ABCr
1972

24ª Reunião da Associação Brasileira de Cristalografia

Livro de Resumos

Organização

UFPR
UNIVERSIDADE FEDERAL DO PARANÁ

Ministério da Saúde
FIOCRUZ - PARANÁ
Instituto Carlos Chagas

2019

25 e 26 de Outubro

Universidade Federal do Paraná
Curitiba

COMITÊ ORGANIZADOR:

Beatriz Gomes Guimarães (FIOCRUZ-Paraná)
Cristiano Luis Pinto de Oliveira (Inst. Física-USP)
Eduardo Granado Monteiro da Silva (IFGW-UNICAMP)
Fábio Furlan Ferreira (UFABC)
Guinther Kellermann (Depto. Física-UFPR)
Javier Alcides Ellena (IFSC-USP)
Maria Cristina Nonato (FCFRP-USP)
Narcizo Marques de Souza Neto (LNLS-CNPEM)

COMITÊ CIENTÍFICO:

Eduardo Granado Monteiro da Silva (IFGW-UNICAMP)
Eduardo Lemos de Sá (Depto. Química-UFPR)
Jaísa Fernandes Soares (Depto. Química-UFPR)
Jorge Iulek (UEPG)
Marcos Tadeu D'Azeredo Orlando (Depto. Física-UFES)
Mario de Oliveira Neto (Inst. de Biociências-UNESP Botucatu)
Nivaldo Speziali (Depto. Física-UFMG)
Ronaldo Nagem (Depto. de Bioq. e Imunologia-UFMG)
Sérgio Ribeiro Teixeira (Inst. Física-UFRGS)
Wagner da Nova Mussel (Depto. Química-UFMG)

COMITÊ LOCAL:

Guinther Kellermann (Depto. Física-UFPR)
Beatriz Gomes Guimarães (FIOCRUZ-Paraná)
Irineu Mazzaro (Depto. Física-UFPR)
Cesar Cusatis (Depto. Física-UFPR)
Jaisa Fernandes Soares (Depto. Química-UFPR)
Eduardo Lemos de Sá (Depto. Química-UFPR)
Daniel da Silva Costa (Depto. Física-UFPR)
Soraya Rodrigues Kulicheski (Depto. Física-UFPR)

APOIO:

Plenárias

Exploring biomolecular dynamics and interactions using advanced sampling methods

Martin Zacharias

Physics Department T38, Technical University of Munich
James-Franck-Str. 1, 85747 Garching, Germany

Understanding the dynamics and stability of biomolecules and biomolecular complexes is of critical importance to better understand its biological function. For many applications currently accessible time scales of molecular dynamics simulations are too short to sufficiently sample relevant conformational states. We employ advanced sampling molecular dynamics (MD) simulations based on Hamiltonian replica exchange (H-REMD) to study the dynamics of proteins and nucleic acids. Methods development concerns both improved sampling of local dihedral transitions but also accelerated sampling of global domain motions in proteins. Applications include the study of peptide and protein folding as well as biomolecular recognition. A second part will focus on the prediction of the geometry of biomolecular complexes using docking approaches. We have developed a flexible protein-protein docking methodology that employs a knowledge-based scoring function for evaluating putative complex structures. The approach also accounts approximately for local and global conformational changes during docking. The application of the methodology to protein-protein and protein-peptide docking and refinement will be presented

Static and dynamic disorder in nanocrystalline metal catalysts

Paolo Scardi

Department of Civil, Environmental & Mechanical Engineering, University of Trento, Trento, Italy.

Metal colloids were already known for centuries when the Romans used gold nanocrystals to dye glass and textiles, and even into medicine [1]. However, only recently have been developed methods for producing nanocrystals of given shape and limited dispersion of sizes. This ability offers extraordinary opportunities for applications such as heterogeneous catalysis, in which nanocrystal shape and dimensional control are fundamental to optimize the performance and selectivity of the catalytic action, as well as to reduce costs, a priority in industrial applications of Platinum Group Metals.

Even if Transmission Electron Microscopy is the elective technique for the direct observation of single nanocrystals, X-ray techniques like EXAFS-XANES and XRD have a strong point in providing information on large statistical ensembles. In addition to the structural information, the study of line profiles and Temperature Diffuse Scattering in XRD powder patterns gives insights into the static and dynamic disorder [2,3], one of the most relevant aspects for catalysis together with the information on the crystal facets exposed to the environment. Concerning the last point, diffraction from powders of metal nanocrystals with the same shape shows features similar to the diffraction from single crystals; as shown recently [4,5], this greatly enhances the detail and reliability of the information carried by the line profiles.

In this presentation a review of Synchrotron Radiation XRD experiments on Pd nanocrystals is presented to illustrate the capability of the technique. Then the most recent results are reported on a combined study by XRD and atomistic simulations (MD and DFT) of the effect of surface capping agents and modifications arising from interactions of the metal nanocrystals with the environment.

[1] C. N. R. Rao, P.J. Thomas, G.U. Kulkarni, "Nanocrystals: Synthesis, Properties and Applications", Springer Series in materials science 95, Springer-Verlag Berlin Heidelberg, 2007.

[2] P. Scardi & A. Flor, *Philosophical Magazine*, 98, **15**, 1412-1435 (2018).

[3] A. Flor, J.M. Feliu, C.-K. Tsung & P. Scardi, *Nanomaterials*, **9**, 609 (2019).

[4] P. Scardi, A. Leonardi, L. Gelisio, M.R. Suchomel, B.T. Sneed, M.K. Sheehan & C-K. Tsung, *Phys. Rev. B.*, **91**,155414 (2015).

[5] P. Scardi & L. Gelisio, *Sci. Reports*., **6**, 22221 (2016).

The MANACA beamline at Sirius, structural biology at 4th Generation

A.C. Zeri[a], A.F.Nascimento[a], C.Y.Hagio[a], E.A. Araujo[a], A.C. Rodrigues[a], H. Westfahl[a].

[a]*Brazilian Synchrotron Light Laboratory – LNLS/CNPEM, Campinas, Brazil.*

.

MANACA (**MA**cromolecular micro and **Na**no Serial **C**ryst**A**llography) will be the first macromolecular crystallography beamline at Sirius, optimised for high flux, micro-beam size and small beam divergence (0.36 mrad). The focus is optimized to 10 x 7 um (HxV) at sample position, but the beam size can be adjusted from 100 x 80 um to 10 x 7 um allowing match the beam to the crystal size. Additionally, the beam can also be cut to achieve smaller sizes (e.g. 5x5 um). The photon flux at sample will be ~$3x10^{12}$ph/s/100mA at 12.5 keV and energy range from 5 to 20 keV. The experimental station has a mini-kappa goniometer that allow the optimal alignment of crystals with long cell axes. Setups for serial crystallography data collection and analyses, as well as automation procedures, are being prepared.

The great beam characteristics provided by Sirius and the high stability and precision of the optics and experimental station will allow the diffraction of challenging samples such as viruses (and other big unit cell crystals), membrane proteins and complexes, which commonly yield small crystals. The energy range and beamline setup will allow native SAD phasing, eliminating the necessity of additional experiments to solve new structures. The experiment control will be done using a user-friendly graphical interface (MXCuBE), and automatic data processing (from data reduction to initial modelling) will be available.

Sessões Temáticas Paralelas

Biologia Estrutural

NP³ PLATFORM: COMBINED PROTEIN CRYSTALLOGRAPHY AND MS-BASED METABOLOMICS TO EMPOWER NATURAL PRODUCT DRUG DISCOVERY

Rafael de Felicio[1]; Cristina F. Bazaano[1,2]; Luiz G. Alves[1]; Gina P. Polo Infante[1]; Marcos G. Cunha[1]; Ianka B. Amador[1]; Karen Velasco-Alzate[3]; Luciana C. Furtado[3]; Juliana R. Gubiani[4]; Everton L. F. Ferreira[4]; Bruna D. Vieira[1]; Raquel O. Ferreira[1]; Andrey F. Nascimento[5]; Ana C. M. Zeri[5]; Guilherme Telles[2]; Roberto G. S. Berlinck[4]; Leticia V. Costa-Lotufo[3]; Daniela B. B. Trivella[1]

[1] Brazilian Biosciences National Laboratory (LNBio), Brazilian Center for Research in Energy and Materials (CNPEM), Zip Code 13083-970 Campinas, Sao Paulo, Brazil.
[2] Institute of Computer Sciences, University of Campinas, Zip Code 13083-852, Campinas, Sao Paulo, Brazil.
[3] Department of Pharmacology, University of Sao Paulo, Zip Code 05508-900, Sao Paulo, Sao Paulo, Brazil.
[4] Chemistry Institute of Sao Carlos, University of Sao Paulo, Zip Code 13566-590, Sao Carlos, Sao Paulo, Brazil.
[5] Brazilian Synchrotron Light Laboratory (LNLS), Brazilian Center for Research in Energy and Materials (CNPEM), Zip Code 13083-970 Campinas, Sao Paulo, Brazil.

Natural substances provide new chemical scaffolds for drug discovery and can probe novel enzyme binding sites and inhibition mechanisms. However, the identification of bioactive natural products and their enzyme binding mechanisms is challenging, sample and time-consuming. We have developed an integrated approach to overcome these gaps, based on high throughput screening of pre-fractionated NP libraries, X-ray protein crystallography and mass spectrometry techniques, all assisted by designed computer algorithms for identifying bioactive natural products and their enzyme binding sites, in the very early stages of natural product-based drug discovery. This approach was named the NP³ platform and works as follows: crystallographic fishing of the bioactive natural product from non-purified and unknown complex chemical samples with crystals of the target protein reveals the active natural product binding site, its mechanism of interaction with the enzyme, and provides initial clues on its chemical structure. LC-MS/MS-based metabolomics is then employed for filtering candidate m/z (compounds) in the unknown mixture and, by an iterative process of crystal electron density and MS/MS spectra interpretation, it is possible to reveal the chemical identity of the bioactive natural product. This iterative approach proved successful even when using low resolution protein crystals and active natural products present in trace amounts in complex chemical samples. The process can be performed in miniaturized scales, in which each step is compatible with high throughput techniques. The NP3 platform is empowering natural product drug discovery in our pipeline, as it will be exemplified by marine fungi and bacterial extracts screened and deconvoluted with the NP³ platform.

Acknowledgements: Serrrapilheira Institute 3659, FAPESP 15/17177-6, 14/10753-9 and 13/50228-8.

The dynamic control of Glutaminase C supramolecular organization with implications on tumor metabolism

M. M. Dias[a]*, J. E. N. Quesnay[b]*, A. Cassago[c], M. van Heel[c], R. V Portugal[c]**, A. L. B. Ambrosio[b]**, and S. M. G. Dias[a]**

[a] *Brazilian Biosciences National Laboratory, CNPEM, Campinas, SP, Brazil.*
[b] *São Carlos Physics Institute, USP, São Carlos, SP, Brazil.*
[c] *Brazilian Nanotechnology National Laboratory, CNPEM, Campinas, SP, Brazil.*

Glutaminase C (GAC), one of the four human glutaminase isozymes, has a distinct cellular localization as well as kinetic properties that provide proliferative advantages to cancer cells [1]; hence, it is considered an important target for the development of novel therapies [2]. We recently described the structural determinants of the long-established phosphate-dependent activation mechanism of GAC that involves the movement of a gating loop and controls substrate accessibility to the active site; this was shown to induce *in vitro* long-range, fiber-like oligomerization and to enhance GAC enzymatic efficiency substantially [3]. However, the existence of such GAC filaments in cells has since remained elusive. We now provide novel information demonstrating that the higher-order mitochondrial assembly of GAC in cancer cells is a dynamic process and necessary for proper enzyme super-activation, upon nutrient withdrawal. We also describe the first experimental structure, at a domain resolution, of the phosphate-induced filament assembled by GAC by cryo-electron microscopy.

[1] Cassago, A., et al., *PNAS*, **109 (4)**, 1092 (2012).

[2] Altman, B. J., Stine Z. E., and Dang, C. V., *Nat Rev Cancer*, **16**, 773 (2016).

[3] Ferreira, A.P.S., et al., *JBC*, **288 (39)**, 28009 (2012).

Acknowlegments: FAPESP.

*Contributed equally:
**Jointly supervised the work: rodrigo.portugal@lnnano.cnpem.br, andre@ifsc.usp.br, and sandra.dias@lnbio.cnpem.br

Fumarases as drug targets against neglected diseases

Maria Cristina Nonato.
Laboratório de Cristalografia de Proteínas, FCFRP, Universidade de São Paulo

Fumarate hydratases or fumarases (FHs) are enzymes that catalyze the reversible hydration of fumarate to L-malate. Eukaryotic cells express two isoforms of fumarase: the canonical role of fumarase is taken by the mitochondrial echoform that participates in the tricarboxylic acid cycle and can also take part in the succinic fermentation pathways by providing fumarate for the enzyme fumarate reductase; the cytosolic echoform has been described as having an important role in the maintenance of genome integrity. By migrating from the cytosol to the nucleus, the cytosolic FHs play a key role in DNA damage response to DNA double strand breaks. Moreover, cytosolic fumarase was suggested to participate as a scavenger of fumarate from the urea cycle and catabolism of amino acids. The crucial role of fumarases in cell metabolism make them potential targets for drug design against infectious diseases.

By using a multidisciplinary approach that combines structural, biophysical, biochemical and genetic studies, it is our aim to validate and exploit fumarases as drug targets against the tropical parasitic diseases: leishmaniasis, schistosomiasis and Chagas disease. They are found among the 20 group of diseases listed by the World Health Organization as neglected diseases due to the lack of investment in the development of effective treatment for their patients.

Leishmania *spp.* and *Trypanosoma cruzi*, the causing agents of cutaneous leishmaniasis and Chagas disease, were found to possess two class 1 fumarases, oxygen sensitive proteins that via an iron-sulfur cluster mediate the reversible conversion of fumarate to S-malate. Intracellular localization studies located FH-1 in the mitochondrion, whereas FH-2 was found predominantly in the cytosol with possibly also some in glycosomes. In *Trypanosoma cruzi*, gene disruption suggested that although the cytosolic or mitochondrial fumarase activities are individually dispensable their combined activity is essential for parasite viability. Based on the mechanistic differences with the human (host) fumarase, we designed and validated 2-thiomalate as a selective inhibitor targeting the parasite enzyme. Our crystal structures of both FH isoforms with inhibitor bound at 2.05 Å resolution and 1.60 Å resolution, not only revealed the new dimeric protein fold adopted by class 1 fumarases, but revealed that the selectivity of 2-thiomalate for class I FHs is due to direct coordination of the inhibitor to the unique Fe of the catalytic [4Fe-4S] cluster that is found in class I parasitic FHs but is absent from class II human FH.

Schistosoma mansoni, responsible for causing schistosomiasis, possesses the two classes of fumarases. Class I fumarase from *S. mansoni* is the mitochondrial enzyme whereas class II fumarase is predicted to be the cytosolic enzyme. Both enzymes are found to be highly expressed in all life stages of the parasite. Class 2 fumarase structure of *S. mansoni* in complex with L-malate was determined by single crystal X-ray diffraction, at 1.85 Å resolution. The differences between classe 2 fumarases between the parasitic and human enzymes were found to be distributed all over the structure, including the prediction of allosteric sites that could be explored to design new selective inhibitors. Differential scanning fluorimetry was shown to be the adequate technique for ligand screening.

For all above enzymes, ligand screening and optimization are underway. This work provides molecular frameworks for the development of chemical leads and innovative drugs against these important neglected diseases.

Acknowlegments: FAPESP; CNPq e CAPES.

Cristalografia de Pequenas Moléculas

Hirshfeld Surfaces and Chemical Bonding in Transition Metals

Bernardo Lages Rodrigues

Chemistry Department, Federal University of Minas Gerais, Belo Horizonte, Brazil

Hirshlfeld Surfaces (HS) are defined from the Hirshfeld stockholder concept (Hirshfeld, 1977) and divides the crystal volume into non-overlapping entities. Distance based properties such as interior distance (d_i), exterior distance (d_e) and the more significant normalized contact distance (d_{norm}) at the HS have been widely used to visualize intermolecular interactions such as hydrogen bonds and π–π stacking in molecular crystals (see, e.g., McKinnon, Fabbiani, Spackman (2007)) . The herein presented work shows the application of Hirshfeld surfaces to understand different behaviours of metal – ligand interactions in transition metals compounds, from the decomposition of the molecule (or polymeric net) into its metal and ligand contributions. Besides the above cited properties, we used the curvedness (C) and the shape index (S) of the HS in the bonding directions to interpret metal-ligand interactions.

Hirshfeld, F. L. (1977) *Theor. Chim. Acta*, **44**, 129-138

McKinnon, J. J.; Fabbiani, F. P. A. & Spackman, M. A. (2007) C*ryst. Growth Des.*, **7**, 755-769

Acknowlegments: CNPq, CAPES, FAPEMIG, FINEP.

Desvendando reações químicas com Difração de raios X

Carlos E. T. Bruzeguini, Matheus B. Alvarenga, Beatriz B. Carvalho, Reginaldo B. dos Santos, Marcos A. Ribeiro

Departamento de Química, Centro de Ciências Exatas, Universidade Federal do Espiríto Santo, Vitória, Brasil.

Ligantes derivados de *o*-aminofenol existem em diferentes estados de oxidação e protonação o que faz com que esses ligantes sejam reconhecidos como redox ativos. O interesse na síntese e caracterização de compostos de coordenação com ligantes *o*-aminofenol é grande porque esses compostos servem de modelo para reações bioquímicas que envolvem espécies radicalares. Não obstante, a presença de elétrons desemparelhados em ligantes coordenados às espécies metálicas cria uma diversidade grande de possibilidades de interação eletrônicas, o que é utilizado no desenvolvimento de materiais moleculares.[1]

Ligantes tetradentados derivados de *o*-aminofenol podem existir como espécies diradicalares onde o centro metálico atua como ponte de comunicação entre os dois elétrons desemparelhados e adicionalmente, dependendo das espécies metálica, diferentes configurações eletrônicas emergem criando distintas propriedades eletrônicas e espectroscópicas. No caso de compostos de cobalto e ligantes redox ativos a distribuição eletrônica metal-ligante, em alguns casos, pode ser controlado por variações de temperatura criando espécies conhecidas como tautômeros de valência.[2][3]

Nesse contexto nosso grupo vem trabalhando na síntese e caracterização de compostos de coordenação de cobalto com ligantes tetradentados redox ativos, especificamente, N,N´-bis(3,5-di-terc-butil-2-hidroxifenil)etilenodiamina (**H4L**) na tentativa de se obter compostos de cobalto que exibam tautomerismo de valência. Três ligantes redox inocentes foram escolhidos, etilenodiamina, piridina e 2,2´-bipiridina, para completar as esferas de coordenação. Duas novas estruturas do composto de coordenação $[Co(H4L)en]^{2+}$ foram determinadas e nelas é possível observar a natureza redox ativa do ligante que se apresenta na forma de um radical iminosemiquinonato, figura **1a**.

No decorrer das pesquisas diferentes espécies orgânicas e inorgânicas foram caracterizadas por difração de raios X de monocristais. Produtos de reações de ciclização (figura **1b**) do ligante tiveram suas estruturas determinadas, assim como compostos de coordenação derivados de reações de oxidação do grupo amina ligado aos anéis aromáticos do ligante redox ativo. A informação estrutural de alta resolução obtida tem permite avaliar as rotas sintéticas assim como propor modificações nas condições afim de se obter os compostos desejados.

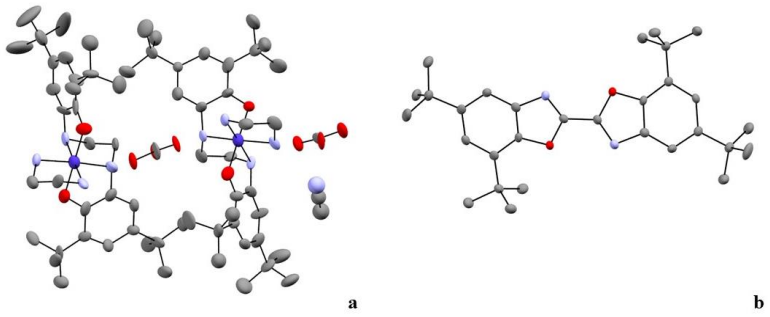

Figura 1: Representação da estrutura do composto $[Co(h_4l)en]CO_3^{2-}$ (**a**) e estrutura do produto da reação de ciclização do ligante H_4L (**b**). Os átomos da cor cinza representam carbono, azul nitrogênio, vermelho oxigênio e roxo cobalto. Os átomos de hidrogênio foram suprimidos para melhor visualização. Os elipsoides são representados a 50% de probabilidade.

As próximas etapas do trabalho incluem estudo cinético da reação de ciclização, melhoria nas condições reacionais para aumento do rendimento nas reações de síntese dos compostos de coordenação de interesse e caracterização das propriedades magnéticas dos compostos.

[1] Chaudhuri, P.; et al. *J. Am. Chem. Soc.*, **123,** 2213-2223(2001).
[2] Min, K. Weyhermüller, T.; Bothe, E.; Wieghardt, K. *Inorg. Chem.* **43**, 2922-2931(2004).
[3] Conner, K.; Arostegui, A.; Swanson, D.; Brown, Seth. *Inorg. Chem.* **57**, 9696-9707(2018).

Agradecimentos: FAPES, MX2 LNLS, CNPq, CAPES

Structural Diversity of 5-Fluorocytosine Multi-Component Crystal Forms: Salts, Drug-Coformer and Drug-Drug Cocrystals

Javier Ellena[a],Matheus S. Souza[a], Luan F. Diniz[a], Cecília C. P. da Silva[a]

[a] *São Carlos Institute of Physics, University of São Paulo, São Carlos, SP, Brazil.*

Aiming to fine-tune the physicochemical profile of active pharmaceutical ingredients (APIs) to circumvent problems related to development and manufacturing, recent studies have examined the solid-state landscape of cytosine derivatives for the synthesis of new crystal forms, whether for use in pharmaceuticals or biological sensors.[1-4] 5-Fluorocytosine (*4-amino-5-fluoro-1,2-dihydropyrimidin-2-one*, 5-FC, **Scheme**) is a synthetic cytosine derivative used in antifungal treatments and as a potential antineoplastic prodrug via gene therapy of mammalian cells. This last use is a promising strategy to reduce undesirable side effects of classical chemotherapy treatment.[1]

In this work we report the supramolecular synthesis of several multi-component solid forms of 5-FC using a wide range of coformers. These forms, that include three drug-drug cocrystals (DDC) with caffeine (an analgesic API), Isoniazid (a tuberculostatic API) and 5-Fluorouracil (an antineoplastic API), were characterized by single crystal and powder X-ray diffraction (SCXRD/PXRD), Fourier Transform Infrared (FT-IR) and Raman spectroscopies. Their thermal stabilities were assessed using hot-stage microscopy (HSM), thermogravimetric analysis (TGA) and differential scanning calorimetry (DSC). In addition, the physical stability analysis at humid environment was performed for the DDCs.

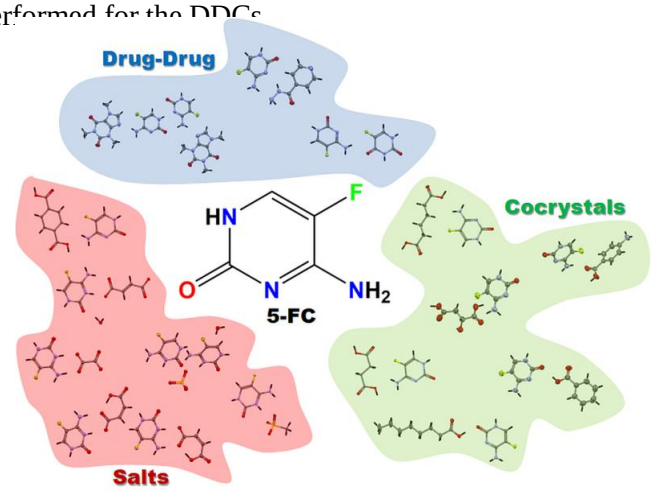

Figure 1: Solid Forms of 5FC.

[1] Da Silva, C.C.P.; de Melo, C.C.; Souza, M.S., Diniz, L.F.; Carneiro, R.L.; Ellena, J. *J. Pharm. Innov.*, **14**(1), 50-56 (2019).

[2] Souza, M.S.; Diniz, L.F.; Vogt, L.; Carvalho-Jr, P.S.; D'vries, R.F.; Ellena, J. *New J. Chem.*, **42**, 14994-15005 (2018).

[3] Souza, M.S.; Diniz, L.F.; Vogt, L.; Carvalho-Jr, P.S.; D'vries, R.F.; Ellena, J. *Cryst. Growth Des.*, **18**(9), 5202-5209 (2018).

[4] Souza, M.S; Da Silva, C.C.P; Almeida, L.R. Diniz, L.F.; Andrade M.B; Ellena, J. J. Mol. Struct., **1161**, 412-423 (2018).

Acknowlegments: The authors acknowledge the Brazilian funding agencies CAPES (C.C.P.S., M.S.S), FAPESP (L.F.D. grant 15/25694-0) and CNPq (J.E. grant #305190/2017-2) for financial support.

Difratometria de Pó

Perovskitas de halogenetos metélicos de baixa dimensionalidade sob condições extremas

A. P. Ayala

Departamento de Física, Universdade Federal do Ceará, Fortleza, Brasil.

Os desenvolvimentos recentes em perovskitas de halogenetos híbridos organo-inorgânicos evidenciaram suas excepcionais propriedades, que incluem uma alta mobilidade de portadores de carga, alto coeficiente de absorção na região visível do espectro solar, longos comprimentos de difusão e simplicidade de fabricação. Essas propriedades fizeram deles materiais optoeletrônicos excepcionais e competitivos para aplicações fotovoltaicas, diodos emissores de luz, fotodetectores, lasers e muito mais. A família de perovskitas de halogenetos inclui várias estruturas baseadas em octaedros de halogenetos metálicos como os da perovskita ABX_3. Estas estruturas têm sido frequentemente classificadas em quatro tipos de estruturas cristalinas considerando o arranjo espacial dos octaedros $[BX_6]^{-4}$: tridimensionais (octaedros de compartilhando os vértices), bidimensionais (planos de octaedros), unidimensionais (cadeias de octaedros) e zero-dimensional (octaedro isolado). As perovskitas de halogenetos de baixa dimensionalidade exibem propriedades notáveis que são significativamente diferentes da contrapartida 3D. Nesta apresentação, investigações estruturais e espectroscópicas de estruturas 0D e 2D sob alta pressão e/ou baixa temperatura serão apresentadas.

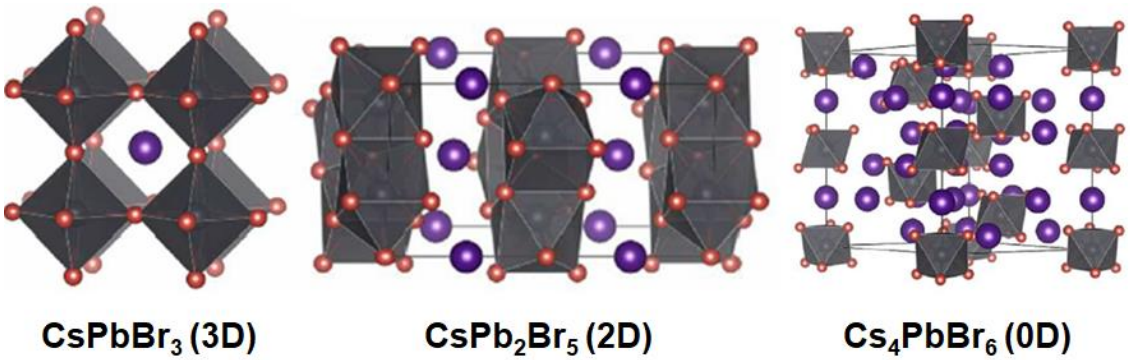

Figura 1: Estruturas cristalinas de perovskitas de halogenetos metálicos .

Agradecimentos: FUNCAP/PRONEX; CNPq; CAPES; CNPEN.

Difração em madeira

I.Mazzaro[a], G. Kellermann, G.I.B. Muniz [b], D.S. Costa

[a]*Departamento Física, Universdade Federal do Paraná, Curitiba Brasil.*
[b]Departamento de Engenharia e Tecnologia Florestal, *Universdade Federal do Paraná*, Curitiba, Brasil.

A madeira pode ser considerada um compósito natural com estrutura formada por conjuntos de células vegetais, com paredes celulares externas ligadas entre si por fibras de celulose, envolvidas por lignina, pectina e minerais. O estudo das propriedades da madeira é de caráter multi disciplinar envolvendo entre eles aspectos biológicos, químicos, físicos e tecnológicos. Do ponto de vista das propriedades mecânicas da madeira, grande importância sé dá ao estudo da celulose e suas propriedades estruturais básicas como, orientação preferencial, cristalinidade, tamanho médio das fibras e ângulo microfibilar (MFA) as quais são determinantes para qualidade da madeira em sí enquanto árvores, como também para seus derivados. Em especial ao MFA são atribuídos o comportamento das propriedades do modulo de elasticidade [1]. Na literatura temos várias técnicas para a avaliação do MFA. As mais usadas são a microscopia com luz polarizada e técnicas com Raios X[2]. Esta ultima sendo preferível, pelo fato da região sondada fazer uma média de área maior do que da anterior. Medimos com a técnica de Difração de Raios X (XRD) três exemplos de madeira: Pinus Taeda Reação, Pinus Taeda Normal e Eucalypitus Grandis. Para a amostra Pinus Taeda Reação, medimos também com a técnica de Espalhamento de Raios X a Baixo Angulo (SAXS). Mostraremos como o MFA pode ser avaliado através da Difração, como também por Espalhamento a baixo ângulo. Foi utilizado o Equipamento D8 Discovery da Bruker com fonte micro foco (50μm) e detector de área VANTEC. A fonte puntual de Raios X usada, foi alvo de Cu e com óptica Montel para obtenção de feixe paralelo, delimitado por fenda de saída circular de1mm. O detector de área com "beam stop" foi colocado a 97cm do eixo do goniômetro, de modo a receber as reflexões de interesse em toda área do detector. Amostras de madeira foram secas, cortadas na convenção RxTxL (1x10x10)mm^3 e lixadas, onde R refere-se a direção Radial no tronco da arvore, direção está que coincide com a direção do feixe incidente; L a direção de crescimento da árvore, isto é, direção das fibras, enquanto T é tangente ao círculo de crescimento. Cada amostra foi colocada no centro do goniômetro de modo que o feixe de Raios X incidente fosse perpendicular a face T e L. O tempo de exposição para cada imagem foi de 40minutos. Do padrão de difração característico de fibras registrado no detector 2D, foi obtido curvas de intensidade versus ângulo 2θ através de um corte radial da imagem na imagem sobre o detector. A curva intensidade azimutal versus ângulo Φ, foi obtido em todo círculo , no intervalo entre os ângulos $21 < 2\theta < 23{,}0$ graus. As curvas de I(Φ) foram ajustadas funções de Lorentz reproduzindo o perfil medido e dessas os valores angulares de interesse. Como resultados obtivemos os seguintes valores para o MFA através da XRD: $28{,}2 \pm 0{,}5$; $15{,}5 \pm 0{,}5$ e $8{,}4 \pm 0{,}5$ respectivamente para o Pinus Taeda Reação, Pinus Taeda normal, e Eucalypitus grandis . O resultado para o MFA através SAXS para o Pinus Taeda Reação foi de $26{,}5 \pm 0{,}5$. Os resultados mostram a coerência entre as medidas realizadas com XRD e SAXS, confirmando o domínio das metodologias de medidas e análises na obtenção do MFA implantadas no Laboratório.

[1] Donaldson, L.A.; **IAWA Journal**, Vol. 29 (4): 345–386; (2008).
[2] S. Andersson, R. Serimaa, M.Torkkeli, T. Paakkari, P. Saranppa, E Pesonen; **J. Wood Sci** 46: 343-349; (2012).

Agradecimentos: a FINEP através dos projetos FINEP CT-INFRA 3080/2011.

X-ray diffraction under extreme conditions at Sirius

Ricardo D. dos Reis and Narcizo M. Souza Neto.

Brazilian Synchrotron Light Laboratory (LNLS), Brazilian Center for Research in Energy and Materials (CNPEM), Campinas, SP 13083-970, Brazil

The EMA beamline (Extreme condition x-ray Methods of Analysis) is one of the hard x-ray undulator beamlines within the first phase of the new synchrotron source in Brazil (Sirius project). This beamline will have a high photon flux (up to 10^{13} photons/s) focused to submicrometer sizes (down to 60x60 nm^2), dedicated to the study of materials under extreme conditions (pressure, temperature, magnetic field).

The beamline will have two experimental stations to cover several extreme condition techniques today employed at synchrotron laboratories worldwide. In addition to the experimental stations, support laboratories will be strongly linked to the experiments at the beamline, covering high pressure instrumentations using diamond anvil cells, handling actinide samples and one laboratory dedicated to high power lasers for in-situ experiments simultaneously to the x-ray techniques. Together with the ideas of the scientific user community, this will be a great opportunity for diverse studies of materials at extreme conditions. In particular, in this talk I will present an highlight of the main scientific results, that were obtained at XDS beamline of the LNLS using powder XRD under high pressure on the last three years and will show what will be the new opportunities to perform both powder and single crystal diffraction under extreme conditions of temperature, pressure and magnetic field at Sirius.

SEARCH OF NEW MULTICOMPONENTS COMPOUNDS OF NEVIRAPINE

Costa, R.N.,[a] , Infantes, L,[b], *Lazarte, D.C., [c],* Cuffini, S.L.[a]

[a]*Instituto de Ciência e Tecnologia (UNIFESP), São José dos Campos, 12231-280, Brazil*
[b]*Rocasolano" - CSIC, C/ Serrano 119, 28006 Madrid, Spain ,[c] CSIC, Granada, Spain.*
scuffini@unifesp.br

ABSTRACT

The antiretroviral drug Nevirapine (NVP) (11-Cyclo-propyl-5,11-dihydro-4-methyl-6H-dipyrido[3,2-b:2′,3′-e][1,4]diazepin-6-one) is a non-nucleoside reverse transcriptase inhibitor, used in the treatment of HIV-1 infection. It is a class II drug according to the Biopharmaceutics Classification System (BSC)[1], exhibiting low solubility and high permeability. Co-crystallisation has shown promise in the tuning of a range of physical properties including dissolution rate, compressibility and physical stability. The potential co-formers can be restricted to a bunch of compounds, to the hundreds compounds considered as safe for human consumption or to the millions of known organic compounds. The number of co-crystallisations that can be attempted experimentally is limited; therefore, it is crucial to improve the probability of success using knowledge-based method for reducing efficiently the initial co-former sample. We are using *in-silico* methods developed from the Cambridge Crystallographic Data Centre (CCDC) for saving time and cost to predict and design co-crystals.[2] Thus, co-formers were used such as, salicylic acid (SA), saccharin (SAC), theophylline (THEOP), theobromine (THEOB), caffeine (CAF), 4-Hidroxibenzoic acid (4-HBZ) and urea (URE) and also different solvents. New compounds were obtained through the liquid-assisted grinding methods and were characterized by solid-state techniques (XRD (powder and single crystal), DSC, Raman, SEM). Results indicates that NVP-SA, NPV-4HBZ, NVP-SAC are co-crystals, whereas NVP-THEOP, NVP-THEOF and NVP-CAF are eutectic materials, and NVP-URE is a solid mixture. Also, several new iso structural solvates were obtained. All these data were used to check the predictions of the new *in-silico* methods developed in collaboration with CCDC.

Keywords: Nevirapine, co-crystals, eutectic,

References:

[1] M. Lindenberg, S. Kopp, J. B. Dressman. *European Journ. Of Pharm. And Biopharmaceutics* **2004**, *58*, 2, 265-278.
[2] P.A. Wood, N. Feeder, M. Furlow, P.T.A. Galek, C.R. Groom, E. Pidcock. *CrystEngComm* **2014**, 16, 5839-5848.

Transition Metal Chalcogenides obtained by Mechanochemistry: challenges and perspectives of its structural/microstructural characterization

C.E.M Campos[a]

[a]*Departamento de Física, Universidade Federal de Santa Catarina, Florianópolis, Brasil.*

Chalcogenides have been deeply studied due to its application possibilities in material science and recently a good review was published to illustrate the progress in chalcogenide mechanochemistry in the last decades [1]. Inspired by this, I would like to modestly present a little of my contribution in this field, focusing on the challenges and perspectives to perform more advanced structural and microstructural characterizations of these nanocrystalline materials using X Ray Powder Diffraction (XRPD). Besides the new iron-rich telluride, Fe_5Te_4, [2] also intended to be presented in this meeting by our group as poster, we have obtained FeSe samples containing large amount of tetragonal superconducting phase by carefully tuning the experimental conditions of the mechanochemical synthesis. More recently, we found that a composite containing Ni and Ni3Te2 nanophases can be used for simultaneous detection of adrenaline and dopamine by electrochemical analysis, being more efficient than the sample containing only the Ni3Te2 phase. Worth to notice that behind all of these achievements is the XRPD analysis, which is the gold-standard technique responsible to attest chemical reactions between reactants, to quantify the crystalline counterparts and even non-crystalline ones. When combined with other techniques, such as transmission electron microscopy (TEM), calorimetry (DSC), Raman spectroscopy (RS), as well as all those techniques accessing the magnetism of the samples (VSM, Mössbauer, etc.), the XRPD analysis can be reviewed and improved given the chance to better explore the information from the microstructure of the nanophases hidden in the tiny details of the experimental results (as the peak profile and linebroadening functions in the Rietveld-like methods or the shape/size-distribution of the virtual nanocrystals built in the Total Scattering method). As a perspective of future developments, I hope to have high energy photons at the new Brazilian synchrotron source (Sirius-CNPEM) to perform good data collections in our next X-ray total scattering experiments and to improve our Debye Function Analysis (DFA) including the anisotropic micro-strain model and bi-modal size distributions of differently shaped nanocrystals. In this times of global economic crises and limited natural resources, mechanochemistry can be an excellent choice to get chalcogenides for nanoscience and nanotechnology mainly because it is an efficient, environment friendly and low-cost synthesis method.

[1] P. Bala´z et al. J Mater Sci vol. 52, pp. 11851–11890 (2017).

[2] K.F. Ulbrich, F. Bertolotti, N. Masciocchi, A. Cervellino, A. Guagliardi and C.E.M. Campos, Journal Materials Chemistry C, vol.6, pp. 3047-3057 (2018).

Acknowlegments: We are grateful to the Brazilian agencies CNPq, CAPES and FAPESC for financial support, multiuser facilities at UFSC (LDRX, LCME and LabCAM), XDS and XRD1 beamlines of Brazilian Sincrotron (LNLS/CNPEM) proposals (20150201, 2018011, 20190070).

Crystal structure of perovskite oxides and its correlation with transport properties for solid oxide fuel cells

F. R. Napolitano[a], J. F. Basbus[a], M. D. Arce[a], H. E. Troiani[a], M. E. Saleta[a, b], J. G. Cuello[c], C. Barbieri Rodella[b], S.J.A. Figueroa[b], A. Caneiro[d], L. V. Mogni[a] and A. Serquis[a].

[a] *Centro Atómico Bariloche (CAB), INN – CNEA - CONICET, Bariloche, Rio Negro, Argentina.*
[b] *Brazilian Synchrotron Light Laboratory (LNLS-CNPEM), Campinas, Brazil*
[c] *Institut Laue-Langevin (ILL), Grenoble, France*
[d] *Y-TEC, Av. del Petroleo s/n, Berisso, Buenos Aires, Argentina.*

The development of clean energy technologies requires to improve the efficiency of electrical systems. For several years, our group has been studying materials based on non-stoichiometric oxides to be used in devices for generating clean and sustainable energy such as solid oxide cells (SOC) in their fuel or electrolyzer modes (SOFC or SOEC).

ABO_3 perovskites oxides provides a very versatile structure, where a large variety of atoms can be included into the A or B sites through distortions of the ideal cubic structure. This characteristic allows the tuning of particular properties that could be relevant for certain applied interest. Due to the strong relationship between the crystallographic structure and the defects with the electronic and transport properties of these materials, it is necessary to explore them with numerous complementary techniques, and simulating operating conditions in order to correlate their characteristics with the properties of interest (properties of transport, thermal, electrochemical, etc.). In this talk I will show some examples of systems in which the correlation between the micro / nanostructural aspects (determined by the processing parameters) and the physical properties that determine the efficiency of some SOC components. In particular, I will present some results regarding two systems: $La_{0.4}Sr_{0.6}Ti_{1-y}Co_yO_{3-\delta}$ (LSTC) and $BaCe_{0.4}Zr_{0.4}Y_{0.2}O_{3-\delta}$ (BCZY) perovskites, which present interesting correlations between the crystallographic and electronic structure with the catalytic activity. LSTC is a good candidate for symmetrical SOC electrodes [1] and BCZY, which is proposed as a potential PC-SOFC electrolyte [2] due to its high bulk protonic conductivity.

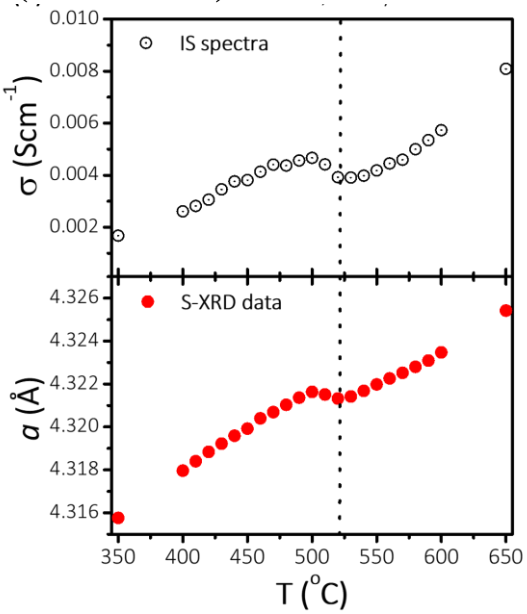

Figure 2: Simultaneous data acquisition of BCZY: Conductivity (above) and lattice parameter (below) obtained from Impedance Spectroscopy (IS) and Synchrotron-XRD simultaneous measurements as function of temperature.

The results include in-situ and in-operando measurements of these oxides both in the laboratory and in large facilities such as synchrotron or neutron sources. All these studies are necessary to find the ideal combination of materials (and synthesis processes) that optimize their performance and long-term stability, to be used in applications.

[1] Napolitano F., Soldati A.L., Geck J., Lamas D. G, Serquis A., *International Journal of Hydrogen Energy*, **38**, 8965-8973 (2014).

[2] Basbus J.F., Arce M.D., Prado F.D., Caneiro A., Mogni L.V., *Journal of Power Sources* **329**, 262-267 (2016).

Acknowlegments: Agencia Nacional de Promoción de Ciencia y Tecnología (ANPCyT) Laboratorio Nacional de Luz Sincrotrón (LNLS), CONICET. CNEA.

Qualitative and quantitative phase analysis of single and multicomponent solid crystalline drug forms

Renata Diniz

Departamento de Química-ICEx, Universidade Federal de Minas Gerais, Belo Horizonte, Brazil

[b]*Physics Institute, University of II, Town, Country.*

[c]*Departamento de Quíimica, Universidad de III, Ciudad, País.*

Drugs or Active Pharmaceutical Ingredients (API) are chemicals that when administered to a living organism interact with it producing some biological effect. Most API (~ 90%) are small organic molecules that can be found in both crystalline and amorphous solid states. However, about 80% of commercially available API solid forms are crystalline. Modifying the crystalline packaging of the API in different solid forms can alter many of their physicochemical properties, such as compressibility, hardness, hygroscopicity, melting and boiling temperatures, stability, solubility and dissolution rate. Therefore, the knowledge of API solid form is very important for pharmaceutic industries. In this work will be presented the analysis by powder X-ray diffraction of single and multicomponent solid forms of antihypertensive (losartan, hydrochlorothiazide, chlorthalidone and captopril) and antimicrobial (lomefloxacin). In special, for the captopril drug will be discuss about its stability in relation to humidity variation and storage time.

Espalhamento de Raios X a Baixo Ângulo

Potencialidades da Técnica de SAXS para Estudo da Correlação entre Estrutura e Propriedades de Materiais Híbridos Orgânicos-Inorgânicos de Interesse Tecnológico

K. Dahmouche

Universidade Federal do Rio de Janeiro, Campus de Duque de Caxias, Duque de Caxias-RJ, Brasil

Uma área particularmente interessante tanto do ponto de vista científico quanto tecnológico concerne os materiais híbridos orgânicos-inorgânicos [1,2]. Esses materiais bifásicos são constituídos de uma fase inorgânica e uma fase orgânica geralmente polimérica. Mas, diferentemente dos compósitos orgânicos-inorganicos usuais, a interpenetração na escala nanométrica entre as fases orgânicas e inorgânicas confere ao material propriedades inéditas impossíveis de se obter com compósitos clássicos, como por exemplo a transparência típica dos vidros. Como as propriedades desses materiais não são descritas pela soma das contribuições individuais de cada fase, visto que a interface tem um papel preponderante, classifica-se as classes de materiais híbridos a partir da natureza da interface orgânica-inorgânica: classe I onde as duas fases são interligadas por ligações fracas (pontes de hidrogênio, Van der Waals, etc) e classe II onde há formação de ligações primárias (covalentes ou ionocovalentes) entre as fases inorgânicas e orgânicas. O composto orgânico confere a esses nanocompósitos propriedades físicas ou químicas específicas: óticas, elétricas, eletroquímicas ou biológicas. Por outro lado, a parte inorgânica do material contribuiu para a resistência mecânica e térmica, permite modular o índice de refração, podendo ainda conferir propriedades óticas, eletroquímicas, elétricas ou magnéticas, interessantes.

Essa palestra visa a mostrar como o uso da técnica de SAXS é fundamental para explicar as propriedades dos materiais híbridos, através da correlação entre a estrutura desses materiais na escala manométrica e suas propriedades De fato, evidenciamos através de exemplos de materiais híbridos podendo ser empregados nas áreas de energia limpa ou da saúde que os processos de nano-estruturação existentes nesses materiais são de extrema importância para obter as propriedades de interesse tecnológico desejadas.

[1] C. Sanchez, B. Julian, P. Belleville, M. Popall, B.C., *Journal of Materials Chemistry*, **15**, 3559 (2005)

[2]: C. Sanchez, L. Rozes, F. Ribot, C. Laberty-Robert, D. Grosso, C. Sassoye, C. Boissière, L. Nicole, *CR. Chimie*, **13**, 3 (2010).

Agradecimentos: Fundação de Amparo a Pesquisa do Rio de Janeiro (FAPERJ); CNPq e CAPES.

Reverse micelles and cloud point approach of Diol triblock copolymer

C. V. Teixeira[a], Y. A. Marques[b] , M. C. A. Fantini[c] . C. L. P. Oliveira[c]

[a]*Departamento de Física, Universidade Federal do Rio Grande do Sul, Porto Alegre, RS, Brasil.*

[b] *Dow Chemical, Polyurethanes Research and Development, Texas, United States.*

[c] *Instituto de Física, Universidade de São Paulo, São Paulo, SP, Brasil.*

Solution behaviour of two commercially used polyether glycols with polyethylene (PEO)-polypropylene (PPO)-polyethylene (PEO) composition - Diol (linear) and Triol (star-like) -was studied, concerning the concentration and temperature effects until the cloud point (CP). Both polymers are practically insoluble in water, reaching their CP at low concentration and temperature. To increase the CP, 2-(2-butoxyetoxy) ethanol (DB) was mixed to the water [1].

Increasing amounts of DB solubilize the polymers at higher concentrations and higher temperatures. The structural study was performed with 25% DB in water, which solubilized all polymers concentrations (from 5% to 95%). Due to the high solubility, the micelles could only be observed above 40% of polymer in solution, when reversed micelles were formed. The solvent nuclei of the reversed micelles increased with increasing polymer concentrations, caused by dehydration of the PPO chains, followed by a decrease at further higher concentrations, when the hydrophobic chains were completely dehydrated. When the CP is reached, the solvent nuclei are segregated but, as they are well separated by large polymer domains, no phase separation occurs. Despite the high polymer concentration and high temperature, neither ordered nor gel phase is formed, probably because of a combination of high solubility and short hydrophobic segments. Both polymers showed very similar behavior. The study was performed by Small-Angle X-ray scattering (SAXS) and complemented by Fourier Transformed Infrared Spectroscopy (FTIR) and Dynamic Light Scattering (DLS).

[1] Schönfeldt, N., *Surface Active Ethylene Oxide Adducts*, New York: Pergamon Press, Oxford (1969).

Acknowlegments: FAPESP; CNPq; Dow Chemical.

Coherent and Small Angle X-ray Scattering at SIRIUS, the Cateretê beamline

F. Meneau[a], A.R. Passos[a], T. Kalile[a], J.P. Zerba[a] and C.C. Polo[a]

[a]*Brazilian Synchrotron Light Laboratory (LNLS), Brazilian Center for Research in Energy and Materials (CNPEM), 13083-970, Campinas, SP, Brazil.*

The Cateretê beamline at Sirius, the new Brazilian synchrotron light source will be dedicated to coherent and time-resolved scattering experiments. It will provide unique capabilities, providing cutting edge research tools that are non-existent today in Brazil, like 3D imaging with nanometer resolution and X-ray photon correlation spectroscopy (XPCS) to study dynamics in hard and soft condensed matter and biological materials.

The SIRIUS storage ring will have a natural horizontal emittance of $\epsilon_x = 245\ pm\ rad$ and a vertical emittance (coupling 1%) of $\epsilon_y = 2.4\ pm\ rad$ [1]. The Cateretê beamline will be equipped with a Delta undulator [2] allowing to tune the beam polarisation. The main three optical elements, vertical and horizontal focusing mirrors [3] and the four-crystal monochromator will be in a horizontal side-bounce configuration, optimising the stability, and delivering a fully coherent beam of 30 x 30 μm^2, with an energy ranging from 4 to 21 keV. The expected coherent flux is expected to reach 10^{12} ph/s at 4 keV. The experimental station will be located 88 meters from the source, followed by a 28 meters vacuum chamber hosting the Medipix (3k x 3k pixels^2) in-vacuum detector. The sample environment is under commissioning and will enable to perform 3D-CDI, ptychography, BraggCDI, XPCS and USAXS measurements. It will be equipped with an interferometry system, a cryogenic device for biological specimens and catalytic reactors for *in situ* studies [4], [5].

In this presentation, I will present the main characteristics and new scientific potentialities of the Cateretê beamline which is expected to receive light by the end of 2019.

[1] L. Liu, N. Milas, A. H. C. Mukai, X. R. Resende, and F. H. De Sá, "The sirius project," *J. Synchrotron Radiat.*, vol. **21**, no. 5, pp. 904–911, (2014).

[2] A. B. Temnykh, "Delta undulator for Cornell energy recovery linac," *Phys. Rev. Spec. Top. - Accel. Beams*, vol. **11**, no. 12, pp. 1–10, (2008).

[3] R. R. Geraldes *et al.*, "the Design of Exactly-Constrained X-Ray Mirror Systems for Sirius," *MEDSI Conf. Proc.*, pp. 173–178, (2018).

[4] A. Rochet *et al.*, "In situ reactor to image catalysts at work in three-dimensions by Bragg coherent X-ray diffraction," *Catal. Today*, vol. **336**, no. December 2018, pp. 169–173, (2018).

[5] A. F. Suzana *et al.*, " In situ three-dimensional imaging of strain in gold nanocrystals during catalytic oxidation ," *Nanoscale Adv.*, vol. **1**, no. 8, pp. 3009–3014, (2019).

Acknowlegments: FAPESP (2014/25964-5), CNPq and MCTIC.

Self-Assemblies Based on Cell Penetrating Peptides: Supramolecular Structure Unveiled by Small-Angle Scattering

E.R. Silva

Departamento de Biofísica, Escola Paulista de Medicina, UNIFESP, São Paulo, Brasil.

Cell penetrating peptides (CPP) are short amino acid sequences able to cross cell membranes. This feature paves the way for diverse biomedical applications, especially those related to intracellular delivery of exogenous compounds. As a rule, these oligopeptides are highly cationic, abundant in arginines and lysines, and have been successfully conjugated to nucleic acids for gene delivery into a wide range of cell lines. Obviously, structure-activity relationships are crucial for optimizing biomaterials based on these assemblies, however, comprehensive information on their nanoscopic organization is still lacking in literature. In this context, small-angle scattering tools may bring a strong contribution since they allow for investigating these systems under near-native conditions. In this Talk, I will discuss aspects of the nanoscopic structure of conjugates formulated between cell-penetrating peptides and nucleic acid sequences. In the first part, I will describe the organization of hybrid conjugates formulated using two classes of model peptide amphiphiles, the lipopeptide PRW-C_{16} and the bolaamphiphile RFL_4FR [1]. A combination of SAXS/SANS and cryo-EM data shows that lipopeptide-based complexes self-assemble into structures with large-scale fractal features, hosting DNA in the interstices whereas bola-amphiphile scaffolds self-assemble into planar structures with DNA strands sandwiched in-between peptide nanotapes. In the second part, I will present results from investigations about the structure of conjugates based on the *CPP Penetratin*. Small-angle scattering was combined with infrared nanospectroscopy (AFM-IR) to provide information on the inner structure and for stablishing relevant structure-activity correlations useful for designing of novel DNA vectors [2].

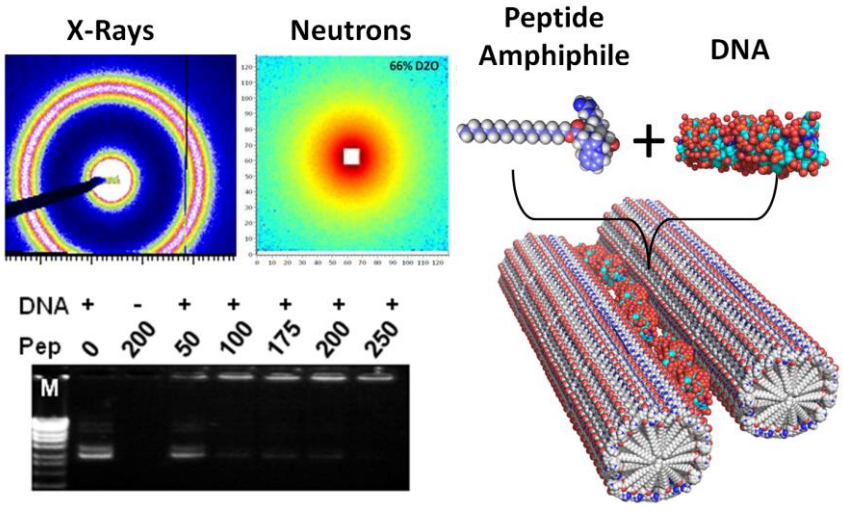

Figure 1: Schematic structure of DNA complexes based on a cell-penetrating peptide [1].

[1] Silva, E.R., Cooney, G., Hamley, I., Alves, W. A., Lee, S., O'Connor, B. F., Reza, M., Ruokolainen, Walls, D., *Soft Matter*, **12**, 9158-9169 (2016).

[2] Mello, L.R., Hamley, I.W., Castelletto, V., Garcia, B. B. M., Han, S.W., Oliveira, C.L.P. and Silva, E.R., submitted (2019).

Acknowlegments: FAPESP (2016/24409-3).

Glycoside hydrolases molecular characterization : a SAXS approach

M. Oliveira Neto[a], C. A. Gandin[a] , W. Garcia[b], I. Polikarpov[c], F. M.Squina[d].

[a]*Institute of Biosciences, Unesp, Botucatu, São Paulo, Brazil.*
[b]*Center for Natural and Human Sciences (CCNH), UFABC, Santo André, Brazil.*
[c]*Institute of Physics of São Carlos, USP, São Carlos, São Paulo, Brazil.*
[d]*Program of Technological and Environmental Processes, UNISO, Sorocaba, SP, Brazil.*

Small-angle X-ray scattering (SAXS) is an experimental technique frequently applied to low-resolution structural studies of macromolecules embedded in a homogeneous liquid medium, over a molecular size scale within the 1–100 nm range. The SAXS method allows for investigations of both, well-structured and disordered macromolecules in solution, neither requiring crystallization procedures nor highly elaborate sample preparations [1]. Knowledge of the stability, molecular weight, oligomeric states, and quaternary arrangements of proteins in solution is fundamental for understanding their molecular functions and activities [2]. Glycoside hydrolases (GHs) play fundamental roles in the decomposition of lignocellulosic biomaterials, the most abundant carbon source in the biosphere; however, its recalcitrance remains a challenge for microbial conversion into biofuel and bioproducts. SAXS has been extensively used to give structural information about GHs, where the relative position of multimodular protein domains has been elucidated, expanding knowledge and establishing a relationship between activity and flexibility of biological systems.

[1] Glatter, O., Kratky, O. Small-Angle X-ray Scattering. *Academic Press: New York*, (1982).

[2] Piiadov, V., Araújo, E.A., Oliveira Neto, M., Craievich, A.F., Polikarpov I. *Protein Science*, **28**, 454-463 (2019).

[3] Liberato, M.V., Silveira, R.L., Prates, E.T., Araujo, E.A., Pellegrini, V.O.A., Camilo, C.M., Kadowaki, M.A., Oliveira, M.O., Popov, A., Skaf, M.S., Polikarpov, I. *Scientific Reports*, **6**, 23473-23489, (2016).

Acknowlegments: Fapesp; CNPq.

Investigating systems at nanoscale using scattering methods

Oliveira CLP [a]

[a]*Physics Institute, University of São Paulo, São Paulo, Brazil*

For the characterization of the structure of matter several experimental methods can be used. Among a large number of techniques, scattering and diffraction methods, particularly using visible light, X-rays and neutrons are widely used. In this talk cutting-edge applications of Small-angle X-ray Scattering (SAXS) and light scattering (both static and dynamic) will be presented for the investigation of nanoparticles, proteins, vesicles, micelles among other cases.

[1] Oliveira CLP, Gerbelli BB, Silva ERT, Nallet F, Navailles L, Oliveira EA, et al. Gaussian deconvolution: a useful method for a form-free modeling of scattering data from mono- and multilayered planar systems. Journal of Applied Crystallography. 2012;45:1278-86.

[2] Oliveira CLP, Santos PR, Monteiro AM, Figueiredo Neto AM. Effect of Oxidation on the Structure of Human Low- and High-Density Lipoproteins. Biophysical Journal. 2014;106(12):2595-605.

[3] Garcia PRAF, Loza K, Daumann S, Grasmik V, Pappert K, Rostek A, Helmlinger J, Prymak O, Heggen M, Epple M , Oliveira CLP. Combining Small-Angle X-ray Scattering and X-ray Powder Diffraction to Investigate Size, Shape and Crystallinity of Silver, Gold and Alloyed Silver-Gold Nanoparticles. Brazilian Journal of Physics. 2019;49(2):183-90

[4] Alves C, Pedersen JS, Oliveira CLP. Calculation of two-dimensional scattering patterns for oriented systems. Journal of Applied Crystallography. 2017;50:840-50

Acknowlegments: FAPESP, CNPQ, CAPES

Comunicações Orais

The role of *Trypanosoma brucei* ribonuclease RRP44 in ribosomal RNA processing

Cesaro, G.[a,b], Carneiro, F.R.G.[a], Legrand, P.[c], Zanchin, N.I.T.[a], Guimarães, B.G.[a,b].

[a] *Instituto Carlos Chagas, FIOCRUZ/PR, Curitiba, Brazil.*

[b] *Programa de Pós-graduação em Ciências-Bioquímica, UFPR, Curitiba, Brazil.*

[c] *Synchrotron SOLEIL, Saint-Aubin, France.*

Parasitic trypanosomatids, such *Trypanosoma brucei*, *T. cruzi* and *Leishmania sp.* present unique features compared with other eukaryotes with regard to RNA processing and maturation. For instance, *T. brucei* ribosomes contain specific rRNA expansions and the 60S subunit is composed of eight rRNAs molecules instead of the three rRNAs found in most eukaryotes. The role of specific endo- and exonucleases in the maturation of the unusual rRNA precursor of trypanosomatids remains largely unknown. One of the nucleases involved in rRNA processing is Rrp44, an exosome associated ribonuclease in yeast, which is involved in several metabolic RNA pathways. Here we investigate functional and structural aspects of the *T. brucei* ribonuclease RRP44. Recombinant full-length and truncated forms of TbRRP44 were produced for crystallization. *T. brucei* knockdown cells were generated using RNA interference (RNAi) to perform phenotypic characterization. Analysis of pre-ribosomal RNA processing were performed by qRT-PCR and Northern blot. Proliferation curves of knockdown cells confirmed that TbRRP44 is essential for the parasite viability. TbRRP44 depletion causes accumulation of the complete LSU rRNA precursor, in addition to 5.8S maturation impairment. The crystal structure of TbRRP44 endonucleolytic PIN domain was refined at 2.3 Å resolution. Structural comparison with *Saccharomyces cerevisiae* Rrp44 revealed differences which could provide molecular bases for the lack of interaction of RRP44 with the exosome complex in *T. brucei*. A TbRRP44 construction including the exonucleolytic RNB domain was also crystallized. Crystals diffract to 3.1 Å resolution and the structure was determined by molecular replacement. Structural analysis reveals that the exonucleolytic active site is conserved when compared with *S. cerevisiae* Rrp44. In conclusion, we have shown that TbRRP44 is essential for cell viability and correct LSU rRNA maturation. The crystal structure of the TbRRP44 endonucleolytic domain revealed key differences relative to the yeast homologue.

Acknowlegments: CNPq, CAPES, COFECUB, FIOCRUZ, Synchrotron SOLEIL.

24th ABCr Meeting , Curitiba, October 2019

Study of Alloy (AuAg) Nanoparticle using Pair Distribution Function (PDF) derived from Precession Electron Diffraction (PED)

L. M. Corrêa, M. H. M. Moreira, V. Rodrigues, D. Ugarte

Physics Institute 'Gleb Wataghin', University of Campinas-UNICAMP, Brazil.

Usual crystal characterization techniques have been developed considering a periodic arrangement of atoms with long range order; these basic assumptions may make their use unsuited to characterize small crystals. Pair Distribution Function (PDF) has been successful in solving the structure of low ordered materials (amorphous, nanoparticles - NP)[1, 2, 3]. PDF can be derived from X-Ray Powder Diffraction (XRPD) data with high signal to noise ratio up to high scattering angles using synchrotron sources. Even using modern instrumentation, NP sample weighting several milligrams are required; this may represent a challenging issue in some research projects. To overcome this difficulty, we propose the use of PDF derived from Electron Diffraction. The strong electron-matter interaction allows a tiny sample quantity to be used (~ few ngr), but the incident electron can scatter several times inside the crystal (dynamical diffraction), complicating the interpretation of measured intensities. Using Precession Electron Diffraction (PED), measured intensities are quase-kinematical, allowing the use of x-ray approaches[4]. NP samples ($Au_{0.70}Ag_{0.30}$) were produced by a home-made cluster source at IFGW-Unicamp[5]. Experiments were realized using a TECNAI G2 200KV microscope equipped with Nanomegas ASTAR systems and axial CCD camera (LCE-DEMa-UFSCar). A home-made software, written in Python, was used for data analysis. Measured PED-PDFs have been quantitatively compared with different NP structures (fcc, decahedral, icosahedral, etc.). The smallest residue was obtained for ~3 nm decahedral NPs (~20%). This NP diameter is smaller than the mean diameter derived microscopy image (~6 nm), suggesting that the these particles are formed by the aggregation of smaller crystallites.

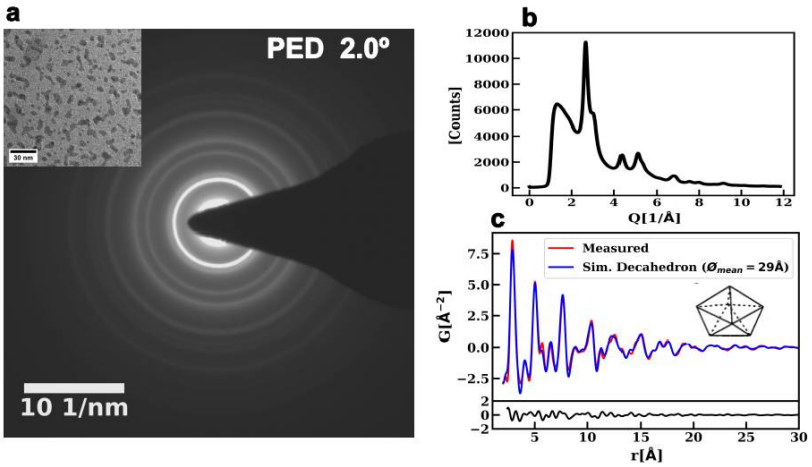

Figure 1: a) PED pattern of AuAg NPs. Inset: microscopy image of clusters. b) Azimuthal integration of ring pattern intensities (equivalent to XRPD). c) reduced PDF calculated from b).

[1] T. Egami, S. J. L. Billinge, Underneath the Bragg peaks: Structural Analysis of Complex Materials, Elsevier, Oxford (2003).

[2] S. Banerjee, et al. , J. Phys. Chem. C, **122**, 29498-29506 (2018).

[3] M. M. Hoque, et al., J. Phys. Chem. C, **123**, 32, 19894-19902 (2019).

[4] P. A. Midgley, A. S. Eggeman, IUCrJ, **2**, 126 – 136 (2015).

[5] A. D. de Sá, et. al., J. Vac. Sci. Technol. B, **32**, 061804 (2014).

Acknowlegments: CNPq; CAPES; FAPESP; LCE-DEMa-UFSCar; We are grateful to D. Coimbrão for assistance during PED work.

Atovaquona incorporada em nanoemulsão não interfere na organização supramolecular da nanoestrutura

F. Bruxel[a], C. Scheuer[a], M. C. Galarça[a], L. B. Wild[b], R. S. Schuh[b], C. A. Perez[c], A. Malachias[d], H. F. Teixeira[b]

[a]*Programa de Pós-Graduação em Ciências Farmacêuticas, Universidade Federal do Pampa, Uruguaiana, Brazil.*
[b] *Programa de Pós-Graduação em Ciências Farmacêuticas, Universidade Federal do Rio Grande do Sul, Porto Alegre, Brazil.*
[c] *Laboratório Nacional de Luz Sincroton, Campinas, Brazil.*
[d] *Departamento de Física, Universidade Federal de Minas Gerais, Belo Horizonte, Brazil.*

Relatos de resistência por parte dos parasitos do gênero *Plasmodium* têm sido descritos para todos compostos antimaláricos atualmente utilizados no tratamento da malaria [1]. Dentre esses compostos, inclui-se também a atovaquona, uma molécula que também apresenta baixa hidrossolubilidade e dificuldade para ultrapassar as barreiras lípidicas das membranas celulares [2]. Neste contexto, sua incorporação em nanoemulsões tem sido sugerida como uma forma de solucionar esses problemas. Entretanto, pouco se conhece ainda sobre a organização estrutural supramolecular dessas emulsões, importante para compreender como o fármaco se associa ou é liberado a partir dos nanossistemas [3]. Assim, o objetivo deste trabalho foi caracterizar aspectos físico-químicos e determinar a organização estrutural de nanoemulsões, antes e após a incorporação de atovaquona no sistema. As formulações brancas foram preparadas por emulsificação espontânea e compostas por triglicerídeos de cadeia média, lecitina, 1,2-dioleil-3-trimetilamônio-propano, glicerol e água ultrapura (NE) [4]. As nanoemulsões contendo atovaquona foram denominadas NE-ATQ. A distribuição e diâmetro médio de gotícula foram caracterizados por difratometria a laser e o potencial zeta por migração eletroforética. Para determinar a organização estrutural, foi utilizada a técnica de difração de raios-X por energia dispersiva, utilizando-se uma fonte de luz Síncroton. As formulações NE e NE-ATQ apresentaram propriedades físico-químicas semelhantes ($p>0,05$), demonstrando diâmetros médios de gotículas entre 190-230nm, com índice de polidispersão <0,2. O potencial zeta apresentou-se positivo (+42 a 55 mV) para ambas as formulações. A formulação NE apresentou os picos de difração: 0,091 e 0,178 $Å^{-1}$, correspondendo a um tamanho de retículo de 69 Å. A formulação contendo atovaquona (NE-ATQ) apresentou picos de difração em 0,097 e 0,195 $Å^{-1}$, correspondendo ao tamanho de retículo de 64,8 Å. Ambas formulações apresentaram razões características de estruturas lamelares, conforme já descrito na literatura para esse tipo de sistema. Também pôde ser identificada a presença de outros picos de menor intensidade na região de 0,083 e 0,104 $Å^{-1}$, sendo provavelmente relacionados à mistura de fosfolipídeos presentes na lecitina, que compõe as formulações [3]. Pode ser concluído que, de acordo com esses resultados, a incorporação de atovaquona não alterou a organização lamelar da nanoemulsão, sugerindo que a molécula está dissolvida em seu núcleo oleoso.

[1] WHO. World Health Organization. Malaria. <https://www.who.int/malaria/en/> (2019).

[2] Rang, H.P., Ritter, J.M., Flower R.J., Henderson, G., in *Rang & Dale: Farmacologia,* 8. ed. Elsevier, Rio de Janeiro, 784 p. (2016).

[3] Bruxel, F., Vilela, J.M.C., Andrade, M.S., Malachias, A., Perez, C.A., Magalhães-Paniago, R., Oliveira, M.C., Teixeira, H.F., *Colloids and Surfaces B*, **112**, 530–536 (2013).

[4] Bruxel, F., Bochot, A., Diel, D., Wild, L., Carvalho, E.L.S., Cojean, S., Loiseau, P.M., Fattal, E., Teixeira, H.F., *Current Topics in Medicinal Chemistry*, **14**, 1-11 (2014).

Acknowlegments: FAPERGS; CNPq; PDA/Unipampa.

HARPIA: High Resolution Powder X-ray Diffraction beamline at Sirius

F. R. Estrada[a], A. Iglessias[a], D. H. Barrett[a,b], V. K. Silva[a], I. B. B. Rêgo[a], C. R. Oliveira[a], C. B. Rodella[a]

[a] *Brazilian Synchrotron Light Laboratory (LNLS), Brazilian Center for Research in Energy and Materials (CNPEM), Campinas, Brazil.*

[b]*Chemistry Department, University of the Witwatersrand, Johannesburg, South Africa.*

Sirius is a fourth-generation synchrotron light source built at the CNPEM and is forecast to begin operations in 2020. Brazil is transitioning from a second-generation synchrotron source (UVX) to a leading position in the design and operation of the brightest 4th-generation machine in its energy class. This multidisciplinary research infrastructure will bring an advanced facility to the structural characterization of polycrystalline samples – HARPIA beamline. The synchrotron radiation source of HARPIA will be an undulator with an 18 mm period length and importantly, without an energy gap. The beamline will be installed in a low-β straight section of the storage ring to increase the beam size in the horizontal direction. HARPIA's optical design aims to be simple, yet highly effective to provide high photon flux at the sample position, H 2.210^{12} ph/s/100 mA at 20 keV, about 1000 times higher than that of the LNLS at 8 keV. Energy selection will be obtained by the Bruker double-crystal-monochromator from the XDS beamline at the LNLS. The two sets of Si crystals, (111) and (311), will allow an energy range from 5 to 30 keV. The beam size at the sample position is calculated to be around 0.85 mm (v) x 1.2 mm (h) with a divergence of 25 μrad (v) x 34 μrad (h) at 20 keV. HARPIA's experimental hutch (Fig. 1) will provide high-resolution X-ray diffraction data with a multi-analyser crystal from FMB Oxford having at least 8 modulus of Si(111) crystals and $NaBr_2$ scintillators detectors. Moreover, it will allow dynamic experiments using a linear fast detector developed in house covering 90° in 2θ range to provide second scale temporal resolution.

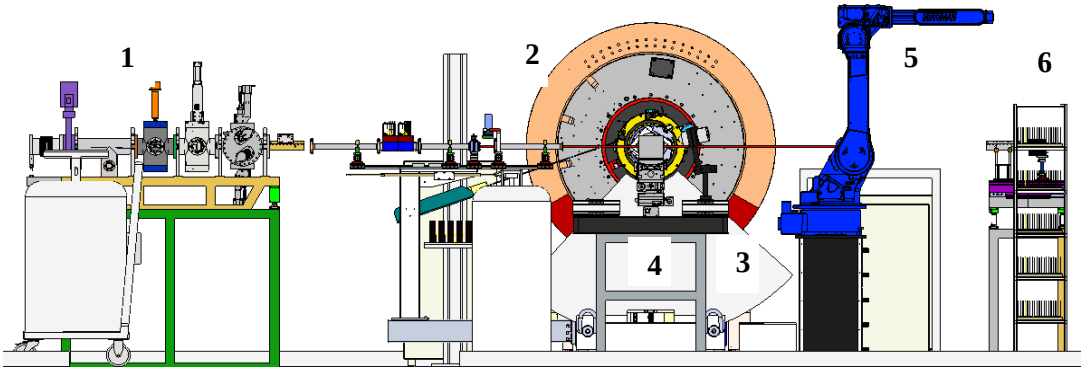

Figure 1: Experimental hutch of HARPIA beamline showing: 1. optical systems (shutter slits, beam monitors, filters); 2. 3-circle diffractometer; 3. in-house linear detector; 4. optical table; 5. robotic arm and 6. sample´s magazine.

The 3 co-axial circle heavy-duty diffractometer from the current XRD1 beamline at LNLS (Fig. 1.2) will be transferred to the HARPIA experimental hutch. X-ray diffraction measurements will be conducted in Debye-Scherrer geometry (capillary geometry). The diffractometer uses high precision rotary stages (Θ, 2Θ and d axes) and are designed to support heavy detector arrays, such as the two sets of detectors in the aforementioned paragraph.

A storage magazine for samples placed into capillaries (Fig. 1.6) allows hundreds of samples to be loaded and measured via the use of a robotic arm which serves as a sample exchanger. The robotic arm allows for the beamline to be programmed and, if necessary, operated remotely providing high levels of efficiency and maximization of the provided beamtime. HARPIA beamline will provide an efficient and user-friendly facility to the structural characterization of polycrystals in a variety of sample environments as well as fast and high-resolution mode detection to Sirius users.

Acknowlegments: FAPESP and CNPEM

Magnetic Structure of RNiSi$_3$ (R = Gd and Tb)

Rodolfo Tartaglia[a], Fabiana R. Arantes[b], Carlos W. Galdino[a], D. Rigitano[a], U. F. Kaneko[c], M. A. Avila[b], and E. Granado[a]

[a] *"Gleb Wataghin" Institute of Physics, University of Campinas, Campinas, Brazil.*
[b] *CCNH, Universidade Federal do ABC, Santo André, Brazil.*
[c] *Brazilian Synchrotron Light Laboratory, Brazilian Center for Research in Energy and Materials, Campinas, Brazil.*

The intermetallic family RNiSi$_3$ (R = rare earth) presents interesting antiferromagnetic ground states evolving with R and under applied magnetic field for some of the compounds.[1] In spite of this, the magnetic structures need to be determined for a better understanding of the physics of this system. In this work, resonant X-ray magnetic diffraction experiments were performed on single crystals of GdNiSi$_3$ and TbNiSi$_3$ at zero field. It is known that photons are also sensitive to the electronic magnetic moments, leading to the appearance of magnetic Bragg peaks in the magnetically ordered phase of the material. Also, when the X-ray energy is close to an absorption edge related to the magnetism of the magnetic element, an enhancement of the signal is observed, causing a resonant scattering condition.[2] The diffraction experiments on GdNiSi$_3$ and TbNiSi$_3$ were done at the XDS (X-ray Diffraction and Spectroscopy) beamline of LNLS. The primitive magnetic unit cell matches the chemical cell below the Néel temperatures T_N = 22.2 and 33.2 K, respectively. The magnetic structure is the same for both compounds, with ferromagnetic *ac* planes stacked in an antiferromagnetic + - + - pattern, with the rare-earth magnetic moments pointing along the **a** direction (magnetic space group *Cmmm'*).[3] This structure contrasts with the + - - + stacking and magnetic moment along **b** axis previously reported for YbNiSi$_3$,[4] indicating a sign reversal of the coupling constant between second-neighbor R planes as R is varied form Gd and Tb to Yb.

[1] F. R. Arantes, D. Aristzabal-Giraldo, S. H. Masunaga, F. N. Costa, F. F. Ferreira, T. Takabatake, L. Mendonça-Ferreira, R. A. Ribeiro, and M. A. Avila, *Phys. Rev. Materials*, **2**, 044402 (2018).

[2] J. P. Hill and D. F. McMorrow, *Acta Cryst.*, **52**, 236 (1996).

[3] R. Tartaglia, F. R. Arantes, C. W. Galdino, D. Rigitano, U. F. Kaneko, M. A. Avila, and E. Granado, *Phys. Rev. B*, **99**, 094428 (2019).

[4] Y. Kobayashi, T. Onimaru, M. A. Avila, K. Sasai, M. Soda, K. Hirota, and T. Takabatake, *J. Phys. Soc. Jpn.*, **77**, 124701 (2008).

Acknowlegments: This work was supported by CAPES and FAPESP (Grant 2017/04913-1).

Functional and structural characterisation of an α-L-arabinofuranosidase from *Thielavia terrestris*. The first β-propeller fold adopted through an exquisite domain-swapping in GH62 family

S. Camargo[a], E. J. Mulinari[a], L. R. de Almeida[a], M. V. Zerbini[a], A. Bernardes[a], F. Segato[b], and J. R. C. Muniz[a]

[a]São Carlos Institute of Physics (IFSC), University of Sao Paulo (USP), Sao Carlos, Brazil.
[b]Engineering School of Lorena, University of São Paulo (USP), Lorena, SP, Brazil.

Genome analyses and experimental data suggested that thermostable enzymes may afford economic advantages in the production of many biotechnological products based on biomass degradation. The fungus *Thielavia terrestris* plays an important role in the global carbon cycle with enzymes highly capable of hydrolysing all major polysaccharides found in biomass, making it an attractive candidate for industrial applications and bioremediation. From prospection to three-dimensional structures, we foster a deeper understanding of the hydrolysis of vegetal biomass and pollutants, applying modern scientific approaches in macromolecular crystallography associated with biophysical and biochemical studies. In this research, we have characterized *Tt*GH62 biochemically and structurally to understand its mechanism and optimal conditions of action. Additionally, the enzyme described here has a structural novelty unusual from all structures that have been reported so far for the GH62 family, an exquisite domain swapping phenomena, located at the supramolecular arrangement due to the presence of a disulphide bond (Cys32 and Cys300) connecting the monomers. The active site is a perfect combination of catalytic residues of both subunits. Similarly, the structure has a calcium-binding site, shared by the dimer-dimer contact interface. All of the crystallographic behaviours go against solution monomeric state, which indicates a crystallographic artefact produces by crystal condition. Nevertheless, the nature of this unusual crystallographic structure brings speculation about inactivation and storage mechanism of high protein concentration producing a compact assembly with additional stabilizing contacts between chains. The *Tt*GH62 was also characterised in synthetic (pNPAraf) and polymeric substrate (arabinan and arabinoxylan), revealing optimum temperature and pH (for pNPAraf) of 30 °C and 4.5-5.0, respectively. Characterisation of the biomass-hydrolysing activity of recombinant enzymes suggests that this organism is highly efficient in biomass decomposition at both moderate and high temperatures. The structural information will form the basis for further studies in site-directed mutagenesis aiming the production of novel enzymes and cocktails with better hydrolytic properties to be used in biotechnological applications.

Acknowledgements: National Synchrotron Light Laboratory (LNLS, Brazil); Fundação de Amparo à Pesquisa do Estado de São Paulo (FAPESP) for the financial support via grants # 2017/16291-5 and 2014/50897-0 (JRCM) and 2016/09152-6 (LRA); São Carlos Institute of Physics/University of Sao Paulo; Conselho Nacional de Desenvolvimento Científico e Tecnológico (CNPq) for the financial support via grant # 308865/2018-9 (JRCM); and Coordenação de Aperfeiçoamento de Pessoal de Nível Superior (CAPES) for fellowship to SC and EJM.

APPLYING THE PDF METHOD IN DRUG ANALYSIS @ LCCEM: POTENTIALITIES

V. D. N. Bezzona, G. L. B. de Araújob, F. F. Ferreiraa

aCenter for Natural and Human Sciences (CCNH), UFABC, Santo André-SP, Brazil
bDepartment of Pharmacy, USP, São Paulo-SP, Brazil

The "Laboratory of Crystallography and Structural Characterization of Materials" (LCCEM) at the Federal University of ABC, Santo André-SP, Brazil, has been developing several types of analysis using X-ray powder diffraction data, which includes structure determination and quantitative phase analysis (QPA) of organic and inorganic materials. Recently, we have developed studies based on X-ray total scattering data and the pair distribution function (PDF) method allowing less ordered structures (amorphous and nanosized samples) to be properly characterized. All the improvements on materials structure characterization are feasible due the use of a high-resolution diffractometer (model STADI-P, STOE®) equipped with a Mo radiation ($K\alpha_1$) source that provides higher momentum transfer (Q_{max}) to be reached – improving considerably the spatial resolution – when compared to Cu radiation data analysis[1].

The main potentiality for PDF application at LCCEM is on drug analysis. An example of such successful PDF use is for the flubendazole active pharmaceutical ingredient. This drug was used as a model structure to compare PDF patterns obtained at LCCEM (using the STADI-P diffractometer) and at the Advanced Photon Source facility (APS beamline 6-ID-D) and the results obtained are shown in figure 1. Although the APS facility allows one to obtain data with higher counting statistics – thus providing low-noise data – as can be seen comparing the structure function $S(Q)$ patterns, the final STADI-P PDF pattern ($G(R)$) is comparable to the APS one, considering the same Q_{max} interval for the data treatment. The results allowed us to find out the intramolecular region up to 3.5 Å from the molecule distances (*i.e.*, from aromatic rings), intra *plus* intermolecular distances where interaction may occur up to 6.0 Å (*i.e.*, when using polymer matrix to load drug), and intermolecular distances beyond 6.0 Å where structural coherence is available. It is worth noting that the use of laboratory data can guide and improve ongoing studies before going to synchrotron facilities.

Finally, LCCEM is able to offer several categories of X-ray powder diffraction analysis – from room temperature up to 1000 ºC – using different methods like Rietveld, PDF and direct methods. In this way, various kinds of researches can be performed.

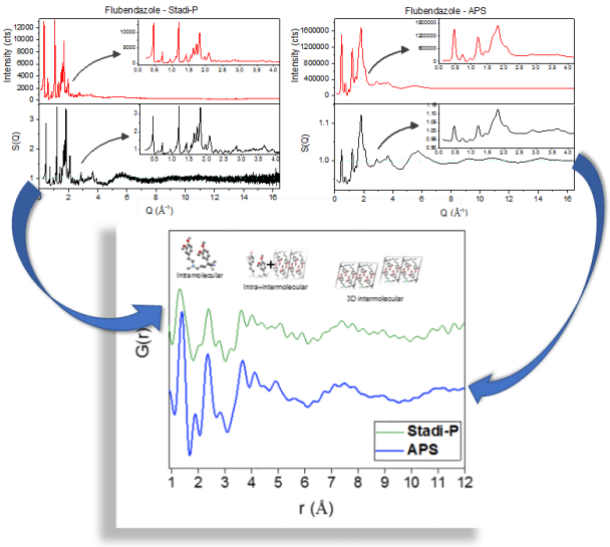

Figure 1: Comparison between LCCEM and APS results.

[1] Dykhne T, Taylor R, Florence A, Billinge SL. *Pharmaceutical Research*, **28**, pp 1041-1048 (2011).

Acknowledgments: Fundação de Amparo à Pesquisa do Estado de SP (FAPESP; proc. n. 11990-5/2018), CNPq (307664/2015-5).

Síntese e estrutura cristalina de dois novos complexos heterolépticos de níquel(II) com 1,1′-bis(difenilfosfino)ferroceno e ditiocarbimatos

R. A. C. Souza[a], S. Guilardi[a], A. E. C. Vidigal[b], M. M. M. Rubinger[b], M. R. L. Oliveira[b], J. A. Ellena[c]

[a]*Instituto de Química, Universidade Federal de Uberlândia, Uberlândia, Brasil.*
[b]*Departamento de Química, Universidade Federal de Viçosa, Viçosa, Brasil.*
[c]*Instituto de Física de São Carlos, Universidade de São Paulo, São Carlos, Brasil.*

Complexos metálicos com ditiocarbamatos ($R_2NCS_2^{-1}$) são empregados no controle de ampla gama de doenças fúngicas em muitas culturas economicamente importantes[1] e na indústria como aceleradores de vulcanização da borracha[2]. Complexos com ditiocarbimatos são estruturalmente semelhantes ($RN=CS_2^{-2}$), porém menos estudados. A literatura reporta a síntese de complexos heterolépticos de Ni(II), Pd(II) e Pt(II) com *N*-R-sulfonylditiocarbimatos e fosfinas[3,4]. Complexos de níquel(II) com 1,1'-bis(difenilfosfino)ferroceno (dppf) e 4-$XC_6H_4SO_2N=CS_2^{2-}$ (X = Cl; Br; Me) foram descritos na literatura[5]. Este trabalho descreve a síntese e estrutura cristalina de dois novos complexos com ditiocarbimatos e dppf (Esquema 1).

Esquema 1. Síntese dos complexos de níquel(II) com *N*-R-sulfonilditiocarbimatos e dppf.

Os complexos **a** e **b** são estáveis a temperatura ambiente e foram caracterizados por espectroscopia no infravermelho e difração de Raios X (Fig. 1).

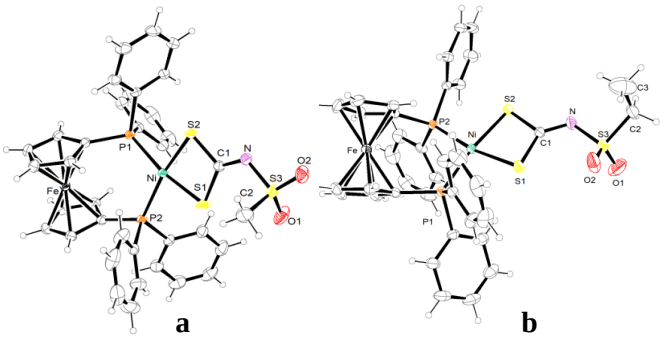

Nos espectros vibracionais de **a** e **b** a banda de νC=N (1433 cm^{-1}) está deslocada para maiores números de onda em relação aos espectros dos ligantes livres (1300 cm^{-1}), enquanto a banda de estiramento do grupo CS_2 (933 cm^{-1}) tem deslocamento oposto (ligantes livres: 960 cm^{-1}) indicando a complexação do Ni(II) pelos átomos de enxofre. O aparecimento da banda νNi-S em torno de 378 cm^{-1} confirma a complexação do ditiocarbimato pelos dois átomos de enxofre nos dois complexos. Monocristais apropriados de **a** e **b** foram obtidos por recristalização lenta em diclorometano/etanol (1:1 v/v) acrescidos de uma gota de água. As intensidades dos feixes de raios X difratados foram coletadas em um difratômetro Bruker APEX II, usando radiação MoKα (0,71073 Å) a temperatura ambiente. O composto **a** cristaliza no sistema monoclínico ($P2_1/c$) e **b** no sistema triclínico ($P\bar{1}$). Em **a** e **b**, o átomo de Ni é coordenado por dois átomos de enxofre do ditiocarbimato e por dois átomos de fósforo de dppf, em uma geometria quadrada plana distorcida. O ângulo S-Ni-S é consideravelmente menor que 90° devido ao ligante bidentado *N*-R-sulfonilditiocarbimato. Os ângulos P-Ni-S são maiores que 90º e o ângulo P-Ni-P apresentam uma distorção ainda maior. As ligações C-S e C-N possuem caráter intermediário entre ligações duplas e simples devido à deslocalização dos elétrons no fragmento S_2CN. Os empacotamentos cristalinos são estabilizados por interações intermoleculares do tipo C-H···O, C-H···S (composto **a**) e C-H···π. Interações intramoleculares do tipo C-H···S também estão presentes no cristal do composto **a**.

[1]Gullino, M. L. *et al. Plant Disease*, **94** (9), 1076-1087 (2010).
[2]Costa, H. M. *et al*. *Polímeros: Ciência e Tecnologia*, **13** (2), 125-129 (2003).
[3]Oliveira, M. R. L. *et al. Inorganica Chimica Acta*, **376**, 238- 244 (2011).
[4] Singh, S. K. *et al. Inorganica Chimica Acta*, **384**, 176–183 (2012).
[5] Singh, S.K. *et al*. *Journal of Organometallic Chemistry*, **190**, 745-746 (2013).

Agradecimentos: Rede Mineira de Química; FAPEMIG; CAPES; CNPq.

Painéis

Biologia Estrutural

Structural and biochemical studies of a cellulosomal thermophilic family 3 β-glucosidase, CtBgl3B from *Clostridium thermocellum*

L. R. Almeida[a], W. Garcia[b] , J. R. C. Muniz[a].

[a]*São Carlos Institute of Physics, University of São Paulo, São Carlos, Brazil.*
[b]*Federal University of ABC, Center for Natural and Human Sciences, Santo André, SP, Brazil.*

The reduction of petroleum reserves, the growing energy demand from emerging countries, and the eminent necessity for reducing carbon dioxide emissions indicate the importance of the pursuit of new sources of renewable energy[1,2]. Thus, the bioethanol production through hydrolysis of lignocellulosic biomass, such as sugarcane bagasse, has received considerable attention[1,2]. Due to its potential for development and cost reduction, the enzymatic hydrolysis of cellulose using cellulases can be a key factor for the production of second-generation bioethanol at a competitive cost in the long term[3]. Some thermophilic bacteria, such as *Clostridium thermocellum*, produces an extracellular multi-enzyme protein complex named cellulosome, which has been demonstrating a high ability to efficiently perform cellulosic biomass degradation, especially in the crystalline portion of cellulose[4]. Thereby, cellulase mixtures are commonly used for the saccharification of cellulose in biotechnological applications. The β-glucosidases (BGls, EC 3.2.1.21), which hydrolyzes the β-linkage between two adjacent molecules in dimers and short oligomers of glucose, it has been shown that enhanced levels of BGls in cellulase mixtures may benefit the conversion of cellulose to glucose[5].

Aiming to characterize cellulosomal BGls from *C. thermocellum*, from different families of glycoside hydrolases (GHs) by structural, biochemical and biophysical techniques herein we describe the CtBgl3B. The cloned CtBgl3B gene had protein expressed in *Escherichia coli* (BL21) and has been successfully purified following affinity chromatography and molecular mass separation. The purified enzyme has a thermophilic characteristic, showing high activity at a temperature above 60 °C at pH 4.5-7.0. Higher activity at pH 5.5 and 70 °C. Interestingly, it has a melting temperature (Tm) of ≈70 °C, determined by differential scanning fluorimetry (DSF) and circular dichroism (CD). In addition, its enzymatic activity was evaluated with the following parameters: Michaelis-Menten constant Km = 0.45 (mM), catalytic constant k_{cat} = 201 (s^{-1}), and catalytic efficiency k_{cat}/Km = 444 (mM^{-1} s^{-1}).

The structure of CtBgl3B was determined by X-ray diffraction (2.34 Å resolution in $P2_12_12_1$; a=63.84, b=148.06, c=198.64 Å) using molecular replacement, demonstrating a dimeric arrangement in the asymmetric unit, indicators of refinement quality R_{work} and R_{free}, respectively 0.21 and 0.24. The structure has three-domain architecture as observed previously for other glycoside hydrolase family 3 Bgls, and in addition, a fourth domain of unknown function at C-terminal that interact with the partner monomer interfacing near to the catalytic cleft. Multi-angle light scattering (MALS) and small-angle X-ray scattering (SAXS) experiments corroborate that CtBgl3B in solution also adopts dimeric arrangement.

[1] Serrano-Ruiz, J. C. *Advanced Biofuels: Using Catalytic Routes for the Conversion of Biomass Platform Molecules*. (Apple Academic Press, 2015).

[2] Liu, J. *et al.* Systems integration for global sustainability. *Science.* **347**, 963 (2015).

[3] Bornscheuer, U., Buchholz, K. & Seibel, J. Enzymatic degradation of (ligno)cellulose. *Angew. Chem. Int. Ed. Engl.* **53**, 10876–93 (2014).

[4] Prawitwong, P. *et al.* Direct glucose production from lignocellulose using Clostridium thermocellum cultures supplemented with a thermostable [beta]-glucosidase. *Biotechnol. Biofuels* **6**, 184 (2013).

[5] Kahn, A., Galanopoulou, A. P., Hatzinikolaou, D. G., Moraïs, S. & Bayer, E. A. Evaluation of Thermal Stability of Cellulosomal Hydrolases and Their Complex Formation. in *Cellulases: Methods and Protocols* (ed. Lübeck, M.) 153–166 (Springer New York, 2018).

Acknowlegments: São Paulo Research Foundation - FAPESP.

The role of *Trypanosoma brucei* ribonuclease RRP44 in ribosomal RNA processing

Cesaro, G.[a,b], Carneiro, F.R.G.[a], Legrand, P.[c], Zanchin, N.I.T.[a], Guimarães, B.G.[a,b].

[a] *Instituto Carlos Chagas, FIOCRUZ/PR, Curitiba, Brazil.*

[b] *Programa de Pós-graduação em Ciências-Bioquímica, UFPR, Curitiba, Brazil.*

[c] *Synchrotron SOLEIL, Saint-Aubin, France.*

Parasitic trypanosomatids, such *Trypanosoma brucei*, *T. cruzi* and *Leishmania sp.* present unique features compared with other eukaryotes with regard to RNA processing and maturation. For instance, *T. brucei* ribosomes contain specific rRNA expansions and the 60S subunit is composed of eight rRNAs molecules instead of the three rRNAs found in most eukaryotes. The role of specific endo- and exonucleases in the maturation of the unusual rRNA precursor of trypanosomatids remains largely unknown. One of the nucleases involved in rRNA processing is Rrp44, an exosome associated ribonuclease in yeast, which is involved in several metabolic RNA pathways. Here we investigate functional and structural aspects of the *T. brucei* ribonuclease RRP44. Recombinant full-length and truncated forms of TbRRP44 were produced for crystallization. *T. brucei* knockdown cells were generated using RNA interference (RNAi) to perform phenotypic characterization. Analysis of pre-ribosomal RNA processing were performed by qRT-PCR and Northern blot. Proliferation curves of knockdown cells confirmed that TbRRP44 is essential for the parasite viability. TbRRP44 depletion causes accumulation of the complete LSU rRNA precursor, in addition to 5.8S maturation impairment. The crystal structure of TbRRP44 endonucleolytic PIN domain was refined at 2.3 Å resolution. Structural comparison with *Saccharomyces cerevisiae* Rrp44 revealed differences which could provide molecular bases for the lack of interaction of RRP44 with the exosome complex in *T. brucei*. A TbRRP44 construction including the exonucleolytic RNB domain was also crystallized. Crystals diffract to 3.1 Å resolution and the structure was determined by molecular replacement. Structural analysis reveals that the exonucleolytic active site is conserved when compared with *S. cerevisiae* Rrp44. In conclusion, we have shown that TbRRP44 is essential for cell viability and correct LSU rRNA maturation. The crystal structure of the TbRRP44 endonucleolytic domain revealed key differences relative to the yeast homologue.

Acknowlegments: CNPq, CAPES, COFECUB, FIOCRUZ, Synchrotron SOLEIL.

Expression of methyltransferases hTrm9L and Trm112 from *Homo sapiens* for future structure solution

R. F. Penteado[a], J. Iulek[a].

[a]*Departamento de Química, Universidade Estadual de Ponta Grossa, Ponta Grossa - PR, Brazil.*

Transporter RNA (tRNA) takes part on the fundamental process of protein synthesis. Its function is to transport aminoacids that will be used during protein synthesis in the ribosome. For this task to be accomplished correctly, many tRNA molecules need chemical modifications, like some nucleoside methylation, to assure their correct folding and its correct decodification[1]. The methylation process is performed by enzymes called methyltransferases (Trm) and uses S-adenosyl-methionine (SAM or AdoMet) as a methyl group donor[2]. The complex Trm9/Trm112 (in which Trm9 is the *de facto* methyltransferase and Trm112 is an auxiliary subunity) is conserved in eukaryotes and Trm9 presents two ortologues in humans, namely, ABH8 e hTrm9L. This work aims at expressing human hTrm9L and Trm112 heterologously for future structure solution.

Escherichia coli BL21(DE3) cells were transformed by electroporation with plasmids pET21b(+) that harbored the coding genes of which subunit. Cells that were effectively transformed were selected by growth in media supplemented with ampicillin. Subsequently, transformed cells were propagated in 5 mL of liquid medium ZYP-5052 (with a composition to specifically express the proteins through self induction)[3] at 37 °C for 22 h. Media were centrifuged and cells were promptly resuspended in lysis buffer (20 mM Tris-HCl, 200 mM NaCl, pH = 7.5); they were sonicated for 5 min. The resulting suspension was centrifuged to separate the cell debris. Samples from total lysis fraction and of the soluble and insoluble fractions were taken for analysis by SDS-PAGE. A Ni^{2+} affinity chromatography of the total lysed fraction was also accomplished. The SDS-PAGE results from expression tests of the Trm112 protein indicated an intense band in the expected position for molecular mass of circa 14 kDa (theoretical mass 14,199 kDa), nevertheless, in the lane that corresponds to the insoluble fraction. Yet, in the SDS-PAGE experiments for subunit hTrm9L, no bands were observed that could be attributed to this enzyme.

We concluded that enzyme hTrm112 is satisfactorily expressed in self induction media and can be purified by means of affinity chromatography. Nevertheless, new tests must be accomplished to stabilize it in solution. Concerning hTrm9L, new cell transformation experiments must be accomplished. Once both proteins are satisfactorily produced, the next step is to solve their structure, either by x-ray crystallography or CryoEM.

[1] Létoquart, J.; van Tran, N.; Caroline, V.; Aleksandrov, A.; Lazar, N, van Tilbeurgh, H.; Liger, D.; Graille, M. Nucleic Acids Research, **43**, 10989-11002, (2015).
[2] Schubert, H. L.; Blumenthal, R. M.; Cheng, X. Trends in Biochemical Sciences, **28**, 329-335, (2003).
[3] Studier, F. W. Protein Expression and Purification, **41**, 207–234, (2005).

Acknowlegments: CAPES, Fundação Araucária.

The urokinase plasminogen activator binding to its receptor: a quantum biochemistry description within an in/homogeneous dielectric function framework with application to uPA-uPAR peptide inhibitors

P. A. Morais[a,c], F. F. Maia Jr.[b], C. Solis-Calero[c], E. W. S. Caetano[d], V. N. Freire[e], H. F. Carvalho[c]

[a]*Instituto Federal de Educação, Ciência e Tecnologia do Ceará, Campus Horizonte, Horizonte, CE, Brasil.*

[b]*Departamento de Ciências Naturais, Matemática e Estatística, Universidade Federal Rural do Semi-Árido, Mossoró, RN, Brasil.*

[c]*Departamento de Biologia Estrutural e Funcional, Instituto de Biologia, Universidade Estadual de Campinas, Campinas, SP, Brasil.*

[d]*Instituto Federal de Educação, Ciência e Tecnologia do Ceará, Fortaleza, CE, Brasil.*

[e]*Departamento de Física, Universidade Federal do Ceará, Fortaleza, CE, Brasil.*

Despite being recognized as a therapeutic target in the processes of cancer cell proliferation and metastasis for over 50 years, the interaction of the urokinase plasminogen activator uPA with its receptor uPAR still needs an improved understanding. High resolution crystallographic data (PDB 2FD6) of the uPA-UPAR binding geometry was used to perform quantum biochemistry computations within the density functional theory (DFT) framework. A divide to conquer methodology considering a mixed homogeneous/inhomogeneous dielectric model and explicitly taking water molecules into account was employed to obtain a large set of uPA-uPAR residue-residue interaction energies. In order of importance, not only were Phe25 > Tyr24 > Trp30 > Ile28 shown to be the most relevant uPA residues binding it to uPAR, but the residues Lys98 > His87 > Gln40 > Asn22 > Lys23 > Val20 also had significant interaction energies, which helps to explain published experimental mutational data. Furthermore, the results obtained with the uPA-uPAR in/homogeneous dielectric function show that a high dielectric constant value $\varepsilon = 40$ is adequate to take into account the electrostatic environment at the interface between the proteins, while using a smaller value of ε (< 10) leads to an overestimation of the uPA-uPAR binding energy. Hot spots of the uPA-uPAR binding domain were identified and enhanced quantum biochemistry based descriptions of both a linear uPA_{21-30} and a cyclic polypeptide $cyclo^{21,29}uPA_{21-29}$[(S21C;H29C)] uPAR-blockers were performed, demonstrating that cyclization improves the stability of mimetic peptides without compromising their binding energies to uPAR.

Acknowlegments: CNPq (465699/2014-6), CAPES and FAPESP (2009/16150-6; 2014/50938-8).

Structural biology of enzymes involved in the (S)-4-amino-2- hydroxybutyrate (AHBA) biosynthesis from the aminoglycoside butirosin

L.A. Rivas[a]; F. C. Rodrigues de Paiva[a]; F. Huang[b]; P. Leadlay[b]; M. V.B. Dias[ac]
[a]*Institute of Biomedical Sciences ICB II, University of São Paulo, São Paulo, Brazil.*
[b]*Department of Biochemistry, University of Cambridge, Cambridge, United Kingdom.*
[c]*Department of Chemistry, University of Warwick, Coventry, United Kingdom.*

Natural products obtained from secondary metabolism of bacteria, plants and fungi represent an important source of antimicrobial agents for the treatment of diverse illness, such as infections. One of these agents is the aminoglycosides, molecules that have precursors from the glycolytic pathway in bacteria, as butirosin, which is produced by *Bacillus circulans*. One of its particularities is the presence of an (S)-4-amino-2- hydroxybutyrate (AHBA) attached to the 2-deoxystreptamine (2-DOS) aglycone ring. The presence of AHBA in butirosin makes this antibiotic less susceptible to bacterial resistance mechanisms through aminoglycosides modifying enzymes. However, the biosynthesis of the AHBA group in the butirosin pathway is not sufficiently understood, although it is known the participation of six enzymes in its biosynthesis whose structures have not been extensively studied. Herein, we aim to perform a structural analysis of three of these enzymes: BtrJ in charge of the addition of molecules of L-glutamate; BtrK which participates catalyzing a decarboxylation reaction of glutamate; and BtrH which participates of the final steps transferring the AHBAs group from an acyl carrier protein to a ribostamycin molecule. Genes *btrJ, btrK* e *btrH* were cloned in pET28a plasmid vector. BL21(DE3) or Rosetta competent cells were used for transformation and expression of the protein. Ni^{2+}NTA affinity and size-exclusion chromatography were performed to purify the proteins and subsequent protein crystallography experiments were performed by sitting drop and hanging drop. Crystal X-ray diffraction data collection was performed at Synchrotron Light Source DESy (PETRA III, Germany) or LNLS (Campinas). Data for BtrK crystals have been obtained at a resolution of about 1,4 Å in the space group P21212. The crystallographic refinement was carried out by the CCP4i software package. BtrK is a two-domain protein, one of them with a TIM barrel folding which comprises of the PLP active site and possibly, the region that interacts with other substrates (*Figure 1*). Comparing to other decarboxylases, the active site is conserved and includes the Schiff base between the catalytic lysine (K49) and the PLP coenzyme. The general electrostatic surface is slightly negative while the PLP pocket is positively charged and mainly hydrophobic. BtrK homodimer structure (functional state of the protein) was obtained through symmetry operations in COOT. Homodimer pocket showed to be mainly electronegative. BtrJ was successfully purified and crystallization assays were developed obtaining crystals with different morphologies; how ever, it was no possible to collect any image after x-ray diffraction. BtrH enzymes experiments are still in progress. Further experiments are proposed to co-crystallize these enzymes with some ligants to see structural changes and elucidate functional features.

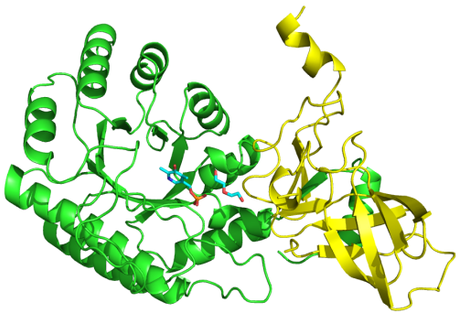

Figure 1. Two domain structure of BtrK protein. TIM barrel domain is identified in green and β-sandwich domain in yellow. PLP active site is represented in stick model.

Acknowlegments: FAPESP, CAPES, CPNq

In silico approaches for structural determination of a *Trypanosoma cruzi* Nitroreductase

P. H. Luccas[a], M. L. Cirqueira[a], M. A. A. Aleixo[a], M. C. Nonato[a].

[a]*Department of Physics and Chemistry, FCFRP-USP, Ribeirão Preto, Brazil.*

Chagas disease affetcs about 8 million people worldwide, causing death of 7 thousand people/year. Initially, the disease was restricted to low income population, on emergent countries, as in South America. But, due to globalization, the infectant protozoan, *Trypanosoma cruzi*, has spread to developed countries, such USA, where is more than 300 thousand cases estimated. The transmition may be mediated by the blood-sucking bug "kissing bug", or by oral transmition. Benznidazole is capable of treat Chagas disease, but it is very toxic and ineffective. Benznidazole is a prodrug activated by action of a nitroreductase [1], which catalyses the reduction of benznidazole to high nucleophylic metabolites, attacking membranes, proteins and DNA. Despite the drug use since 1970s, its mechanism of action is still unclear. Aiming to develop new drugs nitroredutase targeted, this study is directed to TcNTR (Nitroreductase) structure characterization, and its mechanism of action. This enzyme has an unknown structure, and hasn't been crystallized yet. *In silico* approaches could provide some informations about the ollygomeric state, residues of interaction with cofactor, and also about its catalytic mechanism.

Kinetic studies were performed with heterologous TcNTR_72 expressed by *E. coli* Rosetta, purified by affinity chromatography, using Ni-NTA resin. Kinetics assays were performed measuring the NADH consumption by fluorescence, in presence of benznidazole. *In silico* studies were required to explain unexpected kinetic profile. Were run the predictors SwissModel, PsiPred, Phobius, TMHMM.

Kinetic assays with benznidazole showed un undescribed sigmoidal character for TcNTR. Since the appearence of the sigmoidal profile, such as autoinhibition of TcNTR on high substrate concentrations, we investigated the possibility of a dimeric organization, not reported. Through the correlation between different predictors and comparission with bacterial nitroreductases, we were able to propose a new model to TcNTR.

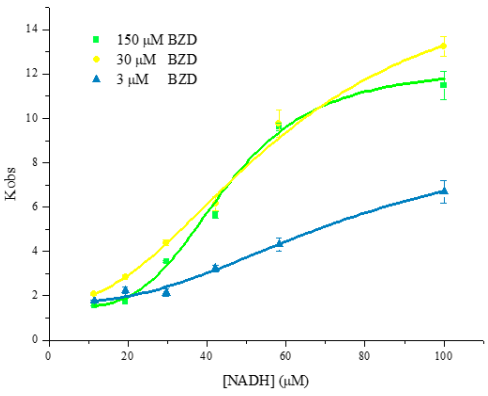

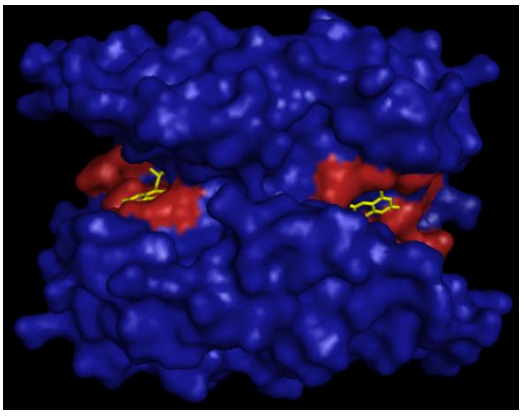

Figure 1a (Left): Enzymatic kinetic assays, of TcNTR_72, showing cooperativity between subunits. BZD at a constant concentration, varying NADH concentration (µM). Figure 1b (Right): Modelo of TcNTR_72 dimer, based on TtNADH Oxidase (Thermus thermophilus), the enzyme with greater structural identity, of 30%.

[1] Hall, B. S., Meredith, et al. Targeting the Substrate Preference of a Type I Nitroreductase To Develop Antitrypanosomal Quinone-Based Prodrugs. *Antimicrobial Agents and Chemotherapy*. **Vol. 56**, 5821-5830 (2012).

Acknowledgements: FAPESP.

Functional and structural characterisation of an α-L-arabinofuranosidase from *Thielavia terrestris*. The first β-propeller fold adopted through an exquisite domain-swapping in GH62 family

S. Camargo[a], E. J. Mulinari[a], L. R. de Almeida[a], M. V. Zerbini[a], A. Bernardes[a], F. Segato[b], and J. R. C. Muniz[a]

[a]São Carlos Institute of Physics (IFSC), University of Sao Paulo (USP), Sao Carlos, Brazil.
[b]Engineering School of Lorena, University of São Paulo (USP), Lorena, SP, Brazil.

Genome analyses and experimental data suggested that thermostable enzymes may afford economic advantages in the production of many biotechnological products based on biomass degradation. The fungus *Thielavia terrestris* plays an important role in the global carbon cycle with enzymes highly capable of hydrolysing all major polysaccharides found in biomass, making it an attractive candidate for industrial applications and bioremediation. From prospection to three-dimensional structures, we foster a deeper understanding of the hydrolysis of vegetal biomass and pollutants, applying modern scientific approaches in macromolecular crystallography associated with biophysical and biochemical studies. In this research, we have characterized *Tt*GH62 biochemically and structurally to understand its mechanism and optimal conditions of action. Additionally, the enzyme described here has a structural novelty unusual from all structures that have been reported so far for the GH62 family, an exquisite domain swapping phenomena, located at the supramolecular arrangement due to the presence of a disulphide bond (Cys32 and Cys300) connecting the monomers. The active site is a perfect combination of catalytic residues of both subunits. Similarly, the structure has a calcium-binding site, shared by the dimer-dimer contact interface. All of the crystallographic behaviours go against solution monomeric state, which indicates a crystallographic artefact produces by crystal condition. Nevertheless, the nature of this unusual crystallographic structure brings speculation about inactivation and storage mechanism of high protein concentration producing a compact assembly with additional stabilizing contacts between chains. The *Tt*GH62 was also characterised in synthetic (pNPAraf) and polymeric substrate (arabinan and arabinoxylan), revealing optimum temperature and pH (for pNPAraf) of 30 °C and 4.5-5.0, respectively. Characterisation of the biomass-hydrolysing activity of recombinant enzymes suggests that this organism is highly efficient in biomass decomposition at both moderate and high temperatures. The structural information will form the basis for further studies in site-directed mutagenesis aiming the production of novel enzymes and cocktails with better hydrolytic properties to be used in biotechnological applications.

Acknowledgements: National Synchrotron Light Laboratory (LNLS, Brazil); Fundação de Amparo à Pesquisa do Estado de São Paulo (FAPESP) for the financial support via grants # 2017/16291-5 and 2014/50897-0 (JRCM) and 2016/09152-6 (LRA); São Carlos Institute of Physics/University of Sao Paulo; Conselho Nacional de Desenvolvimento Científico e Tecnológico (CNPq) for the financial support via grant # 308865/2018-9 (JRCM); and Coordenação de Aperfeiçoamento de Pessoal de Nível Superior (CAPES) for fellowship to SC and EJM.

Nova abordagem no desenvolvimento de antimicrobianos: caracterização estrutural da via biossintética da vitamina B6

A. L. C. Barra[a], A. S. Nascimento[a].

[a]*Instituto de Física de São Carlos, Universdade de São Carlos, São Carlos, Brasil.*

Doenças infecciosas são uma ameaça a humanidade e é crescente o número de infecções por patógenos multirresistentes. *Plasmodium* sp. está entre os principais patógenos que apresentam resistência a vários antimicrobianos, dificultando o tratamento da doença (malária). Segundo a Organização Mundial de Saúde, a malária é responsável por cerca de 2 milhões de mortes/ano sendo que 40% dos casos são devido ao *Plasmodium vivax* [1]. Assim sendo, há uma urgente necessidade de se descobrir novas classes de alvos terapêuticos para o desenvolvimento de antimicrobianos.

Piridoxal fosfato (PLP), forma ativa da vitamina B6, é um cofator essencial para diversas enzimas, tanto de procariotos quanto eucariotos. Grande parte destas estão associadas a vias bioquímicas de amino compostos, como aminoácidos [2]. A síntese *de novo* de PLP está presente em alguns patógenos, mas é ausente em mamíferos, o que torna as enzimas dessa via alvos ideais para o desenvolvimento de novos antimicrobianos. Duas enzimas são responsáveis pela síntese: Pdx1 e Pdx2 que formam um complexo multimérico. Quando o complexo é formado, a enzima Pdx2 transforma glutamina em glutamato liberando uma molécula de amônia (NH_3) para Pdx1, que juntamente com ribose-5-fosfato (R5P) e gliceraldeído-3-fosfato (G3P), sintetiza o piridoxal-5-fosfato (PLP) [3].

Diante disso, o objetivo desse trabalho é caracterizar estruturalmente o complexo Pdx1/Pdx2 assim como as enzimas isoladas de *P. vivax*. Para isso, as proteínas foram expressas em *E. coli Rosetta* (DE3) e purificadas por cromatografia de afinidade a níquel. Em seguida, as proteínas recombinantes foram clivadas com a protease *Tobacco Etch Virus* (TEV) para a remoção da tag e submetidas a uma cromatografia de exclusão molecular.

A enzima PvPdx2 foi bem expressa e purificada com sucesso, no entanto, PvPdx1 apresentou problemas de expressão. Deste modo, foi realizada uma triagem de expressão com diferentes cepas de *E. coli* e foram obtidos resultados promissores. A validação destes resultados está em andamento assim como as triagens de cristalização de PvPdx2. Com ambas proteínas purificadas será possível realizar estudos cristalográficos e biofísicos do complexo enzimático PvPdx1/PvPdx2.

[1] Price, R. N., Tjitra, E. et al, Vivax Malaria: Neglected and Not Benign, *American Journal of Tropical Medicine and Hygiene*, **v. 77**, 79-87 (2007).

[2] Percudani, R., Peracchi, A., A genomic overview of pyridoxal-phosphate-dependent enzymes, *EMBO reports*, **v. 4**, 850-854 (2003).

[3] Müller, I. B. et al. The assembly of the plasmodial PLP synthase complex follows a defined course. *PLoS ONE*, **v. 3**, 1-9 (2008).

Agradecimentos: Fundação de Amparo à Pesquisa do Estado de São Paulo (FAPESP), Instituto de Física de São Carlos (IFSC), USP.

Dynamics and structure refinement of a two-domain protein using MD and SAXS

Maximilia F. de Souza[a], Roberto K. Salinas[b], Phelipe A. M. Vitale[b], Martin Zacharias[c] and Cristiano L. P. Oliveira[a]

[a] *Institute of Physics University of São Paulo, Brazil*
[b] *Institute of Chemistry, University of São Paulo, Brazi*
[c] *Technical University of Munich, Germany*

Small-angle scattering (SAS) of X-rays (SAXS) [1] has proven to be a powerful tool to study structure and dynamics of multi-domain proteins and protein complexes aided by complimentary techniques to increment the resolution information [2]. SAXS allows the determination of the overall shape and shape changes of biological macromolecules in solution, as well as the investigation of macromolecules stability over time, and the degree of monodispersity. In recent years considerable effort has been devoted to explore the synergy between SAXS and other biophysical strategies in order to better characterize multi-domain proteins and protein complexes [3]. The application of SAXS as a tool for the characterization of structure and dynamics of a two-domain protein, CBD12, will be presented. The *Drosophila* Na^+/Ca^{2+} exchanger (CALX) is a membrane protein that catalyzes the exchange of Na^+ and Ca^{2+} across the lipid bilayer. Regulation of the CALX transport function requires the binding of Ca^{2+} to a sensor domain, CBD12, located a large intracellular loop of the exchanger (Figure 1). CBD12 consists of two domains, CBD1 and CBD2, connected by a short linker. The literature indicates that Ca^{2+}-binding to CBD1 modulates the dynamics between CBD1 and CBD2, which is key to understand the mechanism behind the exchanger regulation [3]. We will present SAXS experiments carried out in the CBD12 presence and absence of calcium that made possible the observation of changes in protein flexibility in solution (Figure 1), as well as the analysis using molecular dynamics (MD) to describe for the first time the dynamic of CBD12 in bound of Ca^{2+} and free states up to 3.4μs that allowed to get insights and differences of the dynamics of protein in the bound and free form. Besides that, Ensemble Optimization Method (EOM) [5] was applied using an external pool generated from MD simulations - 15000 models from 0.4-3.3 μseconds demonstrating a quite good fit for the experimental data and with a larger population in the unbound state.

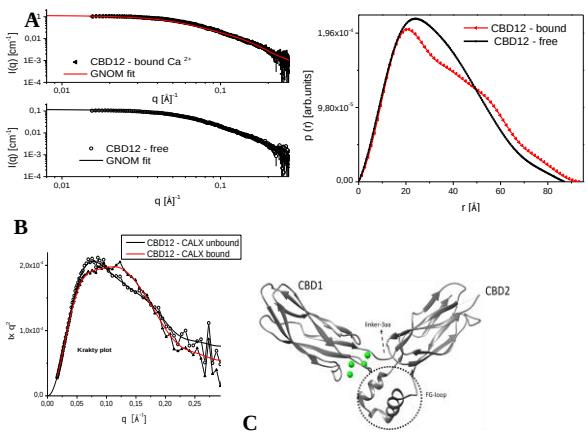

Figure 1. (A) SAXS curves of CBD12-apo and Ca^{2+}-bound, symbols are the experimental data and theoretical fittings are described as lines (B) Kratky plot of SAXS curves from CBD12-apo and Ca^{2+}-bound states. (C) Crystal structures of the CBD12 Ca^{2+}-sensor domain in the bound state (PDB 3RB5) [5]

References

[1] T. Madl, F. Gabel, M. Sattler, *J. Struct. Biol*, 173, 472–482, 2011
[2] C. Dominguez *et al*, *J. Am. Chem. Soc.*, 2013,125, 1731-1737, 2013.
[3] L. A. Abiko *et al*. *Proteins*,84,580-590, 2016.
[5] Wu et al. *Structure*, 19, 1509-1517, 2011.
[6] Bernado, P., Svergun, D.I., et.al,. *J. Am. Chem. Soc.* 129(17), 5656-5664, 2007.

Acknowlegments: This work was supported by CAPES, CNPq and FAPESP.

CTLA-4/ipilimumab binding therapy: quantum biochemistry computations for the development of peptide mimetics and small molecules in cancer immunology

J. L. Amaral[a], P. A. Morais[b,c], F. F. Maia Jr. [d], R. F. Costa[d] , E. M. Bezerra [d], H. F. Carvalho [c] , E. W. S. Caetano [e], G. Zanatta [f] , V. N. Freire [f].

[a]*Depto Bioquímica e Biologia Molecular, Universidade Federal do Ceará, Fortaleza-CE, Brazil.*

[b]*Instituto Federal de Educação, Ciência e Tecnologia do Ceará, Horizonte, CE, Brazil*

[c]*Depto of Structural and Functional Biology, UNICAMP, 13083-863 Campinas, SP, Brazil.*

[d]*Center of Exact and Natural Sciences, Universidade Federal Rural do Semi-Árido, Mossoró-RN, Brazil*

[e] *Instituto Federal de Educação, Ciência e Tecnologia do Ceará, Fortaleza, CE, Brazil.*

[f] *Department of Physics, Universidade Federal do Ceará, Fortaleza-CE, Brazil.*

Over the past decade, several immunotherapeutic agents have become available for the routine clinical management of cancer [1]. To date, several immune checkpoints have been identified and explored as potential therapeutic targets in oncology. Two inhibitory immune checkpoint receptors were intensively studied in the context of clinical cancer immunotherapy: cytotoxic T-lymphocyte-associated antigen 4 (CTLA-4) and programmed cell death protein 1 (PD-1). Remarkable results have led to the regulatory approval of several monoclonal antibodies targeting CTLA-4 or PD-1 receptors. They include ipilimumab (Yervoy; Bristol-Myers Squibb), pembrolizumab (Keytruda; Merck), nivolumab (Opdivo; Bristol-Myers Squibb), and atezolizumab (Tecentriq; Genentech-Roche). On the other hand, small-molecule immune-oncology-based treatments as well as peptides mimetic are being proposed and are supposed to emerge as new types of immunotherapies to modulate immune checkpoint receptors. These new potential immunotherapies present economic advantages, constituting a cost-effective alternative, as stated by Acúrcio et al. [2]. Recently, the inhibition of the checkpoint protein PD-1 by the therapeutic antibody pembrolizumab was outlined by quantum chemistry [3]. By employing quantum chemistry methods based on the Density Functional Theory (DFT), Tavares et al. [3] have investigated in silico the binding energy features of the receptor PD-1 in complex with its drug inhibitor. Their computational results gave a better understanding of the binding mechanisms, being also an efficient alternative towards the development of antibody-based drugs, pointing to hot spots for new treatments in cancer therapy. Based on techniques our group has developed previously [4,5], in this work we present results on the CTLA-4/ipilimumab binding therapy by performing quantum biochemistry computations for the development of peptide mimetics and small molecules in cancer immunology. By performing DFT calculations to describe the interaction between the CTLA-4 antigen and the antibody ipilimumab within a divide to conquer methodology and a nonhomogeneous dielectric function description, we: (1) unveil the hot spots (i.e. the most significative residues) of the CTLA-4/ ipilimumab contributing to their binding; (2) suggest peptides and small molecules that are supposed to block the CTLA-4/ipilimumab interaction effectively, being candidates as drug leads to lower the price of the CTLA-4/ipilimumab-based cancer immunology treatment in the case of associated susceptible patients; (3) point to the possible use of cryo-microscopy to study static and dynamic structural aspects of antigens, antibodies, as well as their binding to mimetic peptides and small molecules [6] which are intended as low cost drugs to be used in the immunology-based cancer treatment.

[1] L. Galluzzi et al, Sci. Transl. Med. 10, eaat7807 (2018);
[2] R.C. Acúrcio, J. Med. Chem. 2018, DOI:10.1021/acs.jmedchem.8b00541;
[3] A. B. M. L. A. Tavares et al, Sci. Rep. (2018) 8:1840;
[4] Solis-Calero et al, Phys. Chem. Chem. Phys. ,2018, 20, 22818;
[5] A. C. V. Martins et al, New. J. Chem. (2017), DOI: 10.1039/c6nj03939a;
[6] Fernandez-Leiro and Scheres, Nature 537, 339 (2016).

Acknowlegments: CNPq e CAPES.

Cristalografia de Pequenas Moléculas

A Case of Coordination Polymer Polimorphism

Pedro Miguel A. F. de Paula, Heitor A. de Abreu, Renata Diniz.

Departamento de Química, UFMG, Belo Horizonte, Brasil.

The structure of a coordination polymer (CP) contains metal ions, which are linked by coordinated organic molecules in a crystalline array. A structure linked by coordination bonds in one direction and by other kinds of intermolecular interactions (e.g. hydrogen bonds) in two directions is a 1D CP. The same logic is applied to define 2D and 3D CP [1]. This work's objective was to synthesize CPs using 4,4'-diamino-2,2'-stilbenedisulfonic acid (DAS) and 4,4'-bipyridine (bipy) as ligands and Zn (II) as metal ion.

Two polymorphs were obtained through different experimental methods: hydrothermal (solid 1) and conventional (solid 2) syntheses. The crystals were measured using molybdenum wavelength and the structures refined with SHELXL[2]. Solid 1 crystallized in Pbca orthorhombic space group, while solid 2 crystallized in P -1 triclinic space group. Both solids show a 1D polymeric by zinc coordinating to DAS, and bipy acts a co-former in the stabilization of the solid state. Zinc(II) shows an octahedral geometry, coordinated to two DAS by N atoms and four water molecules (figure 2). The main difference between solids 1 and 2 is the torsion angle between the aromatic rings of the organic molecules. In solid 1, the torsion angle between the 4,4'-bipyridine rings is 20,79º, and between the 4,4'-diamino-2,2'-stilbenedisulfonic acid rings is 11,5º. In solid 2, there is no torsion between these rings.

In solid 1, the average distance between Zn(II) and the water molecules is 2,06 Å, and 2,24 Å between Zn^{2+} and DAS's amino group. In solid 2, the average distance between Zn(II) and the water molecules is 2,09 Å, and 2,18 Å between Zn^{2+} and DAS's amino group.

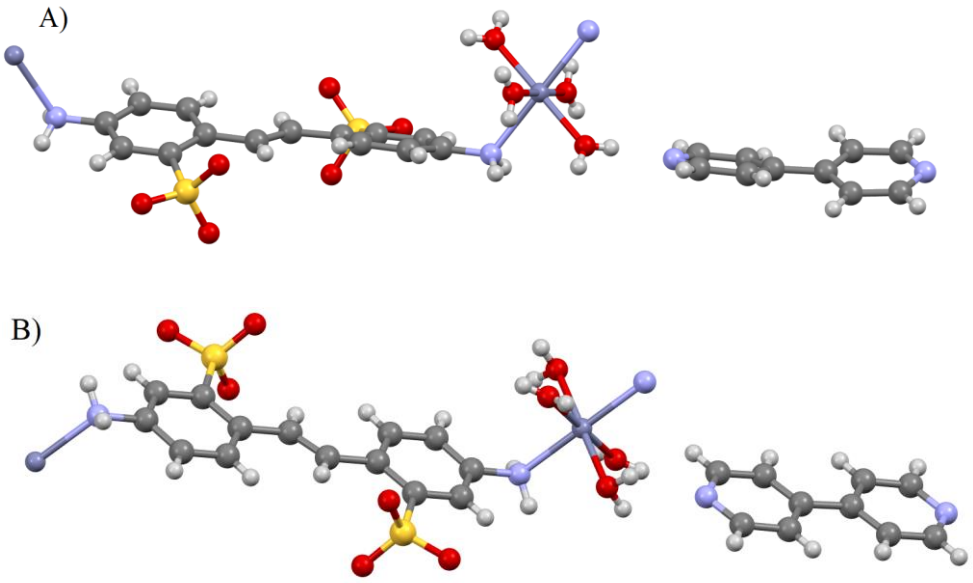

Figure 1: Crystalline structure of A) solid 1 and B) solid 2

These results show the importance of the synthetic methodology in the preparation of coordination polymers and in the solid state stabilization.

[1] XU, Ruren, PANG, Wenqin, HUO Qisheng, *Modern Inorganic Synthetic Chemistry*, Elsevier, City (2011).

[2] G. Sheldrick, *Acta Crystallographica Section C*, 2015, 71, 3-8.

Síntese e estrutura cristalina de dois novos complexos heterolépticos de níquel(II) com 1,1′-bis(difenilfosfino)ferroceno e ditiocarbimatos

R. A. C. Souza[a], S. Guilardi[a], A. E. C. Vidigal[b], M. M. M. Rubinger[b], M. R. L. Oliveira[b], J. A. Ellena[c]

[a]*Instituto de Química, Universidade Federal de Uberlândia, Uberlândia, Brasil.*
[b]*Departamento de Química, Universidade Federal de Viçosa, Viçosa, Brasil.*
[c]*Instituto de Física de São Carlos, Universidade de São Paulo, São Carlos, Brasil.*

Complexos metálicos com ditiocarbamatos ($R_2NCS_2^{-1}$) são empregados no controle de ampla gama de doenças fúngicas em muitas culturas economicamente importantes[1] e na indústria como aceleradores de vulcanização da borracha[2]. Complexos com ditiocarbimatos são estruturalmente semelhantes ($RN=CS_2^{-2}$), porém menos estudados. A literatura reporta a síntese de complexos heterolépticos de Ni(II), Pd(II) e Pt(II) com *N*-R-sulfonylditiocarbimatos e fosfinas[3,4]. Complexos de níquel(II) com 1,1'-bis(difenilfosfino)ferroceno (dppf) e 4-$XC_6H_4SO_2N=CS_2^{2-}$ (X = Cl; Br; Me) foram descritos na literatura[5]. Este trabalho descreve a síntese e estrutura cristalina de dois novos complexos com ditiocarbimatos e dppf (Esquema 1).

Esquema 1. Síntese dos complexos de níquel(II) com *N*-R-sulfonilditiocarbimatos e dppf.

Os complexos **a** e **b** são estáveis a temperatura ambiente e foram caracterizados por espectroscopia no infravermelho e difração de Raios X (Fig. 1).

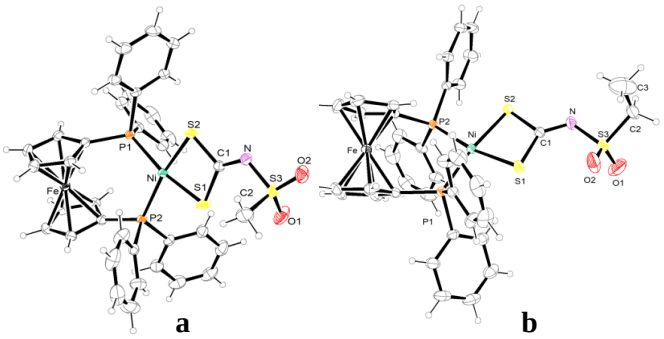

Nos espectros vibracionais de **a** e **b** a banda de νC=N (1433 cm^{-1}) está deslocada para maiores números de onda em relação aos espectros dos ligantes livres (1300 cm^{-1}), enquanto a banda de estiramento do grupo CS_2 (933 cm^{-1}) tem deslocamento oposto (ligantes livres: 960 cm^{-1}) indicando a complexação do Ni(II) pelos átomos de enxofre. O aparecimento da banda νNi-S em torno de 378 cm^{-1} confirma a complexação do ditiocarbimato pelos dois átomos de enxofre nos dois complexos. Monocristais apropriados de **a** e **b** foram obtidos por recristalização lenta em diclorometano/etanol (1:1 v/v) acrescidos de uma gota de água. As intensidades dos feixes de raios X difratados foram coletadas em um difratômetro Bruker APEX II, usando radiação MoKα (0,71073 Å) a temperatura ambiente. O composto **a** cristaliza no sistema monoclínico ($P2_1/c$) e **b** no sistema triclínico ($P\bar{1}$). Em **a** e **b**, o átomo de Ni é coordenado por dois átomos de enxofre do ditiocarbimato e por dois átomos de fósforo de dppf, em uma geometria quadrada plana distorcida. O ângulo S-Ni-S é consideravelmente menor que 90° devido ao ligante bidentado *N*-R-sulfonilditiocarbimato. Os ângulos P-Ni-S são maiores que 90º e o ângulo P-Ni-P apresentam uma distorção ainda maior. As ligações C-S e C-N possuem caráter intermediário entre ligações duplas e simples devido à deslocalização dos elétrons no fragmento S_2CN. Os empacotamentos cristalinos são estabilizados por interações intermoleculares do tipo C-H···O, C-H···S (composto **a**) e C-H···π. Interações intramoleculares do tipo C-H···S também estão presentes no cristal do composto **a**.

[1]Gullino, M. L. *et al. Plant Disease*, **94** (9), 1076-1087 (2010).
[2]Costa, H. M. *et al*. *Polímeros: Ciência e Tecnologia*, **13** (2), 125-129 (2003).
[3]Oliveira, M. R. L. *et al. Inorganica Chimica Acta*, **376**, 238- 244 (2011).
[4] Singh, S. K. *et al. Inorganica Chimica Acta*, **384**, 176–183 (2012).
[5] Singh, S.K. *et al*. *Journal of Organometallic Chemistry*, **190**, 745-746 (2013).

Agradecimentos: Rede Mineira de Química; FAPEMIG; CAPES; CNPq.

Determinação da estrutura cristalina do Ciprofibrato e caracterização de micelas de Pluronic® como nanocarreadores para *Drug Delivery*

R.L.G.Q. Corrêa[a]; L.J.C. Albuquerque[a, b]; F.F. Ferreira [a,b]; F.N. Costa[a, b]

[a] *Centro de Ciências Naturais e Humanas (CCNH), UFABC, Santo André, Brasil*

[b] *Núcleo de Pesquisa em Nanomedicina (NANOMED), UFABC, Santo André, Brasil*

Ciprofibrato (CIP) é um fármaco altamente hidrofóbico, utilizado no tratamento da dislipidemia - doença degenerativa crônica caracterizada por níveis anormais de lipídeos na corrente sanguínea. Esta é uma condição de risco elevado para desenvolvimento de doenças cardiovasculares, consideradas hoje como as maiores causas de morte no planeta [1,2]. O objetivo deste trabalho é determinar a estrutura cristalina do CIP e caracterizar micelas mistas de Pluronic® P123/F127 carregadas com este fármaco, visando desenvolver um nanocarreador para entrega local da droga (*drug delivery*), melhorando sua biodisponibilidade, dado que as micelas podem aumentar a solubilidade do CIP em água.

Neste trabalho foi utilizada a difração de raios X de pó para determinar a estrutura cristalina do CIP (Figura 1). A amostra foi triturada em um almofariz de ágata com pistilo, de forma a obter um pó fino o suficiente para análise por raios X, e colocada entre duas folhas finas (0.014-mm) de acetato de celulose num porta-amostras que permaneceu girando durante a coleta de dados. Os dados foram coletados em temperatura ambiente em um difratômetro de raios X STADI-P, utilizando o comprimento de onda de CuKα_1 (λ=1.54056Å). Os resultados mostram que o CIP cristaliza numa estrutura monoclínica e apresenta parâmetros de rede conforme a Tabela 1. Os fatores R indicam boa concordância entre os dados experimentais e o modelo.

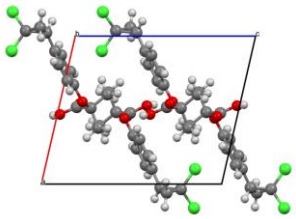

Figura 1: Estrutura cristalina do CIP determinada via DRX

Tabela 1: Estrutura cristalina do Ciprofibrato.

Grupo espacial	a; b; c (Å)	β (°)	V (Å³)	Z;Z´	R_{exp} (%)	R_{wp} (%)	R_{Bragg} (%)	χ (%)
$P2_1/c$	10.7576(3), 10.2652(2), 12.7973(3)	102.9356 (11)	1377.33 (6)	4;1	2.637	5.7462	2.984	2.179

As micelas foram preparadas a partir de uma solução estoque com 100 mg de Pluronic® misto (2:1 – F127:P123) dissolvida em solvente orgânico (Etanol) e acrescentadas diferentes concentrações de CIP (10%, 20%, 30% e 40% m/m) em seguida sendo nanoprecipitadas em água. Após evaporação do solvente, as partículas foram ressuspensas em água para análise de tamanho, polidispersividade e potencial ζ (zeta) utilizando DLS (*Dynamic Light Scattering*) e ELS (*Electrophoretic Light Scattering)*. Foram selecionadas as melhores condições para produção de micelas estáveis, com tamanho em torno de R_H=31nm (micelas não carregadas) e R_H=43nm (micelas carregadas). A quantidade de fármaco encapsulado foi determinada por espectroscopia na região do UV-Vis na melhor condição alcançada, atingindo cerca de 75%. Nas próximas etapas, será investigada a conformação do CIP quando encapsulado nas micelas e comparada a estabilidade das micelas de Pluronic® com outros polímeros biocompatíveis já reportados em literatura [3], como PEO_{45}-b-PLA_{174} e PEO_{113}-b-PCL_{118}.

[1] Staels B., et al, *Circulation*, 1998, 98, 2088.

[2] World Health Organization (WHO). *A global brief on hypertension. Silent killer, global public health crisis*. Geneva: WHO; 2013.

[3] C. E. de Castro, et al. *Langmuir* 2014, 30, 32, 9770-9779

Agradecimentos: Os autores agradecem o financiamento do CNPq (# 307664/2015-5).

Atovaquona incorporada em nanoemulsão não interfere na organização supramolecular da nanoestrutura

F. Bruxel[a], C. Scheuer[a], M. C. Galarça[a], L. B. Wild[b], R. S. Schuh[b], H. F. Teixeira[b].

[a]*Programa de Pós-Graduação em Ciências Farmacêuticas, Universidade Federal do Pampa, Uruguaiana, Brazil.*

[b] *Programa de Pós-Graduação em Ciências Farmacêuticas, Universidade Federal do Rio Grande do Sul, Porto Alegre, Brazil.*

Relatos de resistência por parte dos parasitos do gênero *Plasmodium* têm sido descritos para todos compostos antimaláricos atualmente utilizados no tratamento da malaria [1]. Dentre esses compostos, inclui-se também a atovaquona, uma molécula que também apresenta baixa hidrossolubilidade e dificuldade para ultrapassar as barreiras lípidicas das membranas celulares [2]. Neste contexto, sua incorporação em nanoemulsões tem sido sugerida como uma forma de solucionar esses problemas. Entretanto, pouco se conhece ainda sobre a organização estrutural supramolecular dessas emulsões, importante para compreender como o fármaco se associa ou é liberado a partir dos nanossistemas [3]. Assim, o objetivo deste trabalho foi caracterizar aspectos físico-químicos e determinar a organização estrutural de nanoemulsões, antes e após a incorporação de atovaquona no sistema. As formulações brancas foram preparadas por emulsificação espontânea e compostas por triglicerídeos de cadeia média, lecitina, 1,2-dioleil-3-trimetilamônio-propano, glicerol e água ultrapura (NE) [4]. As nanoemulsões contendo atovaquona foram denominadas NE-ATQ. A distribuição e diâmetro médio de gotícula foram caracterizados por difratometria a laser e o potencial zeta por migração eletroforética. Para determinar a organização estrutural, foi utilizada a técnica de difração de raios-X por energia dispersiva, utilizando-se uma fonte de luz Síncroton. As formulações NE e NE-ATQ apresentaram propriedades físico-químicas semelhantes ($p>0,05$), demonstrando diâmetros médios de gotículas entre 190-230nm, com índice de polidispersão <0,2. O potencial zeta apresentou-se positivo (+42 a 55 mV) para ambas as formulações. A formulação NE apresentou os picos de difração: 0,091 e 0,178 $Å^{-1}$, correspondendo a um tamanho de retículo de 69 Å. A formulação contendo atovaquona (NE-ATQ) apresentou picos de difração em 0,097 e 0,195 $Å^{-1}$, correspondendo ao tamanho de retículo de 64,8 Å. Ambas formulações apresentaram razões características de estruturas lamelares, conforme já descrito na literatura para esse tipo de sistema. Também pôde ser identificada a presença de outros picos de menor intensidade na região de 0,083 e 0,104 $Å^{-1}$, sendo provavelmente relacionados à mistura de fosfolipídeos presentes na lecitina, que compõe as formulações [3]. Pode ser concluído que, de acordo com esses resultados, a incorporação de atovaquona não alterou a organização lamelar da nanoemulsão, sugerindo que a molécula está dissolvida em seu núcleo oleoso.

[1] WHO. World Health Organization. Malaria. <https://www.who.int/malaria/en/> (2019).

[2] Rang, H.P., Ritter, J.M., Flower R.J., Henderson, G., in *Rang & Dale: Farmacologia,* 8. ed. Elsevier, Rio de Janeiro, 784 p. (2016).

[3] Bruxel, F., Vilela, J.M.C., Andrade, M.S., Malachias, A., Perez, C.A., Magalhães-Paniago, R., Oliveira, M.C., Teixeira, H.F., *Colloids and Surfaces B*, **112**, 530–536 (2013).

[4] Bruxel, F., Bochot, A., Diel, D., Wild, L., Carvalho, E.L.S., Cojean, S., Loiseau, P.M., Fattal, E., Teixeira, H.F., *Current Topics in Medicinal Chemistry*, **14**, 1-11 (2014).

Acknowlegments: FAPERGS; CNPq; PDA/Unipampa.

Experimental Charge Density Study of the Pharmaceutical Cocrystal Isoniazid:5-Fluorocytosine

J. C. Tenorio[a], A. Formiga[a] , J. Ellena[b], A. Wanderley[b], C. W. Lehmann[c]

[a]*Institute of Chemistry, University of Campinas, Campinas-SP, Brazil.*
[b]*São Carlos Institute of Physcis, University of São Paulo, São Carlos - SP, Brazil.*
[c]*Max-Planck Institute for Coal Research, Mülheim a.d. Ruhr, Germany.*

In this work is described the experimental charge density (CD) study of a new solid form derived of the combination of two used widely active pharmaceutical ingredients (API): the antimetabolite prodrug 5-Fluorocytosine (5-FC) and the tuberculostatic drug Isoniazid (INH).

The result of the combination of these molecules yields the formation of a pharmaceutical cocrystal (5-FC:INH), which is stabilized by the supramolecular synthon held by strong hydrogen bond of N-H…N type, between the amine and imine fragments of the 5FC molecule and the hydrazide fragment of INH molecule. The crystal structure of this cocrystal is already known in room temperature, but no charge density study has been published as far. [1]

In that vein, we have carried out a single-crystal X-ray diffraction experiment in high resolution ($\sin(\theta_{max})/\lambda$=1.15 Å^{-1}) at 150 K, in a conventional diffractometer equipped with a X-ray source of Molybdenum rotating anode. After the collection and processing data, Hasen & Coppens aspherical multipolar refinement was proposed, [2] in order to determine the CD distribution of this cocrystal.

The good quality of the data allowed to carry out a topological analysis and electron density partitioning using the Quantum Theory of Atoms in Molecules (QTAIM) analysis. Insights about the intermolecular interactions, the presence of fluorine atom, and crystal lattice energy were some of the aspects which were assessed from the multipolar refinement model and theoretical quantum calculations.

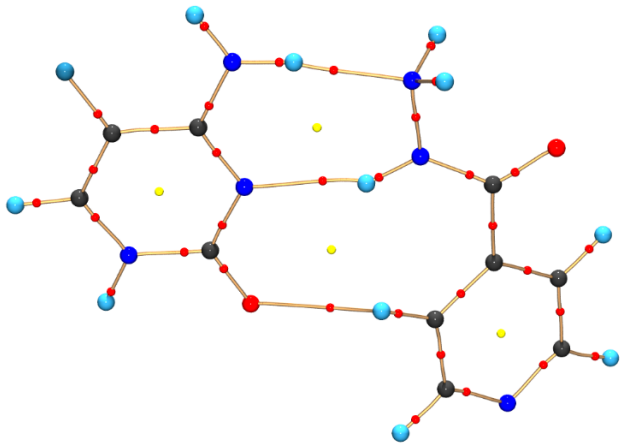

Figure 1: Molecular graph of the Charge Density topology in INH:5FC cocrystal.

[1] Souza, M. S., Diniz, L. F., Vogt, L., Carvalho Jr, P. S., D'vries, R. F., Ellena, J., *Crystal Growth & Design*, **18**, 5202 (2018).

[2] Hansen, N., Coppens, P., *Acta Cryst*, **A34**, 909 (1978)

Acknowledgments: This study was financed in part by the Coordenação de Aperfeiçoamento de Pessoal de Nível Superior - Brasil (CAPES) - Finance Code 001 & FAPESP (Fundação de Amparo à Pesquisa do Estado de São Paulo)

Synthesis and characterization of two new hexavanadates

G. B. Baptistella[a], F. S. Santana[a], D. L. Hughes[b], J. F. Soares[a], E. L. de Sá[a], G. G. Nunes[a]

[a] *Departamento de Química, UFPR, Curitiba, PR, Brasil.*

[b] *School of Chemistry, University of East Anglia, Norwich, NR47TJ, UK.*

Abstract

The functionalization of polyoxometalates with covalently or noncovalently linked organic species has attracted attention by their richer structural patterns and broad application in fields as medicine, material science and magnetism.[1] The reaction between V_2O_5, oxalic acid and 1,1,1-tris(hydroxymethyl)ethane (tme) or 1,1,1-tris(hydroxymethyl)propane (tmp) (1:3:1) in the presence of triethylamine produced orange parallelepiped crystals with similar structures of $(C_6H_{16}N^+)_2[C_{10}H_{20}O_{19}V_6]$ (**I**) and $(C_6H_{16}N^+)_2[C_{12}H_{22}O_{19}V_6]$ (**II**) (Figure 1). Single crystal X-ray diffraction showed that **I** crystalized in the triclinic system, P-1, and **II** crystalized in the monoclinic system, P2(1)/n. Both structures were comprised of an aggregate containing 6 vanadium centers, 13 oxide groups and two triol ligands in a tridentate way. The charge of the aggregates is balanced by two triethylammonium cations. All vanadium centers exhibit an octahedral-distorted geometry and contain a terminal vanadyl (VO) group. Elemental analysis contents were consistent with theoretical values demonstrating the purity of the compounds.

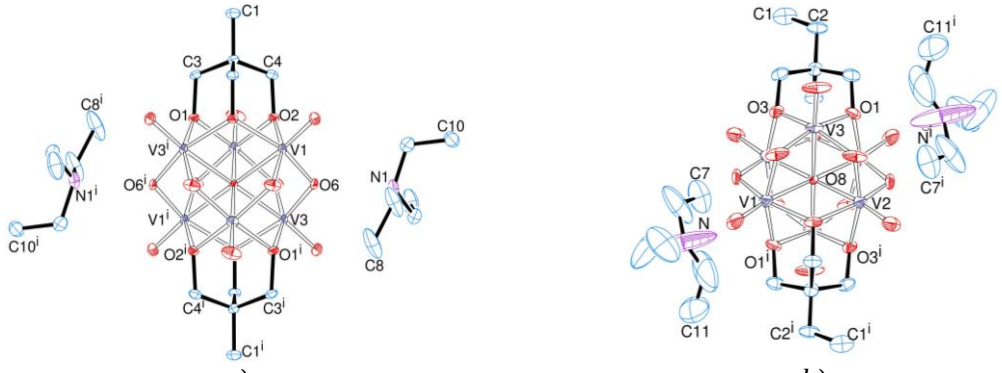

a) *b)*

Figure 1. ORTEP–3 representation of *(a)* $(Et_3NH)_2[V_6O_{13}(tme)_2]$ (**I**) and *(b)* $(Et_3NH)_2[V_6O_{13}(tmp)_2]$ (**II**). Hydrogen atoms were omitted for clarity. Thermal ellipsoids were drawn at the 50% probability level.

Compound **I** have two strong hydrogen bonds that occur between carbons (C8 and $C8^i$) of the triethylammonium anion and two vanadyl oxygen and four weak bifurcated hydrogen bonds that occur between carbons (C10 and $C10^i$) with oxygen coordinated to two vanadium. For **II**, the hydrogen bonding involves the carbons (C7 and $C7^i$) and (C11 and $C11^i$).

The IR spectra of **I** and **II** presented bands characteristic of the polyoxidovanadates (POV) and the organic parts. The UV/vis/NIR spectrum presents two bands with maximum absorption below 360 nm and an intense band at 452 nm which is characteristic of the TCLM transition. The spectrum doesn't show bands in the visible region, which indicates that the products have only vanadium(V).

Compounds **I** and **II** are examples of functionalized hexavanadate structures synthesized by a simple and reproducible methodology. In the next steps, attempts will be made to functionalize organic molecules in their structure.

References:

[1] DOLBECQ, A. Chem. Rev., **v. 110, n.10,** p. 6009–6048 (2010)

Acknowledgments: UFPR/CAPES/CNPq/FUNDAÇÃO ARAUCÁRIA/PROEX

Influence of the hydration degree of decavanadate associated with tris(hydroxymethyl)aminomethane to the supamolecular assembly

Juliana M. Missina[a*], Luiza B. P. Leme[a], Kahoana Postal[a], Francielli S. Santana[a], David L. Hughes[b], Eduardo L. de Sá[a], Ronny R. Ribeiro[a], Jaísa F. Soares[a], and Giovana G. Nunes[a].

[a]*Departamento de Química, Universidade Federal do Paraná, Curitiba-PR, Brazil.*
[b]*School of Chemistry, University of East Anglia, Norwich NR4 7TJ, UK.*

The decavanadate anion, $[H_xV_{10}O_{28}]^{(6-x)-}$ (V_{10}), has a rich chemistry determined by its combination with several organic or inorganic counterions, and by the variation of reaction conditions, such as pH, reaction time and temperature.[1] [2] In this work, we obtained two decavanadate salts containing protonated tris(hydroxymethyl)aminomethane (tris) as counterion through variation of the vanadium starting material. From the reaction with $NaVO_3$, orange crystals of $[trisH]_4[H_2V_{10}O_{28}]\cdot 10H_2O$ (**1** –Figure 1a) were isolated, while the reaction with V_2O_5 produced orange parallelepipeds of $(trisH)_6[V_{10}O_{28}]$ (**2** – Figure 1b).

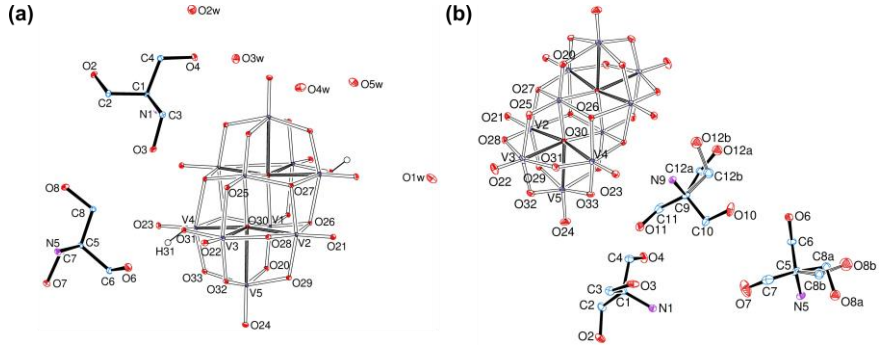

Figure 1: ORTEP diagrams of ***(a)*** *$[trisH]_4[H_2V_{10}O_{28}]\cdot 10H_2O$ (**1**) and* ***(b)*** *$(trisH)_6[V_{10}O_{28}]$ (**2**). Ellipsoids are drawn at the 50% probability level.*

Product **1** crystallizes in the P-1 triclinic space group. The doubly protonated V_{10} anion and the presence of lattice water molecules in this structure define a complex 3-D hydrogen bond network that connects all species in the lattice. Moreover, the O–H···O interactions promote the formation of cyclic octamers made up of water molecules and tris cations that are interleaving with the decavanadate anions along the *b* axis.

Product **2** crystallizes in the $P2_1/n$ monoclinic space group. Due to the absence of water molecules and protonation on V_{10}, the tris cations are the sole hydrogen bond donors of O–H···O, N–H···O and C–H···O interactions in the structure, creating a compact 3-D network. Atoms O(29), O(31) and O(33) in **2**, for instance, exhibit BVS values of 1.715, 1.714 and 1.651, respectively, and participate in hydrogen bonds whose angles are above 175°, characterising strong interactions.

The novel route that gave **2** is rather convenient for future syntheses, since the use of V_2O_5 promotes the formation of products with high a degree of purity, and solubilization of the oxide increases yield as compared to other methodologies found in the literature.[2]

[1] Hayashi, Y., *Coordination Chemistry Reviews*, **255**, 2270-2280 (2011).

[2] Pavlović, N. B., Prévost, J., Biré, A. S., *Crystal Growth & Design*, **11**, 3778-3789 (2011).

Acknowledgements: CAPES; CNPq; Fundação Araucária; Universidade Federal do Paraná.

Crystal structure of two novel binuclear complexes of Gd^{III} and Dy^{III} with oxalate bridges and chelating *N,N'*-bis(2-oxidobenzyl)-*N,N'*-bis(pyridin-2-ylmethyl)ethylenediamine ($bbpen^{2-}$)

G. A. Barbosa[a], F. S. Santana[a], G. G. Nunes[a], J. F. Soares[a].

[a]*Departamento de Química, Universidade Federal do Paraná, Curitiba-PR, Brasil.*

Lanthanide(III) complexes have been largely studied concerning their intrinsically high magnetic anisotropy barrier [1], [2]. The preparation of compounds containing both 3*d* and 4*f* ions is interesting from the point of view of the improvement in magnetic response provided for the 4*f* ions compared to 3*d*-only complexes [3]. In this context, our attempt to obtain the heterometallic, tris-chelate complexes of general formula $[M^{III}(\mu\text{-ox})_3\{Gd(\text{bbpen})\}_3]$ (H_2bbpen = *N,N'*-bis(2-hydroxybenzyl)-*N,N'*-bis(pyridine-2-ylmethyl)ethylenediamine; ox = oxalate) employing [Gd(bbpen)Cl] and $K_3[M(\text{ox})_3]$ (M^{III} = Cr or Co) as starting materials in a 3:1 molar proportion led to the unexpected formation of colorless parallelepipeds. Single crystal X-ray diffraction analysis revealed the novel binuclear compound $[\{Gd(\text{bbpen})\}_2(\mu\text{-ox})]\cdot 4CH_3OH \cdot 4H_2O$ (**1**). This finding motivated us to successfully design and perform the rational preparation of the product, not only from Gd^{III} but also from Dy^{III} (yields of *ca* 70 %) [4].

The isostructural and centrosymmetric compounds **1** (with Gd) and **2** (Dy), Figure 1 for complex **1**, crystalize in the triclinic system with space group P(−1). In the products, the lanthanide(III) ions experience eight-coordination with distorted square-antiprismatic geometry as confirmed by the use of the SHAPE program [5]. The unit cell contains one neutral binuclear moiety together with four water and four methanol molecules from which two of each type refined well. For both structures, there is an extensive three-dimensional intermolecular hydrogen-bonding network from which the individual O···H–O hydrogen bonds may be described as medium-strength.

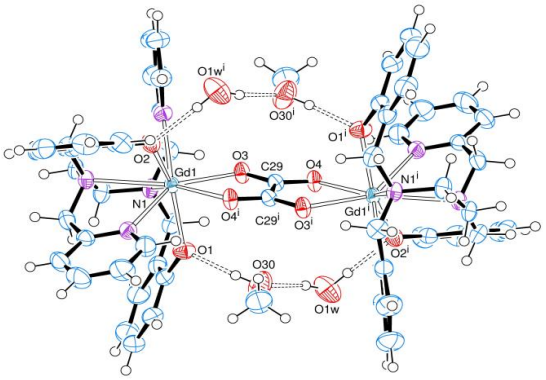

*Figure 1: View of **1** showing some hydrogen-bonding interactions (double-dashed lines). Displacement ellipsoids are drawn at the 50% probability level. Symmetry code: (i) –x, –y + 1, –z + 1.*

The supramolecular features involve the hydrogen atoms from the crystallizing solvents and the oxygen atoms belonging to phenolate groups, which are themselves 'bridged' by one water and one methanol molecule (Figure 1). These interactions seem important to the stabilization of the relatively compact shape of the dimer. Additionally, weak hydrogen bonds of the C–H···O type, involving solvating water molecules, connect the dimeric molecules to one another. Residual electron density associated with one additional water and one methanol molecule was removed with the SQUEEZE routine in *PLATON* [6]. Despite this, it was possible to infer the contribution of these molecules to the assembly of the hydrogen-bonding network.

[1] Goodwin, C.A.P., *et al*. *Nature*, **548**, 439-442, (2017).
[2] Guo, F.-S., *et al*. *Science*, **362**, 1400-1403 (2018).
[3] Piquer, L. R. and Sañudo, E.C. *Dalton Transactions*, **44**, 8771-8780 (2015).
[4] Barbosa, G.A., *et al*. *Acta Crystallographica Section E*. **75**, 418-422 (2019).
[5] Llunell M., *et al*. *SHAPE - Program for the stereochemical analysis of molecular fragments by means of continuous shape measures and associated tools.* Barcelona (2013).
[6] Spek, A. *Acta Crystallographica Section C*. **71**, p. 9-18 (2015).

Acknowlegments: CNPq; CAPES; PPGQ - UFPR. The authors thank Dr. David L. Hughes (University of East Anglia, UK) for training and discussions, and the late Professor Sueli M. Drechsel for helpful suggestions.

Desafios práticos-teóricos para determinação da estrutura de uma porfirazina com Magnésio.

C. H. J. Franco[a], J. P. S. C. Leal[a], L. G. Rezende[a], J. L. S. Milani[a], T. T. Tasso[b].

[a]*Departamento de Química, Universdade Federal de Juiz de Fora, Juiz de Fora, Brasil.*
[b]*Departamento de Química, Universidade Federal de Minas Gerais, Belo Horizonte, Brasil.*

As porfirazinas e metaloporfirazinas são uma importante e emergente classe de compostos devido às propriedades como alta conjugação eletrônica, eficiente absorção de luz, e possibilidade de coordenação com diferentes íons metálicos, que permitem aplicações em dispositivos eletrônicos, sistemas biológicos (e.g. terapia fotodinâmica) e em catálise homogênea [1]. As propriedades químicas da porfirazina são altamente moduláveis pelo metal central e substituintes ligados ao anel, e a escolha destes pode ser racionalizada dependendo da aplicação desejada. Nesse trabalho, descrevemos a estrutura cristalina de uma porfirazina de magnésio (MgPz) contendo grupos retiradores de elétrons, que foi sintetizada com o intuito de investigarmos sua eficiência catalítica para fixação química de CO_2. O composto MgPz sintetizado foi recristalizado utilizando uma quantidade mínima de solvente. Diferentes métodos e solventes (éter dietílico, acetato de etila, hexano) foram testados a fim de controlar a solubilidade e perda de solvente da amostra. Após algumas semanas de evaporação lenta de uma solução concentrada da MgPz em éter dietílico, foi observada a formação de pequenos cristais com dimensões (0,24 x 0,12 x 0,049 mm) altamente frágeis. Durante os pré-experimentos foi observado que os cristais difratavam somente a baixo ângulo com intensidades muito fracas. Os experimentos de difração de raios X por monocristais foram realizados em um difratômetro Rigaku SuperNova com radiação CuKα (λ = 1,5406 Å), detector CCD AtlasS2 e mantidos a baixa temperatura (145K) com um alto tempo de exposição para a coleta das reflexões, o que ocasionou em um tempo de medida de 144 horas. A estrutura foi resolvida usando o Charge Flipping [2] e refinada com o pacote de refinamento ShelXL [3] usando o método dos mínimos quadrados. Esse elevado tempo de exposição por imagem levou a uma alta contribuição de radiação de fundo, que, combinado com a formação de gelo sobre a superfície do cristal durante a medida, contribuíram para uma redução das estatísticas do refinamento e para o processo de indexação da célula unitária. O composto MgPz ($C_{72}H_{34}F_{24}MgN_8O$ e M = 1507.38 g/mol) cristalizou-se no sistema triclínico e grupo espacial P-1, onde a = 15,402(2) Å, b = 17,143(3) Å, c = 17.345(2) Å, α = 111,456(14), β = 98,015(11)°, γ = 110,827(15)°, V = 3787,6(11) Å^3, Z = 2 *e* μ(CuKα) = 1,148 mm^{-1}. Foram observadas 27642 reflexões medidas e 10842 únicas (R_{int} = 0,1150, R_{sigma} = 0,1224). O valor final de R foi de 0,1586 ($I > 2\sigma(I)$) e wR de 0,4879 (para todos os dados). Tentativas de introduzir correções empíricas de absorção dos conjuntos de dados não melhoraram a qualidade dos resultados. Os mapas de diferença de densidade eletrônica para o composto mostram picos residuais significativos, indicando que, além da água ligada ao centro metálico, outras moléculas de solvente (aparentemente 8 moléculas de éter dietílico) estão contidas nas cavidades de porfirazina. Os solventes foram introduzidos nos refinamentos correspondentes com ocupações parciais. O conteúdo exato de solvente dos cristais não pôde ser avaliado com confiabilidade nem pelo refinamento do fator de estrutura, devido à alta correlação entre os parâmetros de ocupação e de movimento térmico, ou por análise elementar. Portanto, a composição estequiométrica porfirazina-solvente desse cristal representa apenas uma aproximação.

[1] Rodríguez-Morgade, M. S.; Stuzhin, P. A. *J. Porphyrins Phthalocyanines* **v.8**, p. 1129-1165 (2004).

[2] Prathapa, S. J., van Smaalen, S., *J. Appl. Cryst.* **v.45**, p. 575-580 (2012).

[3] Sheldrick, G.M., *Acta Cryst. C*, **71**, 3-8 (2015).

Agradecimentos: CNPq (processo #422685/2018-6); CAPES e UFJF.

Estrutura cristalina de dois novos sais de alilditiocarbimatos de tetrafenilfosfônio

R. A. C. Souza[a], S. Guilardi[a], N. M. Albuini[b], M. M. M. Rubinger[b], E. C. Tavares[c], C. H. C. Zacchi[d], L. Zambolim[e], M. R. L. Oliveira[b], A. E. C. Vidigal[b], J. A. Ellena[f]

[a]*Instituto de Química, Universidade Federal de Uberlândia, Uberlândia, Brasil.*
[b]*Departamento de Química, Universidade Federal de Viçosa, Viçosa, Brasil.*
[c]*Universidade Federal de Itajubá, Itajubá, Brasil.*
[d]*Centro Federal de Educação Tecnológica de Minas Gerais, Belo Horizonte, Brasil.*
[e]*Departamento de Fitopatologia, Universidade Federal Viçosa, Viçosa, Brasil.*
[f]*Instituto de Física de São Carlos, Universidade de São Paulo, São Carlos, Brasil.*

Ditiocarbamatos $(R_2NCS_2)^-$ têm sido usados em vários cultivos há décadas como fungicidas[1]. Estudos recentes evidenciaram que alilditiocarbimatos $(RN{=}CS_2)^{2-}$ possuem propriedades antifúngicas, mas ainda sem aplicações comerciais[2]. Este trabalho reporta a caracterização estrutural, por difração de raios X, de dois novos sais de *N*-R-sulfonilditiocarbimatos de tetrafenilfosfônio que apresentam atividade antifúngica[3].

Monocristais amarelos dos compostos **1** e **2** foram obtidos por evaporação lenta de uma solução de etanol/água (1:1 v/v) a 298 K. Os dados de raios X foram coletados em um difratômetro Bruker APEX II, a temperatura de 293(1) K, usando radiação MoKα (0,71073 Å). A estrutura foi resolvida por Métodos Diretos e refinada por mínimos quadrados. Os dados de difração de raios X confirmaram a estereoquímica (Z) para os ânions de alilditiocarbimatos.

O composto **1** cristaliza no grupo espacial $P\bar{1}$ e **2** no grupo espacial P2/c. Na unidade assimétrica, há um ânion (Fig. 1) e um cátion. Existem quatro fragmentos planares nos ânions de alilditiocarbimatos: C1-S1-C10-S2-N2-S3, C1-C2-C3-C4-C11 e dois anéis aromáticos. Em ambos os compostos, os ângulos de torção em torno das ligações S3-C1' e C1-C2 mostram as diferentes conformações dos três fragmentos em relação ao plano C1-S1-C10-S2-N2-S3. No composto **2**, o átomo de fósforo do tetrafenilfosfônio está em posição especial (0, y, 1/4).

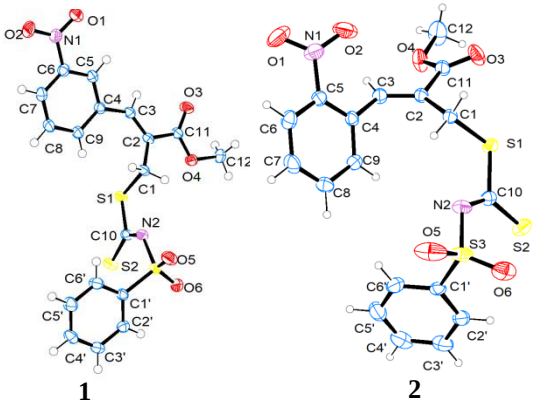

O empacotamento cristalino é estabilizado pelas interações eletrostáticas entre íons de cargas opostas. No ânion dos compostos existem interações intramoleculares do tipo C-H···O. Além dessas, há outras interações intramoleculares: C-H···S e C-H···π (composto **1**) e C-H···N (composto **2**) e na unidade assimétrica há contatos entre cátions e ânions: C-H···O e C-H···π (composto **1**). No composto **1**, as interações intermoleculares C8-H8···O6 entre ânions e C18-H18···O5 entre cátions e ânions formam fitas ao longo do eixo *a* que são conectadas por interações intermoleculares C-H···S e C30-H30···O1 formando camadas. Essas camadas são ligadas por interações C4'-H4'···O3 ao longo do eixo *a*. Além disso, há três interações intermoleculares C-H···π entre cátions e ânions, dando origem a uma rede supramolecular. No composto **2**, as interações intermoleculares C-H···O entre cátions e ânions formam cadeias em ziguezague ao longo do eixo *c*.

[1]Gullino, M. L., *et al*.. *Plant Disease,* **94** (9), 1076-1087 (2010).
[2]Tavares, E. C., *et al*.. *J. Molec. Struct.*, **1106**, 130-140 (2016).
[3]Albuini N. M., *et al*.. 40ª Reunião Anual da Sociedade Brasileira de Química, Syntheses and Antifungal Activity of New Allyldithiocarbimate Salts, São Paulo-SP, 2017.

Agradecimentos: Rede Mineira de Química; FAPEMIG; CAPES; CNPq.

Crystalline Structure of Cooper Triazole Coordination Polymer

O. B. O. Moreira[a] , B. A. Rodrigues,[b] J. A. L. C. Resende[b].

[a]*Departamento de Química, Universidade Federal de Juiz de Fora, Juiz de Fora, Brasil.*
[b]*Insittuto de Ciências Exatas e da Terra, Campus Universitário do Araguaia, Universidade Federal do Mato Grosso, Barra do Garças, Brasil.*

Triazois são uma classe de compostos heterocíclicos nitrogenados sintéticos de cinco membros que apresenta um vasto campo de aplicações, que vão desde usos como explosivos, agroquímicos e farmacológico, devido sua atividade antifúngica, antiviral e anticancerígena.[1] Além dessas características biológicas, compostos de coordenação desses compostos tem despertado interesse em ciências de materiais em decorrência das formação de polímeros de coordenação e aplicação em sistemas para armazenamento de gases. [2]

O composto foi produzido através da reação do ligante ácido de partida com perclorato de cobre hexahidratado, na proporção de 1:1, em metanol. Foram adicionadas algumas gotas de trietilamina. A solução límpida permaneceu em repouso por 72hrs até a obtenção do monocristais de coloração azulada. Dados de difração de raios X foram coletados no equipamento Bruker Kappa CCD com radiação MoKα a temperatura ambiente. A estrutura foi resolvida por métodos diretos utilizando o programa SIR-2014. O modelo estrutural foi refinado pelo método dos mínimos quadrados, utilizando o programa SHELXL. Dados Cristalográficos - Fórmula química: $[Cu\ (C_{10}H_9N_4O_2)_2]_n$; Grupo espacial: P-1; a=9,0896(5) Å; b=10,3191(6) Å; c=11,9955(8) Å; α = 99,118(2)°; β =91,428(2)°; γ =106,982(2)°; Reflexões coletadas= 32989; Reflexões únicas= 3880; Reflexões observadas =3038; Parâmetros refinados = 303; $R[F^2> 2\sigma(F^2)] = 0,043$, $wR(F^2)= 0,116$; S = 1,08.

A análise estrutural possibilitou descrever que a unidade assimétrica do cristal é formada por dois átomos de cobre independentes, localizados sobre centros de inversões da célula unitária. Além destes dois átomos de cobre, observa-se também duas moléculas do ácido independentes na unidade assimétrica. Um dos átomos de cobre apresenta coordenação do tipo N2O2 coordenado por dois nitrogênios triazólicos e dois oxigênios carboxilatos, apresentando geometria quadrado planar. O outro átomo de cobre possui esfera de coordenação do tipo N2O4 coordenado por quatro oxiogênios carboxilatos e dois nitrogênios triazólicos do ligante com geometria octaédrica distorcida.

A coordenação dos átomos de cobre ao ligante leva a formação de um polímero de coordenação unidimensional na direção [110]. Os grupamentos aminas são muito relavantes para o empacotamento cristalino do composto, pois realizam importantes ligações de hidrogênio. Tais interações expandem as características supramoleculares do sistema para planos bidimensionais, resultando em um sistema supramolecular com características lamelares.

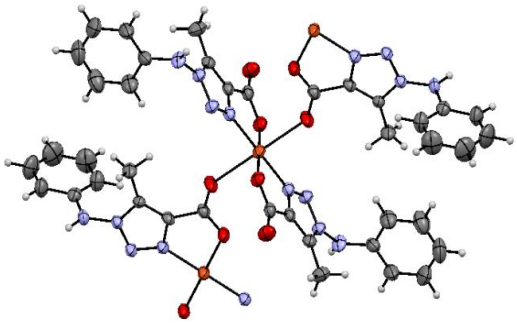

Figura 1: Representação da estrutura cristalina

[1] MELO, J. O. F. et al.. *Química Nova*, v. 29, p. 569-579 (2006).

[2] MUKHERJEE, S., et al. *J. Mater. Chem. A* , v. 7, p. 1055–1068 (2019).

Acknowlegments: CNPq, LDRX-UFF

Caracterização estrutural de um novo complexo trinuclear de gálio

J. S.C. Neto[a], S. O. K. Geise [a], G. G. Nunes[a] , D. L. Hughes[b], J. F. Soares[a], E. L. de Sá[a]

[a] *Departamento de Química, UFPR, Curitiba, PR, Brasil.*

[b] *School of Chemistry, University of East Anglia, Norwich, NR47TJ, UK.*

Resumo

Calcogenetos de gálio têm sido aplicados nas áreas de óptica, fotônica ou ainda como componentes de computadores da próxima geração[1]. A reação entre o pré-ligante (*N,S*-phox)$^-$ com o precursor [$GaCl_3(thf)_2$] (2:1) na presença de thf, possibilitou a obtenção de cristais amarelo-claros com formato de agulhas, em baixo rendimento. A análise de difração de raios X de monocristal evidenciou que **I** cristalizou no sistema trigonal com grupo espacial R-3:H. A estrutura de [$Ga_3(\mu\text{-}S)_3$(*N,S*-phox)$_3$] (**I**) apresenta três centros de gálio(III) ligados através de pontes sulfetos S^{2-}, com uma unidade do ligante oxazolínico coordenado a cada gálio (Figura 1). Os principais ângulos e comprimentos de ligação encontrados em torno gálio(III) conferem um valor de parâmetro tau (τ) igual a 0,86, ao qual é atribuído uma geometria tetraédrica distorcida. A conformação barco adotada pelo anel de 6 membros contendo os centros metálicos e as pontes sulfetos, pode ser atribuída as tensões conformacionais geradas pelo efeito quelato presente no ligante.

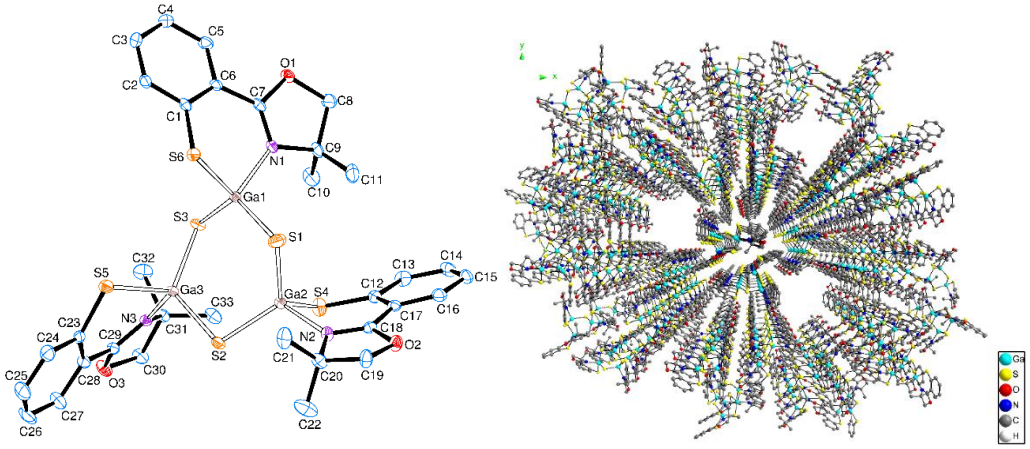

Figura 1: Diagrama ORTEP de [$Ga_3(\mu\text{-}S)_3$(*N,S*-phox)$_3$] e crescimento ao longo de z.

A cela unitária de **I** apresenta um valor de Z igual a 18. Os valores singulares dos parâmetros reticulares, a = 45,644(11) Å, b = 45,644(11) Å e c = 10,344(2) Å conferem a cela um formato de nanoplaca com uma estimativa de área em torno de 605 nm^2. A estrutura supramolecular de **I** apresenta canais definidos pelos anéis aromáticos do ligante. O preenchimento dos canais com uma esfera de diâmetro de 13 Å permitiu realizar uma segunda estimativa da área relativa à circunferência central do buraco em 132,7 Å. O produto I foi obtido acidentalmente, onde sua formação provavelmente ocorreu através de processos redox que são frequentemente observados em reações que o ligante possui átomos de enxofre [2]. Estudos de síntese racional estão em andamento no nosso laboratório.

Referências:

[1] Ricica, T. *et al*. Chem. Eur. J., v. 22, p. 18817–18823, **2016**.

[2] Bottini, R.C.; *et al*. Eur. J. Inorg. Chem. v. 2010, p. 2476-2487, **2010**.

Acknowledgments: UFPR/CAPES/CNPq/FUNDAÇÃO ARAUCÁRIA/PROEX

Structural and vibrational characterization of 1-(diaminomethylene)-thiouron-1-ium 4-aminobenzoate

G. J. Perpétuo[a], J. A. Coleman[b], J. Janczak[c]

[a] *Departamento de Física, Universidade Federal de Ouro Preto, Ouro Preto-MG, Brazil*
[b] *Department of Physics, Imperial College London, London, United Kingdom*
[c] *Institute of Low Temperature and Structure Research, Polish Academy of Sciences, Wrocław, Poland*

This work is a continuation of the study of supramolecular solid-state architectures formed by self-assembly of thiourea derivates[1-3], which can form multiple hydrogen bonds and are useful as building blocks in supramolecular synthesis. Crystals of 1-(diaminomethylene)thiouron-1-ium 4-aminobenzoate were obtained from a hot solution of diaminomethylene thiourea, aminobenzoic acid and water. When the solution became homogenous it was cooled and kept at room temperature. After several days, well-developed colourless crystals suitable for the X-ray analysis were formed.

The crystals of the title compound were dissolved in heavy water and was left in the atmosphere saturated with heavy water for several days in order to avoid the contamination of the crystals. After deuteration the deuterated analogue has quite similar lattice parameters as H-compounds. The structures of H- and its deuterated analogue were investigated in a single-crystal diffractometer. The arrangement of oppositely charged units in the crystal, i.e. 1-(diaminomethylene)thiouron-1-ium cations and aminobenzoate anions, is mainly determined by the ionic and the N-H···O hydrogen bonding interactions.

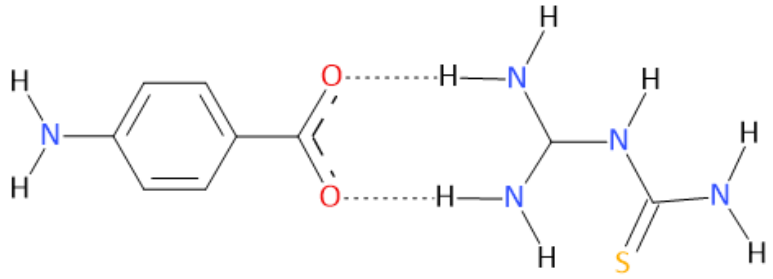

Figure 1: Structure of $(C_2H_7N_4S)(NH_2C_6H_4COO)$

[1] Janczak, J., Perpétuo, G.J., *Acta Cryst. C*, **64**, p. o114-o116 (2008).

[2] Janczak, J., Perpétuo, G.J., *J. Mol. Struct.*, **975**, p. 166-172 (2010).

[3] Perpétuo, G.J., Gonçalves, R.S., Janczak, J., *J. Mol. Struct.*, **1096**, p. 74-83 (2015).

Acknowlegments: Universidade Federal de Ouro Preto, Polish Academy of Sciences.

Difratometria de Pó

Evaluation of Cobalt Dopping Effect in Zinc Oxide

J.P. Dias[a], G.B. Ferreira[a,b], J.M. Siqueira Júnior[a,b].

[a]*Programa de Pós-graduação em Química, Universdade Federal Fluminense, Rio de Janeiro, Brasil.*

[b]*Departamento de Química Inorgânica, Universdade Federal Fluminense, Rio de Janeiro, Brasil.*

Zinc oxide has been widely studied due to its several applications. In industry, this oxide can be used as a catalyst, displacing titanium oxide and when doped, can be applied as a gas sensor[1]. The present work approaches pure zinc oxide synthesis and doped with cobalt through coprecipitation method[2], using ammonium hydroxide as precipitant agent.

The products were analyzed by X-Ray Diffraction (XRD) and Diffuse Reflectance Ultraviolet Spectroscopy (DRS). These techniques allow to study structural and electronic properties of the obtained products. From XRD data, the Rietveld refinement was performed and it abled the study of the oxides microstrains. From DRS data, the optic band gap analysis of the zinc oxide and its doped systems was possible.

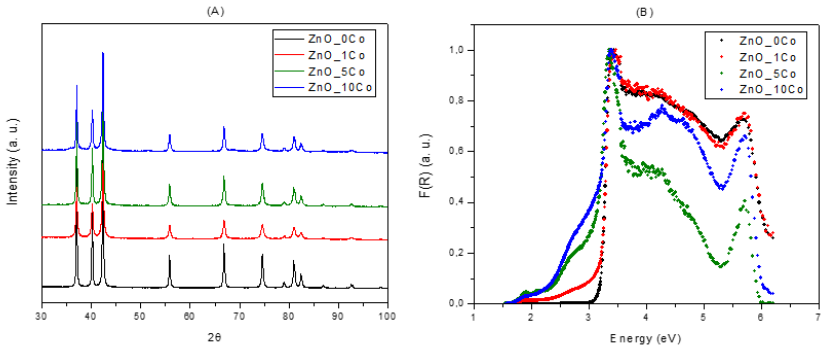

Figure 1. Analysis of (A) XRD and (B) DRS from the samples.

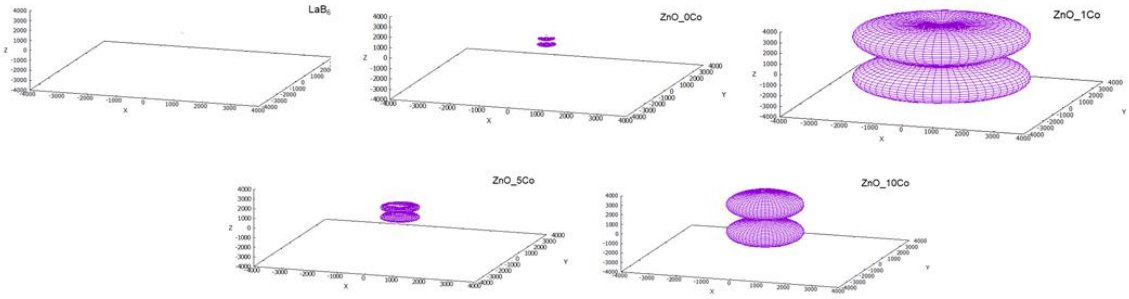

Figure 2. 3D plot microstrains for standard (LaB_6) and samples.

As shown in Fig. 1, there were no structural changes in XRD and slight variations in band gap, 3.24 eV for ZnO, 3.22 eV for ZnO (1% Co), 3.10 eV for ZnO (5% Co) and 3.15 eV for ZnO (10% Co). The 3D plot microstrains (Fig. 2) indicate that the samples with the largest microstrains were those which contain cobalt ions on the lattice. These microstrains can be attributed to the variation of the Shannon radii for the Zn^{2+} and Co^{2+} ions, 0,74 e 0,72 Å, respectively.

[1] RUAS, B. O. **Análise Microestrutural do Óxido de Zinco e do Óxido de Zinco Dopado.** 2018. 60 f. Monografia (Graduação em Química) – Instituto de Química, Universidade Federal Fluminense, Rio de Janeiro, 2018.

[2] Giovanelli, F.; Ndimba P. N. *et. al. Powder Tecnology*, **v. 262**, p. 203-208 (2014).

Acknowledgements: FAPERJ; CNPq; UFF; LAME-UFF; LDRX-UFF.

Síntese de nanopartículas superparamagnéticas de ferrita de cobalto ($CoFe_2O_4$), utilizando um forno de lâmpadas halógenas

A. O. G. Maia[a,b], J. M. Sasaki[b] , E. S. Teixeira[b].

[a] *De licença do Instituto Federal do Rio Grande do Norte, Mossoró-RN, Brasil.*
[b]*Departamento de Eng. e Ciências de Materiais, Universidade Federal do Ceará, Fotaleza-CE, Brasil.*

.

Atualmente, nanopartículas superparamagnéticas têm sido o alvo de muitos estudos devido as suas inúmeras aplicações tecnológicas, como por exemplo em ferrofluidos, em separadores de células e em removedores de poluentes. A propriedade de superparamagnetismo está diretamente ligada ao tamanho das nanopartículas magnéticas. Somente nanopartículas com diâmetro menor que 30 nm podem ser superparamagnéticas. Quanto mais esférica e maior uniformidade da amostra, maior será a eficiência das nanopartículas. Nesse trabalho, nanopartículas de ferrita de cobalto ($CoFe_2O_4$) foram produzidas pelo método sol-gel protéico, que utiliza gelatina como precursor orgânico[1]. A solução foi calcinada a 400^{o}C por 30, 60, 90 e 120 min em um forno bipartido tubular, cuja fonte de calor são 6 lâmpadas halógenas, com potência de 1000W por lâmpada [1, 2]. O forno atinge uma taxa de aquecimento de 100^{o}C/min e um sistema de refrigeração (água) é acionado após o tempo de síntese, a uma taxa de resfriamento média de 20^{o}C/min. Um fluxo de ar de 100 ml/min foi utilizado na oxidação das amostras no momento das calcinações. Essas altas taxas de aquecimento e resfriamento produziram nanopartículas, aproximadamente esféricas, com tamanho médio de 6 nm. Os refinamentos dos dados extraídos da medida de DRX das amostras foram feitos utilizando o Método Rietveld[3]. O tamanho de partícula e a microdeformação foram calculados pela equação de Scherrer[4], pelo gráfico de Williamson-Hall[4] e pelo gráfico Size-Strain[4]. Medidas de MET foram feitas e o tamanho reduzido das nanopartículas foi comprovado. Medidas de VSM foram feitas e o caráter superparamagnético das nanopartículas foi comprovado.

[1] J. A. Carvalho, Dissertação de Mestrado, Universidade Federal do Ceará - UFC, Fortaleza-CE (2011).

[2] J. M. Sasaki, C. T. Menezes, *Acta Crystallographica*, A64, C180-181 (2008).

[3] R. A. Young, *The Rietveld Method*, Oxford Science Publications - IUCr (1995).

[4] S. Sarkar, R. Das, *Journal of Nondestructive Evaluation,* Vol. 38, Pages 9-16 (2018).

Agradecimentos: UFC, IFRN, LRX, CNPq e CAPES

New iron telluride obtained by mechanochemistry

K.F. Ulbrich[a], C.E.M Campos[a]

[a]*Departamento de Física, Universidade Federal de Santa Catarina, Florianópolis, Brasil.*

A new nanocrystalline iron-rich telluride, Fe_5Te_4, was prepared mechanochemically using ball milling procedures in an inert atmosphere. Elemental Fe and Te powders were used in binary mixtures with nominal compositions Fe_xTe, with x = 1.0, 1.25 and 1.5, with x = 1.25 leading to the pure phase. Its crystal structure has a tetragonal (I4/m) symmetry and shows an anomalously short Fe–Fe interaction of 2.52 Å. The microstructure of the nanocrystalline material was studied by synchrotron X-ray total scattering techniques and the Debye scattering equation (DSE) method. Anisotropic micro-strain model developed with ε_{ab} = 0.85% and ε_c = 0.35%, suggest a much larger plasticity of the material in the *ab*-plane. DSE simulations shows bi-modal size distributions, one centered in 20.0 nm and other in 4.0 nm, the relative weight percentages were estimated to be 56% and 44%, respectively [1].

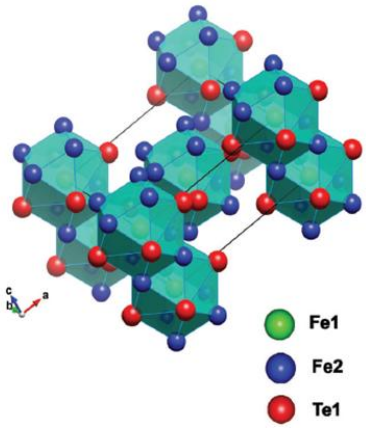

Figure 1: A view of the crystal packing of Fe_5Te_4, highlighting the fused pseudo-cuboctahedral coordination polyhedra about Fe1 atoms [1].

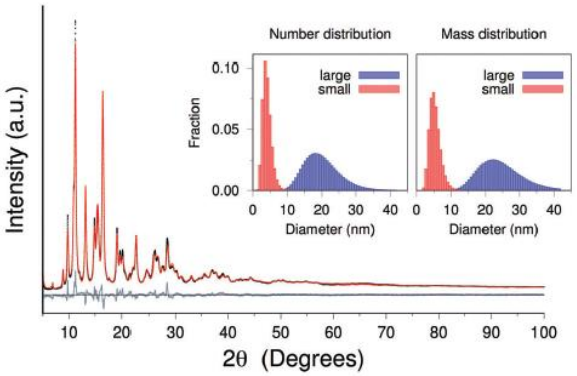

Figure 2: The full pattern matching of synchrotron X-ray total scattering data by the DSE model and the pertinent (number- and mass-based) bi-modal log-normal distributions [1].

[1] K.F. Ulbrich, F. Bertolotti, N. Masciocchi, A. Cervellino, A. Guagliardi and C.E.M. Campos, Journal Materials Chemistry C, vol.6, pp. 3047-3057 (2018).

Acknowlegments: We are grateful to the Brazilian agencies CNPq, CAPES and FAPESC for financial support and X04SA-MS beamline of the Swiss Light Source for technical support. Powder diffraction experiments were performed at LDRX multiuser laboratory at UFSC.

Síntese e caracterização estrutural, óptica e morfológica do nanocompósito híbrido baseado em polifluoreno e nanopartículas de óxido de európio

André A. Ferreira[a], Dennis A. Turchetti[b], Alisson J. Santana[b], Leni Akcelrud[b], Yvonne P. Mascarenhas[c].

[a] *Universidade de São Paulo, Escola de Engenharia de São Carlos, SP, Brazil.*
[b] *Universidade Federal do Paraná, Departamento de Química, PR, Brazil.*
[c] *Universidade de São Paulo, Instituto de Física de São Carlos, SP, Brazil.*

O objeto desta pesquisa foi a síntese e caracterização de um nanocompósito híbrido baseado em polifluoreno (PFO) e nanopartículas de óxido de európio (n-Eu_2O_3). Iniciando-se pela técnica de difração de raios X (DRX), verificou-se o caráter semicristalino do PFO e o perfil cristalino das nanopartículas (n-Eu_2O_3) e do contaminante $Eu(OH)_3$ que passaram a ser designadas como n-Eu_2O_3/$Eu(OH)_3$. O perfil de difração do nanocompósito híbrido n-Eu_2O_3/$Eu(OH)_3$@PFO mostrou a superposição dos perfis da fase amorfa e da semicristalina de PFO e das fases cristalinas de n-Eu_2O_3/$Eu(OH)_3$. A desconvolução dos picos de difração mostrou que o percentual de cristalinidade do PFO no nanocompósito híbrido aumenta cerca de 11% em relação do PFO puro. O refinamento dos parâmetros de cela unitária pelo método de Le Bail confirmou a cela unitária com dimensões $a=13{,}63Å$ $b=21{,}26Å$ e $c=33{,}71Å$ e $\alpha=\beta=\gamma=90^o$ para a fase-β do PFO. Além disso observou-se o aumento do tamanho médio dos cristalitos do PFO no nanocompósito. Foram obtidas também as celas unitárias cúbicas e hexagonais do Eu_2O_3 e do $Eu(OH)_3$ que compõem as n-Eu_2O_3/$Eu(OH)_3$ e notou-se que estas não sofrem alteração no nanocompósito. A microscopia eletrônica de varredura (MEV) mostrou a morfologia de nanopartículas do PFO e das nanopartículas n-Eu_2O_3/$Eu(OH)_3$ e constatou-se o sistema core@shell, com nanopartículas do PFO de fase β recobrindo placas de nanopartículas n-Eu_2O_3/$Eu(OH)_3$ e que estas apresentam uma forma oblata. A realização de espectroscopia por transformada de Fourier (FTIR) mostrou que o nanocompósito se forma a partir de interações físicas. A análise dos espectros de fotoluminescência das amostras poliméricas mostrou que a emissão do polímero foi favorecida devido à adsorção das cadeias poliméricas sobre as nanopartículas n-Eu_2O_3/$Eu(OH)_3$ e consequente aumento tanto da cristalinidade dos nanocristais como do tamanho médio dos cristalitos de PFO no nanocompósito.

Referências:

[1] PECHER, J.; MECKING, S.; **Chemical Reviews**, v. 110, p. 6260–6279, 2010.

[2] PECHARSKY, V.; ZAVALIJ, P. Y.; **Springer US**, v. 2, p. 348-405, 2005.

[3] LIU, C.; Wang, C.; **Macromolecules**, v. 46, p. 3025–3030, 2013.

Agradecimentos: Fundação de Amparo CAPES No. 88882.180154/2007-01, André A. Ferreira. CNPq No. 306036/2016-9, Yvonne P. Mascarenhas. CNPq No. 150757/2017-4, Denis A. Turchetti

INFLUENCE OF CONSTRUCTION WASTE GYPSUM DRYING CONDITIONS ON THEIR CRYSTALLINE CHARACTERISTICS

H.C. Cordon[a,c], B.S. Domingues[b], K. Andreola[b], M. Nitz[b], L.F.G. Souza[b], F.F. Ferreira[c].

[a]Eng. Civil, [b]Eng. Química, Instituto Mauá de Tecnologia, São Caetano do Sul, Brasil.
[c]Centro de Ciências Naturais e Humanas, Universidade Federal do ABC, Santo André, Brasil.

Due to its fast setting time, which corresponds to the useful life of the material from its mixing with water to its hardening, construction plaster (β-hemihydrate – $CaSO_4 \cdot 0.5H_2O$) is a widely used material for the internal lining of walls, as it improves productivity. However, this characteristic also contributes to the high material waste, which hardens before application, generating a large amount of residue (dihydrate – $CaSO_4 \cdot 2H_2O$). If ground and calcined at temperatures between 120 °C and 150 °C, the gypsum waste becomes a binder material having the same chemical formula as the source material[1].

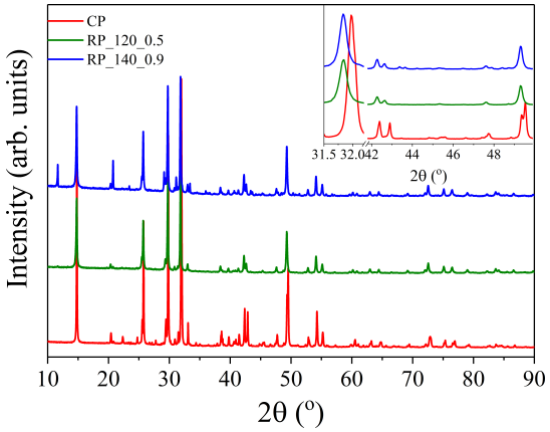

Figure 1: Comparison of diffractograms of plaster samples.

In this work, the construction plaster acquired in São Paulo construction market was hydrated with a 60%-mass content of water to produce the residue, and thus dried and ground in an electric hammer mill. Then, it was calcined under different drying conditions (120 °C with air velocity equal to 0.5 $m \cdot s^{-1}$ and 140 °C with air velocity equal to 0.9 $m \cdot s^{-1}$) in a tray dryer.

X-ray powder diffraction (XRPD) data were used to perform quantitative phase analyses (QPA) by means of Rietveld refinements and the results are shown in Table 1.

Table 1: QPA (wt%) of the compounds present in the samples.

Sample	Gypsum	Bassanite	Anhydrite	Dolomite
CP	-	93.8(4)	4.1(3)	2.2(2)
RG_120_0.5	0.6(2)	94.2(9)	3.3(5)	1.9(4)
RG_140_0.9	10.1(10)	85.9(13)	2.7(3)	1.3(3)

The inset in Figure 1 displays three important differences between the commercial and recycled samples: (i) the displacement to lower angles of the peak located between 31.6° and 32.0° (2θ); (ii) approximation of the peaks in the 42.5° (2θ) region and (iii) the change in the peak located at 49.5° (2θ), which was "split" in two in the commercial sample and became unique in the recycled samples, indicating some structural change in the bassanite phase. This same effect was reported by Schmidt et al.[2] using X-ray powder diffraction data of calcium sulfate subhydrates ($CaSO_4 \cdot 0.5H_2O$ and $CaSO_4 \cdot 0.625H_2O$) samples submitted to 30% and 75% relative humidity, respectively. The change in the crystal structure of bassanite phase is due to the probable difference between the calcination conditions of the gypsum that gave rise to the plaster, which was not controlled once the product was purchased ready, and the waste produced in laboratory.

[1] Cordon, H.C.F., Cagnoni, F.C., Ferreira, F.F., *J Build. Eng.*, **22**, 504-12 (2009).

[2] Schmidt, H., Paschke, I., Freyer, D., Voigt, W., *Acta Crystallogr. B*, **67**, 467–75 (2011).

Acknowledgments: Instituto Mauá de Tecnologia, LCCEM (UFABC), CNPq (307664/2015-5).

Non-Ambient Analysis at HARPIA bemaline at Sirius

F. R. Estrada[a], I. B. B. Rêgo[a], C. R. Oliveira[a], D. H. Barrett[a,b], A. Iglessias[a], C. B. Rodella[a]

[a] *Brazilian Synchrotron Light Laboratory (LNLS), Brazilian Center for Research in Energy and Materials (CNPEM), Campinas, Brazil.*

[b]*Chemistry Department, University of the Witwatersrand, Johannesburg, South Africa.*

At Sirius, the new 4th generation synchrotron facility, HARPIA beamline is the planned Powder X-ray diffraction beamline, which is going to provide outstanding capabilities for time resolved data acquisition as well as for the highest resolution XRD measurements possible in South America. The beamline aims to support a wide range of *in-situ* and *operando* experiments to investigate the structural modification of function materials of a wide range of areas, such as minerals, catalysis, storage energy materials and devices, electronics, ceramics, metallurgy, and pharmaceutical sciences, for instance. This undulator beamline is going to operate from 5 to 30keV in Debye-Scherrer geometry (3-circle diffractometer) to deliver high photon flux (10000 times higher than at LNLS) and an array of fast detectors (*in-house* development). HARPIA's design permits not only ambient, cryogenic or high temperatures (up to 800°C) but also dynamic experiments using cell reactors in capillary geometry, which the instrumentation is draw at Figure 1.

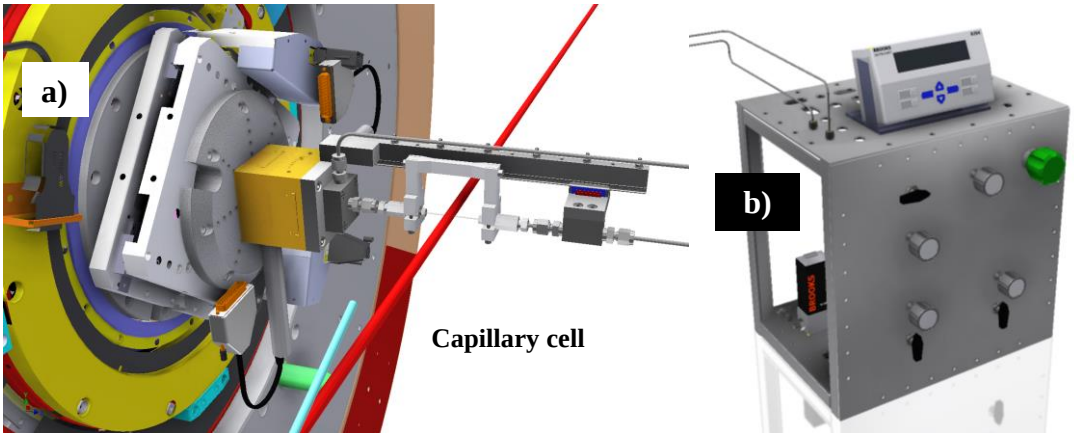

Figure 1: a) Capillary cell installed in the theta-circle of the HARPIA´s diffractometer; red line indicates the x-ray beam direction and b) support installation supplying equipment to pressure control, gas and liquid flow controllers and valves.

Plug and flow capillary cell reactors developed at the LNLS (Fig. 1a) were upgraded to operate in high pressure (up to 50bar) with gaseous flow as well as liquids phase through the powder sample. The samples can be heated up or cooled down at controlled ratios with a hot air blower or a cryojet, respectively. Moreover, the gas and liquid phases will be separated in the outlet of the cell to the gas composition be analyzed in a mass spectrometer or micro-GC. Mas flow meters, back pressure valve and HPLC pumps will be installed in box (Fig. 1 b) which will be placed in table close to the cell reactor. Furthermore, a new motorized mini Newport goniometer will be purchased to the capillary cell be connected at the theta-circle of the diffractometer. This will allow a fast and precise sample alignment during the experiment. The entire set up was planned to be robust, easy and fast to be installed at the beamline.

Acknowlegments: FAPESP (2015/22711-1 and 2017/50261-6) and CNPEM.

Largura intrínseca de absorção

A. N. C. Lima[a], M. A. R. Miranda[b], J. M. Sasaki[b]
[a]*Departamento de Engenharia Metalúrgica e de Materiais, Universidade Federal do Ceará, Fortaleza, Brasil.*
[b]*Departamento de Física,Universidade Federal do Ceará, Fortaleza, Brasil.*

A difração de raios X é bem compreendida, graças a mais de um século de estudos. Suas diversas formulações facilitam seu entendimento e uso como técnica de caracterização, pois pode-se optar pela formulação mais simples que descreve satisfatoriamente o caso estudado. Com o avanço dos síncrotrons são desenvolvidas novas técnicas de caracterização por difração de raios X, e com elas há a necessidade de formulações simples que as descrevam. Por exemplo, a difração ressonante de raios X mole, que teve seu desenvolvimento nas últimas duas décadas, é a única técnica para a medição atômica seletiva de correlações spin, carga e orbital. No trabalho intitulado: *X-ray diffraction in superabsorbing crystals: absorption intrinsic width*[1] desenvolvemos uma expressa analítica que descreve o perfil de difração de raios X mole. Consideramos a difração de raios de comprimento de onda λ por um cristal de coeficiente de absorção μ_0, espessura D, e formado por planos atômicos de extensão lateral ilimitada, para o caso Bragg simétrico com ângulo de Bragg θ_B. Para raios X mole a absorção dos cristais é muito grande, por isso chamamos de cristais superabsorvedores, e podemos desprezar efeito de extinção. O perfil de difração de cristal superabsorvedor é o resultado da interferência entre as ondas espalhadas e da atenuação causada pela absorção. Obtemos o perfil em função da espessura do cristal, do coeficiente de absorção, do ângulo de Bragg e do comprimento de onda. Para cristal pequeno e/ou $\mu_0=0$ o perfil de difração de cristal superabsorvedor coincide com o perfil da teoria cinemática. A largura a meia altura do perfil de difração de cristal superabsorvedor ($FWHM_\mu$) foi calculada numericamente em função da espessura do cristal, ver Figura 1a. A $FWHM_\mu$ diminui com o aumento de D até atingir a largura intrínseca de absorção dada por

$$\Delta_\mu = \frac{2\mu_0\lambda}{\pi \sin 2\theta_B} .$$

Com o aumento de D o perfil de difração de cristal superabsorvedor perde as franjas de interferência até atingir o perfil intrínseco de absorção, que tem forma lorentziana, ver Figura 1b. A largura intrínseca de absorção, expressa em termo da parte imaginária do fator de estrutura, se assemelha à largura de Darwin, pois ambas são causadas pela atenuação dos raios X com a penetração. A formulação do perfil de difração de cristal superabsorvedor fornece novas perspectivas para a difração ressonante de raios X mole.

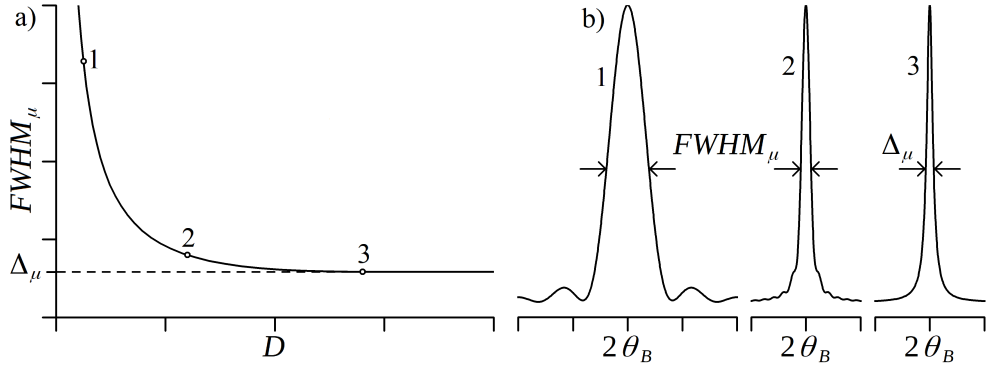

Figura 1: a) Comportament da $FWHM_\mu$ com D. b) Perfil de difração de raios X de cristal superabsorvedor para diferentes espessuras.

[1] Lima, A. N. C., Miranda, M. A. R., Sasaki, J. M., Acta Cryst. A, **75**, 772–776, (2019).

Agradecimentos: FUNCAP; CNPq; CAPES.

HARPIA: High Resolution Powder X-ray Diffraction beamline at Sirius

F. R. Estrada[a], A. Iglessias[a], D. H. Barrett[a,b], V. K. Silva[a], I. B. B. Rêgo[a], C. R. Oliveira[a], C. B. Rodella[a]

[a] *Brazilian Synchrotron Light Laboratory (LNLS), Brazilian Center for Research in Energy and Materials (CNPEM), Campinas, Brazil.*

[b]*Chemistry Department, University of the Witwatersrand, Johannesburg, South Africa.*

Sirius is a fourth-generation synchrotron light source built at the CNPEM and is forecast to begin operations in 2020. Brazil is transitioning from a second-generation synchrotron source (UVX) to a leading position in the design and operation of the brightest 4th-generation machine in its energy class. This multidisciplinary research infrastructure will bring an advanced facility to the structural characterization of polycrystalline samples – HARPIA beamline. The synchrotron radiation source of HARPIA will be an undulator with an 18 mm period length and importantly, without an energy gap. The beamline will be installed in a low-β straight section of the storage ring to increase the beam size in the horizontal direction. HARPIA's optical design aims to be simple, yet highly effective to provide high photon flux at the sample position, H 2.210^{12} ph/s/100 mA at 20 keV, about 1000 times higher than that of the LNLS at 8 keV. Energy selection will be obtained by the Bruker double-crystal-monochromator from the XDS beamline at the LNLS. The two sets of Si crystals, (111) and (311), will allow an energy range from 5 to 30 keV. The beam size at the sample position is calculated to be around 0.85 mm (v) x 1.2 mm (h) with a divergence of 25 μrad (v) x 34 μrad (h) at 20 keV. HARPIA's experimental hutch (Fig. 1) will provide high-resolution X-ray diffraction data with a multi-analyser crystal from FMB Oxford having at least 8 modulus of Si(111) crystals and $NaBr_2$ scintillators detectors. Moreover, it will allow dynamic experiments using a linear fast detector developed in house covering 90° in 2θ range to provide second scale temporal resolution.

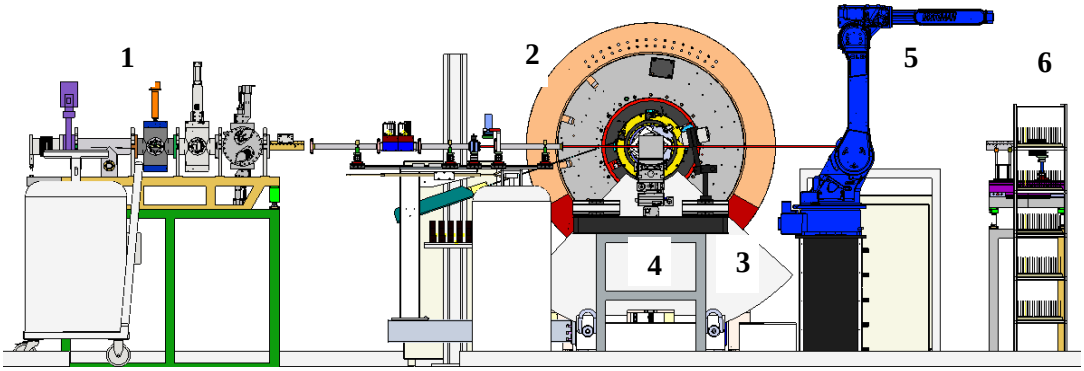

Figure 1: Experimental hutch of HARPIA beamline showing: 1. optical systems (shutter slits, beam monitors, filters); 2. 3-circle diffractometer; 3. in-house linear detector; 4. optical table; 5. robotic arm and 6. sample´s magazine.

The 3 co-axial circle heavy-duty diffractometer from the current XRD1 beamline at LNLS (Fig. 1.2) will be transferred to the HARPIA experimental hutch. X-ray diffraction measurements will be conducted in Debye-Scherrer geometry (capillary geometry). The diffractometer uses high precision rotary stages (Θ, 2Θ and d axes) and are designed to support heavy detector arrays, such as the two sets of detectors in the aforementioned paragraph.

A storage magazine for samples placed into capillaries (Fig. 1.6) allows hundreds of samples to be loaded and measured via the use of a robotic arm which serves as a sample exchanger. The robotic arm allows for the beamline to be programmed and, if necessary, operated remotely providing high levels of efficiency and maximization of the provided beamtime. HARPIA beamline will provide an efficient and user-friendly facility to the structural characterization of polycrystals in a variety of sample environments as well as fast and high-resolution mode detection to Sirius users.

Acknowlegments: FAPESP and CNPEM

SYNTHESIS AND CHARACTERIZATION OF $Cs_2AgSbCl_6$ DOUBLE PEROVSKITE

C. A. Escanhoela Jr[a], G. Sombrio[a], J. A. Souza[a], and F. F. Ferreira[a].

[a]*Centro de Ciências Naturais e Humanas, Universidade Federal do ABC, Santro André, Brazil.*

The double perovskites ($A_2B'B''O_6$) are derived from the ABO_3 perovskites when half of the octahedrally coordinated B'-cations are replaced by the suitable B"-cations. They have been attracting attention due to their interesting physical properties, which could be explored for several applications, such as ferromagnetism, giant dielectric characteristics, and magnetoresistance. The B'-O-B'' electronic interaction plays an important role in charge carries transport. Furthermore, theoretical studies predict bandgap absorption between 1.4 and 1.9 eV resulting in a strong sunlight absorption [1]. They also have small carrier life, small carrier effective masses and high defect tolerance which are favourable characteristics for photovoltaic and photocatalysis [2].

The aim of this study was the synthesis and characterization of $Cs_2AgSbCl_6$ powdered samples looking for solar cell application. The samples were synthesized by solid state reaction using different solvents (Ethanol, Isopropyl, Toluene and Oleic Acid). The crystalline phase and morphological features were investigated by X-ray powder diffraction (XRPD) and scanning electron microscopy (SEM). The results showed that this synthesis method proved to be efficient to obtain polycrystalline-$Cs_2AgSbCl_6$ samples. In Figure 1, the X-ray diffractograms showed that the samples mainly crystallized in a cubic phase (Fm-3m) and a minor amount AgCl phase was also observed. The SEM images showed the obtained crystals have an octahedral shape. The size of the octahedral particles was about 25-50 µm, depending of the synthesis solvent.

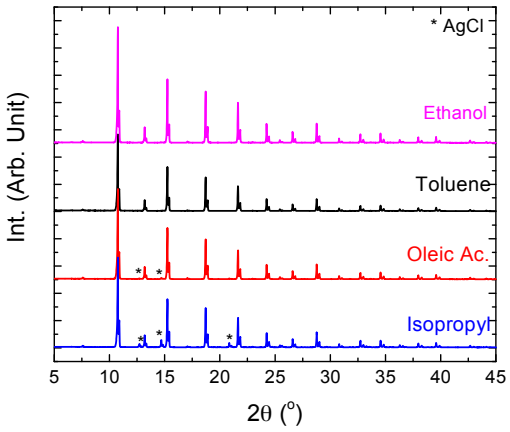

Figure 1: The diffraction pattern of $Cs_2AgSbCl_6$ samples obtained with different solvents.

The electrical and optical properties of the samples will be evaluated looking their application as solar cells.

[1] Sun, Q. et al. Oxide perovskites, double perovskites and derivatives for electrocatalysis, photocatalysis, and photovoltaics. Energy Environ. Sci. **12**, (2018).

[2] Deng, W. et al. Synthesis of $Cs_2AgSbCl_6$ and improved optoelectronic properties of $Cs_2AgSbCl_6/TiO_2$ heterostructure driven by the interface effect for lead-free double perovskites solar cells. Appl. Phys. Lett. **111**, 2–7 (2017).

Acknowledgments: This work is supported by the Brazilian agency CNPq under grants No. 307950/2017-4 and 307664/2015-5, FAPESP under grants No. 2019/01785-8, 2017/02317-2 and 2018/15682-3 and CAPES-PNPD under grants No. 88887 337951/2019-00.

Síntese e recristalização da etringita ($3CaO.Al_2O_3.3CaSO_4.32H_2O$)

T. R. S. Nobre[a], L. Leone[b] , M. H. Maciel[a], S. C. Angulo[a], A. C. V. Coelho[b].

[a]*Escola Politécnica, Departamento de Engenharia Civil (PCC), USP, São Paulo, Brasil.*
[b]*Escola Politécnica, Departamento de Engenharia Metalúrgica e de Materiais (PMT), USP, São Paulo, Brasil.*

As sínteses laboratoriais convencionais, em relação as obtidas por ativação mecanoquímica requerem maior tempo, maior consumo de energia e, algumas vezes, geram emissões de CO_2. Além disso, a ativação mecanoquímica pode melhorar a reatividade e rendimentos dos produtos formados. Especificamente nesta pesquisa, esse processo foi empregado para sintetizar a etringita, $3CaO.Al_2O_3.3CaSO_4.32H_2O$, também denominada de trissulfoaluminato de cálcio hidratado (AFt), uma fase importante formada durante a hidratação do cimento Portland [1]. A etringita é composta por uma estrutura de duas colunas de $[Ca_3Al(OH)_6 \bullet 12H_2O]^{3+}$, de natureza catiônica, preenchida, dentro do canal interlamelar, por ânions, como sulfato (SO_4^{2-}) e hidroxilas (OH^-) [2]. O mecanismo de decomposição térmica desta fase tem sido amplamente estudado nos últimos anos. Sua estabilidade térmica é afetada pela faixa de temperatura. Alguns autores reportam complementarmente a sua capacidade de reidratação e recristalização na presença de água; porém ainda pouco investigada na literatura. Sabe-se que em cimentos reciclados em temperaturas até 600 graus, a reformação da etringita é observada. Nesta pesquisa estudou-se a decomposição, a reatividade e reformação da etringita, após reidratação, procurando compreender melhor seu processo de reciclagem e formas de controle durante a mistura com a água. Para a síntese da etringita os reagentes utilizados foram hidróxido de cálcio p.a., hidróxido de alumínio p.a., sulfato de cálcio dihidratado p.a. e água destilada. Na moagem utilizou-se moinho planetário Fritsch, jarro de aço com capacidade 500 mL e esferas de aço. As misturas foram realizadas em temperatura ambiente com 600 rpm de rotação. Utilizou-se a técnica de Difratometria de Raios X (DRX) para identificação de fases, incluindo outros ensaios como calorimetria e microscopia eletrônica de varredura (MEV).

Observou-se que a síntese da etringita foi otimizada e obtida em apenas 3 h. Após a calcinação, à temperatura de 300°C por 2 h, ocorreu a perda de cristalinidade da etringita, tornando-se parcialmente amorfa devido às perdas de moléculas de H_2O. Fases de bassanita e gipsita foram detectadas por DRX, as quais sugerem que a reação não é totalmente por desidratação, mas pela decomposição da etringita em outras duas fases, conforme descrito na Equação 1.

$$3CaO \cdot Al_2O_3 \cdot 3CaSO_4 \cdot 32H_2O \underset{+H_2O}{\overset{300°C\ 4h}{\rightleftarrows}} 3CaO \cdot Al_2O_3 \cdot CaSO_4 \cdot 12H_2O + CaSO_4 \cdot 0{,}5H_2O + CaSO_4 + 19{,}5H_2O \quad (Equação\ 1)$$

A regeneração da etringita foi comprovada por meio da calorimetria isotérmica e por meio de DRX. Verificou-se um pico exotérmico logo nos primeiros minutos de reidratação. A reidratação da AFt ocorreu de forma rápida, com estrutura e morfologia em forma acicular semelhantes à inicial, porém, com aspectos menos cristalinos (Figura 1). Assim, o processo de regeneração da AFt foi confirmado dentro das condições adotadas nesta pesquisa.

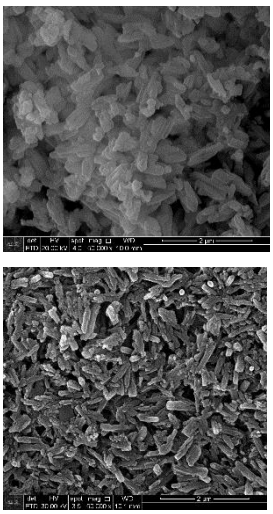

Figura 1: Micrografia da etringita antes e após a regeneração.

[1] KANO, J.; YAMASHITA, H.; SAITO, F. **Powder Technology**, v. 98, n. 3, p. 279–280, 1998.

[2] ZHOU, Q.; LACHOWSKI, E. E.; GLASSER, F. P. **Cement and Concrete Research**, v. 34, n. 4, p. 703–710, 2004.

Agradecimentos: à FUSP, INCT — Advanced Eco-efficient Cement-based Technologies (aeCEM) e ao CNPq pelo suporte financeiro - Projeto Nº 28/2018 - Universal.

APPLYING THE PDF METHOD IN DRUG ANALYSIS @ LCCEM: POTENTIALITIES

V. D. N. Bezzona, G. L. B. de Araújob, F. F. Ferreiraa

aCenter for Natural and Human Sciences (CCNH), UFABC, Santo André-SP, Brazil
bDepartment of Pharmacy, USP, São Paulo-SP, Brazil

The "Laboratory of Crystallography and Structural Characterization of Materials" (LCCEM) at the Federal University of ABC, Santo André-SP, Brazil, has been developing several types of analysis using X-ray powder diffraction data, which includes structure determination and quantitative phase analysis (QPA) of organic and inorganic materials. Recently, we have developed studies based on X-ray total scattering data and the pair distribution function (PDF) method allowing less ordered structures (amorphous and nanosized samples) to be properly characterized. All the improvements on materials structure characterization are feasible due the use of a high-resolution diffractometer (model STADI-P, STOE®) equipped with a Mo radiation ($K\alpha_1$) source that provides higher momentum transfer (Q_{max}) to be reached – improving considerably the spatial resolution – when compared to Cu radiation data analysis[1].

The main potentiality for PDF application at LCCEM is on drug analysis. An example of such successful PDF use is for the flubendazole active pharmaceutical ingredient. This drug was used as a model structure to compare PDF patterns obtained at LCCEM (using the STADI-P diffractometer) and at the Advanced Photon Source facility (APS beamline 6-ID-D) and the results obtained are shown in figure 1. Although the APS facility allows one to obtain data with higher counting statistics – thus providing low-noise data – as can be seen comparing the structure function $S(Q)$ patterns, the final STADI-P PDF pattern ($G(R)$) is comparable to the APS one, considering the same Q_{max} interval for the data treatment. The results allowed us to find out the intramolecular region up to 3.5 Å from the molecule distances (*i.e.*, from aromatic rings), intra *plus* intermolecular distances where interaction may occur up to 6.0 Å (*i.e.*, when using polymer matrix to load drug), and intermolecular distances beyond 6.0 Å where structural coherence is available. It is worth noting that the use of laboratory data can guide and improve ongoing studies before going to synchrotron facilities.

Finally, LCCEM is able to offer several categories of X-ray powder diffraction analysis – from room temperature up to 1000 ºC – using different methods like Rietveld, PDF and direct methods. In this way, various kinds of researches can be performed.

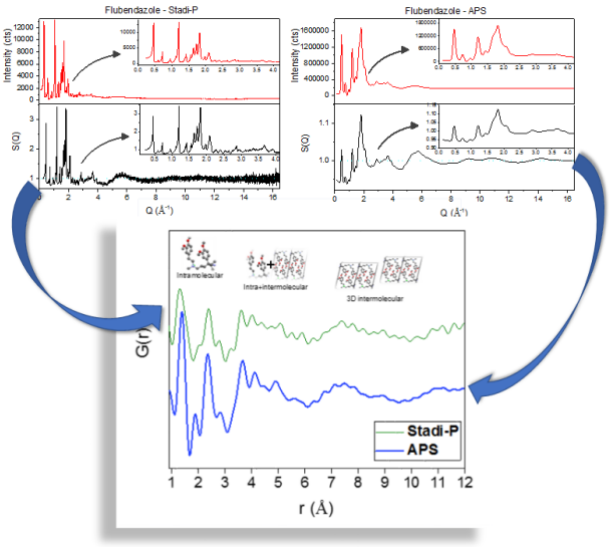

Figure 1: Comparison between LCCEM and APS results.

[1] Dykhne T, Taylor R, Florence A, Billinge SL. *Pharmaceutical Research*, **28**, pp 1041-1048 (2011).

Acknowledgments: Fundação de Amparo à Pesquisa do Estado de SP (FAPESP; proc. n. 11990-5/2018), CNPq (307664/2015-5).

Correlação entre estrutura cristalina e espectro vibracional no sistema $(Sr_{1-x}A_x)_2IrO_4$ (A=Ca, Ba)

A. I. Morales, K. Samanta, e E. Granado.

Instituto de Física "Gleb Wataghin", Universidade Estadual de Campinas, São Paulo, Brasil.

Sistemas eletrônicos com alta correlação eletrônica e acoplamento spin-órbita são ingredientes que podem levar a propriedades atraentes nos materiais. Um material com esta particularidade é o sistema Sr_2IrO_4, com características eletrônicas similares ao cuprato La_2CuO_4. No entanto, o Sr_2IrO_4 e suas variantes dopadas podem apresentar outras fases eletrônicas que precisam ser melhor compreendidas. Uma maneira de induzir variações estruturais e correlaciona-las com possíveis alterações eletrônicas é através da aplicação de pressão, seja ela de natureza química ou física. Nosso grupo recentemente completou um estudo envolvendo espalhamento Raman e difração de raios-X aplicando pressão hidrostática acima de 17GPa, que indica anomalias sutis nos parâmetros de rede mas grandes variações no espectro fonônico, que poderiam estar associados a uma mudança no estado fundamental eletrônico deste material [1]. Entretanto a pressão física também destrói a ordem magnética de longo alcance. Já a substituição de cátions isoeletrônicos como Ca e Ba no lugar do Sr, caracteriza uma pressão química no sistema, e tem mantido a ordem antiferromagnética. Neste estudo foram preparadas amostras policristalinas de Sr_2IrO_4 com substituição de Ca e Ba no sitio do Sr, através do método de reação em estado sólido. A caracterização estrutural das amostras foi realizada através de medidas de difração de pó no difratómetro Bruker D2 Phaser com radiação de raios X gerada pelo tubo de Cu com os comprimentos característicos $K\alpha1=1.5405Å$ e $K\alpha2=1.5443Å$. Estas medidas foram analisadas pelo método de Rietveld usando o software GSAS- EXPGUI (2001) com base da informação cristalográfica da estrutura Sr_2IrO_4 (ICSD N°195952) com simetria $I4_1/acd$. Os resultados foram uma compressão dos parâmetros de rede até $\Delta a/a_0 \sim 0.21\%$ e $\Delta c/c_0 \sim 0.18\%$ no caso da substituição de até 10% de Ca. No caso do Ba foi uma expansão de até $\Delta a/a_0 \sim 0.22\%$ e $\Delta c/c_0 \sim 0.28\%$ com 10% de Ba. Além disso, se observou um limite de miscibilidade de Ca e Ba na estrutura do Sr_2IrO_4 apresentando outras fases cristalinas coexistentes onde se identificou a fase $Sr_3CaIr_2O_4$ (ICSD N°196059) na amostra com 10% de Ca e na amostra com Ba não foi identificada. Também realizamos medidas de espectroscopia Raman, onde se observou uma mudança nas energias dos fônons. Discutiremos neste trabalho a correlação entre as variações no espectro Raman fonônico e a variação dos parâmetros de rede induzidos pela substituição de Ca e Ba na estrutura.

[1] K. Samanta, F. M. Ardito, N. M. Souza-Neto, E. Granado, Phys. Rev. B **98**, 094101 (2018).

Agradecimentos: Fundação de Amparo FAPESP; CNPq.

24th ABCr Meeting , Curitiba, October 2019

Study of Alloy (AuAg) Nanoparticle using Pair Distribution Function (PDF) derived from Precession Electron Diffraction (PED)

L. M. Corrêa, M. H. M. Moreira, V. Rodrigues, D. Ugarte

Physics Institute 'Gleb Wataghin', University of Campinas-UNICAMP, Brazil.

Usual crystal characterization techniques have been developed considering a periodic arrangement of atoms with long range order; these basic assumptions may make their use unsuited to characterize small crystals. Pair Distribution Function (PDF) has been successful in solving the structure of low ordered materials (amorphous, nanoparticles - NP)[1, 2, 3]. PDF can be derived from X-Ray Powder Diffraction (XRPD) data with high signal to noise ratio up to high scattering angles using synchrotron sources. Even using modern instrumentation, NP sample weighting several milligrams are required; this may represent a challenging issue in some research projects. To overcome this difficulty, we propose the use of PDF derived from Electron Diffraction. The strong electron-matter interaction allows a tiny sample quantity to be used (~ few ngr), but the incident electron can scatter several times inside the crystal (dynamical diffraction), complicating the interpretation of measured intensities. Using Precession Electron Diffraction (PED), measured intensities are quase-kinematical, allowing the use of x-ray approaches[4]. NP samples ($Au_{0.70}Ag_{0.30}$) were produced by a home-made cluster source at IFGW-Unicamp[5]. Experiments were realized using a TECNAI G2 200KV microscope equipped with Nanomegas ASTAR systems and axial CCD camera (LCE-DEMa-UFSCar). A home-made software, written in Python, was used for data analysis. Measured PED-PDFs have been quantitatively compared with different NP structures (fcc, decahedral, icosahedral, etc.). The smallest residue was obtained for ~3 nm decahedral NPs (~20%). This NP diameter is smaller than the mean diameter derived microscopy image (~6 nm), suggesting that the these particles are formed by the aggregation of smaller crystallites.

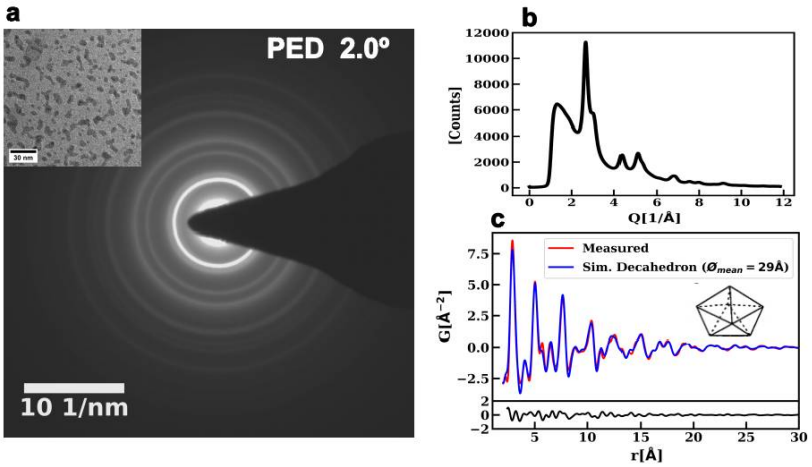

Figure 1: a) PED pattern of AuAg NPs. Inset: microscopy image of clusters. b) Azimuthal integration of ring pattern intensities (equivalent to XRPD). c) reduced PDF calculated from b).

[1] T. Egami, S. J. L. Billinge, Underneath the Bragg peaks: Structural Analysis of Complex Materials, Elsevier, Oxford (2003).

[2] S. Banerjee, et al. , J. Phys. Chem. C, **122**, 29498-29506 (2018).

[3] M. M. Hoque, et al., J. Phys. Chem. C, **123**, 32, 19894-19902 (2019).

[4] P. A. Midgley, A. S. Eggeman, IUCrJ, **2**, 126 – 136 (2015).

[5] A. D. de Sá, et. al., J. Vac. Sci. Technol. B, **32**, 061804 (2014).

Acknowlegments: CNPq; CAPES; FAPESP; LCE-DEMa-UFSCar; We are grateful to D. Coimbrão for assistance during PED work.

Temperature and pressure dependent x-ray powder diffraction study of $Ce_2Rh_{1-x}Ir_xIn_8$

R. P. Amaral[a], R. L. Serrano[a].

[a]*Instituto de Física, Universdade Federal de Uberlândia, Uberlândia, Brasil.*

Two superconducting (SC) phases were observed in the heavy-fermion system $Ce_2Rh_{1-x}Ir_xIn_8$: SC1 phase appears at Rh rich region and is induced by pressure; SC2 phase appears already at ambient pressure (as a dome centered around x ~ 0.6) and, in sharp contrast with the first transition, is progressively eliminated by application of pressure[1]. These strikingly opposite behaviors under the same tuning parameter indicate that the two phases may have different natures[2]. In order to study the evolution of unit cell parameters and to complement x-ray absorption studies we performed x-ray diffraction experiments. Small amounts of powdered samples were introduced into a diamond anvil cell (DAC) controlled by a membrane coupled to a gas pressure controller. The measurements were collected at 20 keV of incident x-ray energy. The overall evolution of the diffraction patterns with T and P shows no phase transition. The unit cell is compressed to higher pressures and this shifts the peaks positions to higher angles (Figure 1). No remarkable difference is observed among the four different measured temperatures. Figure 2 shows the evolution of volume compression and the c/a relation as a function of pressure (inset).

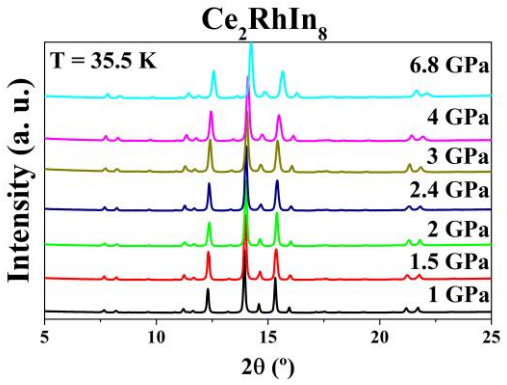

Figure 1: Ce_2RhIn_8 powder diffraction at different pressures.

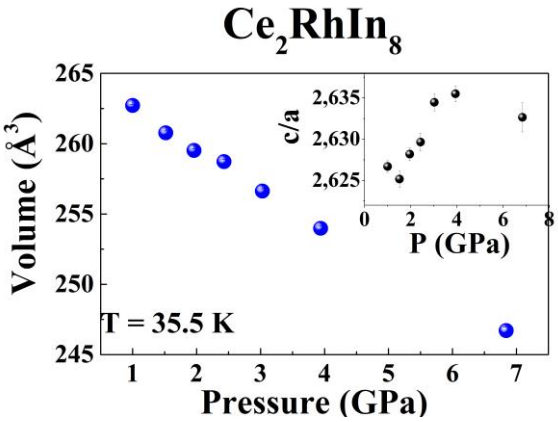

Figure 2: Ce_2RhIn_8 volume and c/a (inset) as a function of pressure.

[1] Hering, E. N., *Physics Review B*, **82**, 184517 (2010).

[2] Moshopoulou, E. G., *Acta Crystal. B*, **62**, 173 (2006).

Acknowlegments: Fundação de Amparo FAPEMIG; UFU; LNLS; for financial support.

Espalhamento Total: Desafios Experimentais na Redução de Dados e na Modelagem da Microestrutura de materiais nanoCristalinos feitos por Síntese Mecanoquímica

M. A. Malagutti, C. E. M. Campos*

Departamento de Física, Centro de Ciências Físicas e Matemática, Universidade Federal de Santa Catarina, Florianópolis, Brasil. (**calos.campos@ufsc.br*)

Através do estudo da cristalografia, pode-se compreender as duas principais metodologias para a análise de padrões de difração de raios X em policristais (XRPD, do termo em inglês X-Ray Powder Diffraction), uma usando o método de Rietveld[1] (via fator de estrutura) e a outra usando métodos de espalhamento total[2] (via equação de Debye) especialmente quando se almeja o estudo e caracterização de nanomateriais. Portanto, para esse trabalho, produziu-se alguns sulfetos e teluretos de Co através de sínteses mecanoquímicas, o que possibilitou fazer a análise dessas amostras usando tanto experimentos de XRPD em equipamentos de laboratório, como também através da realização de experimentos de espalhamento total de raios-X (do termo Wide Angle X-Ray Total Scattering - WAXTS) realizados na linha XRD1[3] da fonte de luz sincrotron Brasileira (LNLS) em maio deste ano. A partir dessas medias, pôde-se aprender o manejo de ferramentas computacionais para as análises supramencionadas, as quais estão implementadas nos pacotes de programas GSAS-II[4] (General Structure Analysis System) e DebUsSy[5] (Sistema para Usuários da função de Debye, tradução livre do inglês).

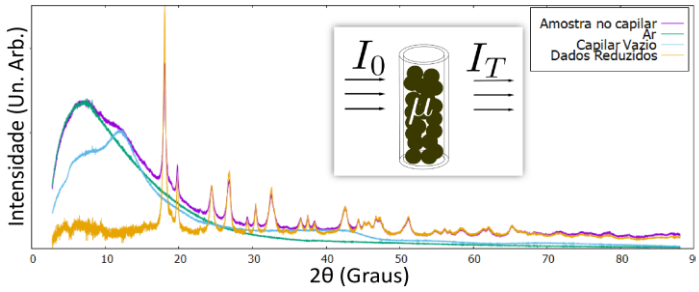

Figura 1: Padrões de difração da amostras no capilar, só do capilar e só do ar, obtidos em experimentos WAXTS usando geometria de transmissão. Podemos destacar também a redução dos dados levando em conta os fenômenos acima. A direita, temos uma ilustração da radiação a atravessar o capilar cilíndrico com a amostra.

Os motivos que levam a utilizar a equação de Debye é que a mesma toma em consideração o espalhamento difuso do material de forma não fenomenológica e permite modelar efeitos de deformação da rede cristalina em função do tamanho dos domínios cristalinos, os quais por sua vez podem ser modelados incluindo diferentes formas (esférica, cilíndrica, cúbica, etc.) junto a distribuições de tamanhos (monomodal, bimodal, etc.). Por esses motivos, técnicas baseadas na equação de Debye (notadamente WAXTS e PDF, do termo em inglês Pair Distribuction Function) são altamente recomendadas para análise de materiais em escala nanométrica. Porém, para atingir esse objetivo é necessário obter dados de difração isentos de contribuições experimentais (instrumentais, espalhamento do ar, sinal do porta amostra, capilar, etc.) e com as devidas correções devido a absorção e a densidade da amostra.

Com isso, essa apresentação visa mostrar detalhes dos experimentos de WAXTS na linha XRD1-LNLS e os primeiros avanços na redução de alguns dos dados obtidos para uso no DebUsSy. Também pretende-se ilustrar os passos na modelagem da microestrutura dos nanocristais (com forma esférica e distribuição monomodal) e as perspectivas de implementar efeitos de microdeformação (isotrópica e anisotrópica) a exemplo do que foi feito pelo nosso grupo de pesquisa em parceria com os pesquisadores Italianos do ToScaLab para amostras de Fe-Te[6]. Vale destacar que também foram realizados testes catalíticos e eletroanalíticos com as amostras produzidas a fim de poder correlacionar características da estrutura e microestrutura da(s) fase(s) cristalina(s) presente(s) nessas amostras com seu potencial de aplicação em produtos tecnológicos.

[1]McCysker, L. B., Von Dreele, R. B., Cox, D. E., Louër, D., Scardi, P.,*J. Appl. Cryst.* , **32**, 36-50 (1999).

[2]Gelisio, L., Scardi, P., *Acta Cryst*, **A 72**, 608-620 (2016).

[3]Carvalho, A. M. G., Araújo, D. H. C., Canova, H. F., Rodella, C. B., Barrett, D. H., Cuffini, S. L., Costa, R. N. Nunes, R. S., *J. Synchrotron Rad.*, **23**, 1501-1506 (2016).

[4]Toby, B. H., & Von Dreele, R. B. (2013). "GSAS-II: the genesis of a modern open-source all purpose crystallography software package". *Journal of Applied Crystallography*, **46**(2), 544-549.

[5]Cervellino, A., Giannini, C., Guagliardi, A.,*J. Appl. Cryst*, **43**, 1543-1547 (2010).

[6]Ulbrich, K. F., Bertolotti, F., Masciocchi, N., Cervellino, A., Guagliardi, A., Campos, C. E. M., J. Mater. Chem. C, 2018, **6**, 3047.

Agradecimentos: CNPq; CAPES; PPGFSC.

CHARACTERIZATION OF SEDIMENTS FROM THE FUNDÃO DAM FAILURE

M. T. D. ORLANDO[a], C. V. G. T. RANGEL[b], E. S. GALVÃO[a], C. G. P. ORLANDO[a], A. C. BASTOS[a] and V. S. QUARESMA[a]

[a] *Universidade Federal do Espírito Santo, Vitória, Brasil.*
[b] *Universidade Federal do Sul da Bahia), Porto Seguro, Bahia, BA, Brazil.*

RESUMO

O acidente com a barragem de Fundão, Mariana, MG, lançou toneladas de rejeitos de minério de ferro no sistema fluvial do Rio Doce [1]. Apesar da composição natural dos sedimentos fluviais, caracterizada por fases minerais relativamente comuns como quartzo, muscovita, caulinita e illita e até mesmo certos teores de hematita e goethita, é importante verificar a abundância de hematita e magnetita após o acidente. Os sedimentos pós-acidente da cidade de Mariana foram analisados por difração de raios X Sincrotron, EDXRF e suscetibilidade AC. Foi encontrado (além de magnetita e hematita num teor significativo maior que o naturalmente encontrado antes o acidente) a presença de $K_2Mn_2(SO_4)_3$ e $FeSO_4!H_2O$, que não foram registrados nos sedimentos naturais da mesma região antes do acidente com a barragem de Fundão, Mariana, MG. Algumas fases cristalinas encontradas são originadas em processos de processamento na indústria de extração mineral, pois seus cristais são de origem sintética (não encontrados na natureza). Uma dessas fases cristalinas sintéticas é a "Szomolnokite" – $FeSO_4!H_2O$.

Palavras chaves: Sincrotron DRX, Fluorescência RX, AC Susceptibilidade Magnética.

ABSTRACT

The accident with the Fundão dam, Mariana, MG, launched tons of iron ore tailings into the Rio Doce river system [1]. Despite the natural composition of the river sediments, characterized by relatively common mineral phases such as quartz, muscovite, kaolinite and illite and even certain hematite and goethite contents, it is important verify the abundance of hematite and magnetite after the accident. The Mariana city post-accident sediments were analyzed by Syncrotron X-ray diffraction, EDXRF and AC Susceptibility. The presence of K2Mn2 (SO4) 3 and FeSO4! H2O was found (in addition to magnetite and hematite at a significantly higher content than was naturally found before the accident), which were not recorded in the natural sediments of the same region prior to the accident with the dam Fundão, Mariana, MG. Some crystalline phases found originate from processing processes in the mineral extraction industry, as their crystals are of synthetic origin (not found in nature). One of these synthetic crystalline phases is the "Szomolnokite" - FeSO4! H2O.

Keywords: Sincrotron DRX, Fluorescence RX, AC Magnetic Susceptibility.

REFERENCE

[1] Almeida, C. A, Oliveira, A. F., Pacheco, A. A., Lopes, R. P.,, Neves, A. A., and Queiroz, M. E. L. R., *Characterization and evaluation of sorption potencial of the iron mine waste after Samarco dam disaster in Doce River basin – Brazil*, Chemosphere, **209**, pg.411-420,(2018). DOI:10.1016/j.chemosphere.2018.06.071

Acknowledgements: The authors would like to acknowledge the Brazillian Synchrotron Light Source (LNLS, CNPEM - Campinas) for the technical support and use of its beam line XRD-1, Proposals 20170383 and 20170108, as well as to Brazilian Funding Agency CNPQ, CAPES and the Local Funding Agency FAPES for supporting this research.

Espalhamento de Raios X a Baixo Ângulo

SAXS APPLIED TO THE STUDY OF THERMOSENSIVE LIPOSOMES

Costa, O. M. M. M.[a,c], Gaziola L., de la Torre[b], Gasperini, A. A. M.[c], Júnior, S. A.[a], Malta, O. L.[a]

[a]*Federal University of Pernambuco, Center for Exact and Natural Sciences, Department of Fundamental Chemistry, Postgraduate Program in Materials Science, Recife - PE, Brazil.*

[b]*Campinas State University, Faculty of Chemical Engineering, Department of Biotechnological Processes, Campinas - SP, Brazil.*

[c]*National Center for Energy and Materials Research, National Synchrotron Light Laboratory, Campinas - SP, Brazil.*

Liposomes are very attractive systems because they naturally have several desirable characteristics to act in nanomedicine, such as biocompatibility, biodegradability, stability in biological fluids, having different chemical environments in their structure and not being immunogenic. [1] The microfluidic technique produced nanometric liposomes (<100 nm) using zwitterionic and anionic phospholipids (DMPC, DMPG, DSPE-PEG) with controlled structural properties (shape, size, polydispersity and lamellarity) and controlled physicochemical properties (colloidal stability, temperature transition). By the SAXS technique, it was possible to observe the unilamellar profile of the formed structures, changes in the structure through the evaluation of the electron density profile of the bilayer with temperature variation, showing its thermosensitive character (Figure 1).

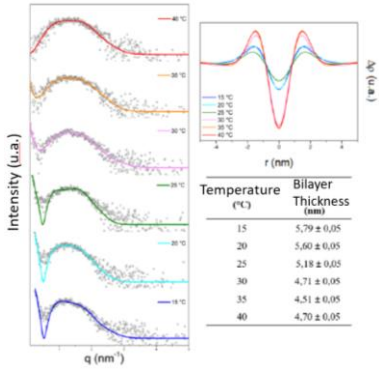

Figure 1: SAXS intensity profiles and electronic density and bilayer thickness profiles

Microfluidics is a powerful technique in the production of nanosystems providing control in the properties of formed materials, as well as the SAXS technique is a valuable tool in the study of structural and physicochemical behavior under external stimulus, in this case, temperature.

Reference: [1] Balbino, T. A., Gasperini, A. A. M, et al. *Chem Eng J*. **226.** 423-33. (2013)

Acknowledgments: *FACEPE, CNPEM – LNLS, CAPES, CNPQ.*

Desenvolvimento de um Sistema de Colimação de Raios X para um Equipamento de SAXS

R. C. Costa[a], J. B. Campos[a], P. R. B. Marinho[b], H. P. Lima[c], R. A. C. Felix[d].

[a]*Departamento de Engenharia Mecânica, Universidade do Estado do Rio de Janeiro, Rio de Janeiro, Brasil.*

[b]*Coordenação de Instalações Nucleares/Diretoria de Radioproteção e Segurança Nuclear, Comissão Nacional de Energia Nuclear, Rio de Janeiro, Brasil.*

[c]*Coordenação de Matéria Condensada Física Aplicada e Nanociência, Centro Brasileiro de Pesquisas Físicas, Rio de Janeiro, Brasil.*

[d]*Coordenação de Desenvolvimento Tecnológico, Centro Brasileiro de Pesquisas Físicas, Rio de Janeiro, Brasil.*

Com o aumento da utilização de nanomateriais, busca-se cada vez mais a criação de técnicas e equipamentos que determinem propriedades de interesse na escala nanométrica. Desta forma, as técnicas de SAXS (Small Angle X-Ray Scattering), permitem a análise de nanomateriais e determinam diversos parâmetros como tamanho de nanopartículas, densidade, morfologia e etc. Este trabalho contribui na construção de um equipamento fundamental no estudo das características nanométricas de novos materiais, que são empregados largamente na indústria por apresentarem propriedades diferentes em comparação com as propriedades microscópicas. A técnica de SAXS abrange uma vasta gama de aplicações e vem ganhando notoriedade entre os pesquisadores, tornando-se uma ferramenta essencial. É precisa, não-destrutiva e geralmente requer apenas um mínimo de preparação da amostra. As áreas de aplicação são muito amplas e incluem materiais biológicos, polímeros, colóides, produtos químicos, nanocompósitos, metais, minerais, alimentos, produtos farmacêuticos e pode ser empregado em pesquisas, bem como no controle de qualidade [1]. Diante deste fato, a instrumentação utilizada nos equipamentos vem evoluindo durante décadas, e com isso, novas possibilidades de uso incorporam a lista de novos campos de aplicação. Nos dias atuais, a técnica de SAXS vem se destacando no campo da investigação dos nanomateriais por se tratar de uma ferramenta poderosa, capaz de desvendar a estrutura da matéria com informações sobre o formato e as dimensões das nanopartículas, densidade da estrutura cristalina, bem como o grau de ordem ou desordem do arranjo estrutural do sistema. Como as propriedades dos materiais estão relacionadas aos parâmetros de rede, e com os tipos de ligações que elas estabelecem entre si, esta técnica é de suma importância para se obter êxito na criação de nanomateriais com as características e propriedades desejadas.

Duas formas principais se destacam em como os raios X interagem ao incidir sobre um objeto. Os raios X podem ser absorvidos e/ou espalhados de forma distinta ao atingir um objeto, dependendo do elemento em que este é constituído [2]. Sem estes fenômenos não seria possível analisar as características observáveis de cada material. Os espalhamentos provocados pela interação com a matéria estão correlacionados com a densidade de elétrons que esta possui.

Existem vários equipamentos que utilizam câmaras com fenda de colimação, onde o feixe primário utilizado é linear [3]. Em geral, as câmaras que utilizam este tipo de colimação têm uma intensidade de fluxo de fótons suficientemente elevado utilizando-se fontes de raios X convencionais em comparação com instrumentação de colimação pontual [4]. As amostras que podem ser analisadas e o tempo das medidas dependem principalmente da instrumentação utilizada no equipamento, onde um dos principais sistemas que interfere neste aspecto é o sistema de colimação.

Um sistema de colimação linear consiste basicamente em duas aberturas distanciadas uma da outra e alinhadas paralelamente entre si [5]. Já o sistema de bloco de colimação bloqueia parte do feixe e é conseguida por três elementos de construção [6]. Dois blocos $\boldsymbol{B_1}$ e $\boldsymbol{B_2}$ e a aresta $\boldsymbol{E}$, onde se projetam perpendicularmente para fora do plano do papel, como apresentado na figura 1. É fundamental que o plano $\boldsymbol{F_1}$ definido pelo bloco $\mathbf{B}_1$ coincida exatamente com o plano $\boldsymbol{F_2}$ do bloco $\boldsymbol{B_2}$ [7].

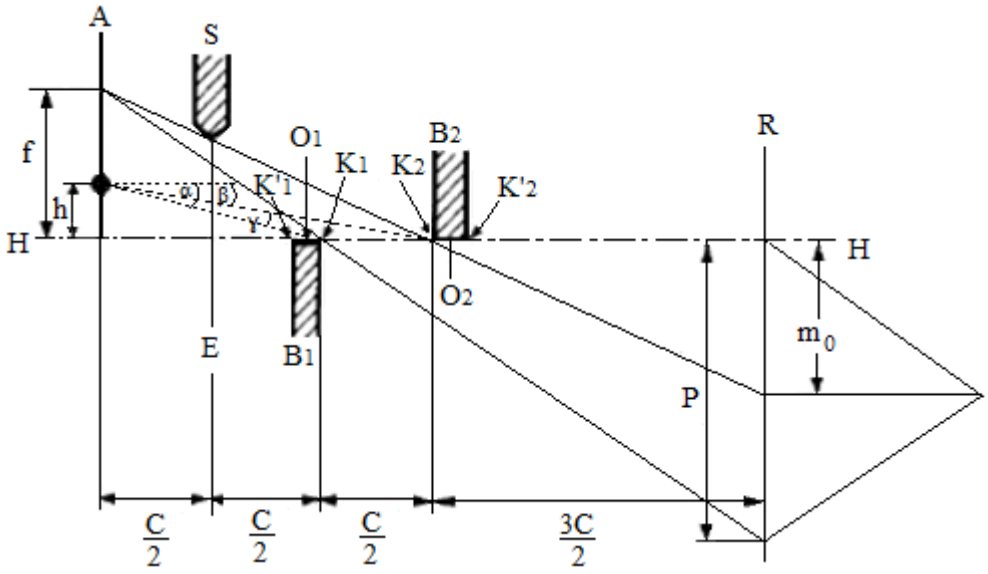

Figura 1: Seção do sistema de colimação em bloco mostrando o arranjo das partes [2].

Máquinas que dispõem de sistemas de controle por comando numérico computadorizado (CNC) integrado com sistemas de gerenciamento CAM (Manufatura Assistida por Computador) foram utilizadas na usinagem do bloco de colimação. Os processos de usinagem como furação, corte por eletroerosão a fio [8] e fresamento foram realizados no LNA (Laboratório Nacional de Astrofísica).

A figura 2 apresenta o bloco de colimação projetado utilizando-se software 3D e a peça real usinada. Este componente exige técnicas apuradas no acabamento de superfícies e precisões mecânicas altíssimas, tornando-a uma peça de difícil fabricação. Devido a sua funcionalidade, os acabamentos superficiais exigidos, e principalmente a sua tolerância de forma, devem ser da ordem do comprimento de onda dos raios X. Entretanto, precisões mecânicas tão altas em peças com dadas dimensões são impossíveis de serem atingidas, restando então, empregar o máximo de cuidado na execução da usinagem e nas várias etapas de acabamento superficial realizada.

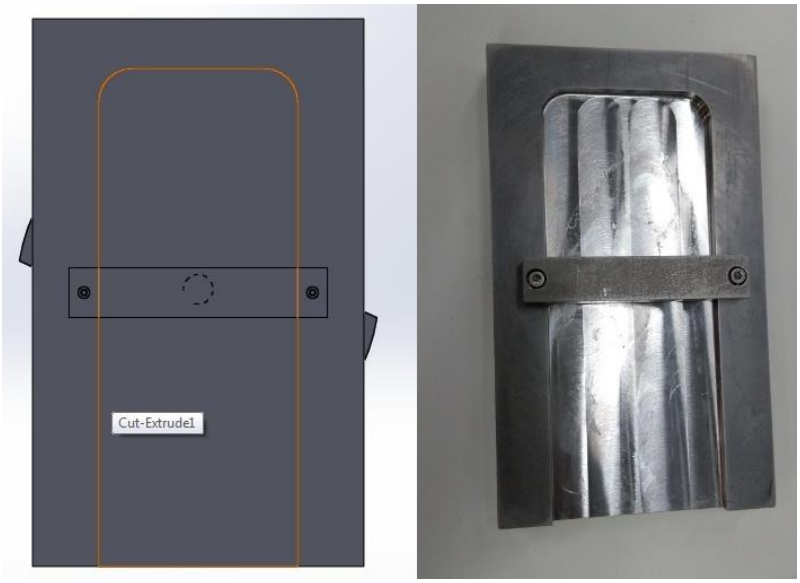

Figura 2: (a) Bloco de Colimação Projetado e (b) a Peça Real Usinada.

Na realização dos testes comprobatórios do sistema de colimação, foram utilizados um detector unidimensional sensível a posição e uma fonte de raios X de 55Fe com linha de emissão de fótons com energia de 5,9 KeV atrelado a uma interface de um sistema de aquisição

de dados. A caracterização do detector foi realizada para uma mistura gasosa Ar – C2H6 (75/25) operando a uma pressão de 2,5 atm acima da pressão atmosférica. O detector opera baseado na técnica da linha de retardo para a determinação da posição de incidência dos fótons. Após o levantamento da curva de ganho, foi definida a faixa de operação do detector com uma tensão de operação HV = 2300 V com Ganho = 105. Foi levantada também a resposta em homogeneidade do detector à iluminação direta de sua janela, a linearidade (coeficiente da reta de conversão b = 19,537) e feito o cálculo da resolução em posição intrínseca do detector (RES = 0,683 mm) [9].

O espectro da figura 3 foi estabelecida com tempo de coleta de 40 h e abertura da fenda ajustada para 1 mm. Fazendo a análise gráfica do espectro, observam-se picos secundários emergindo do lado esquerdo do gráfico juntamente com o pico principal, chegando a uma contagem de aproximadamente 150 e 300 respectivamente. Estes picos secundários são originados devido ao efeito de sombra (que é indesejável neste tipo de experimento). Isto ocorre, pois o diâmetro da fonte é consideravelmente grande (diâmetro da fonte radioativa ^{55}Fe d = 5 mm).

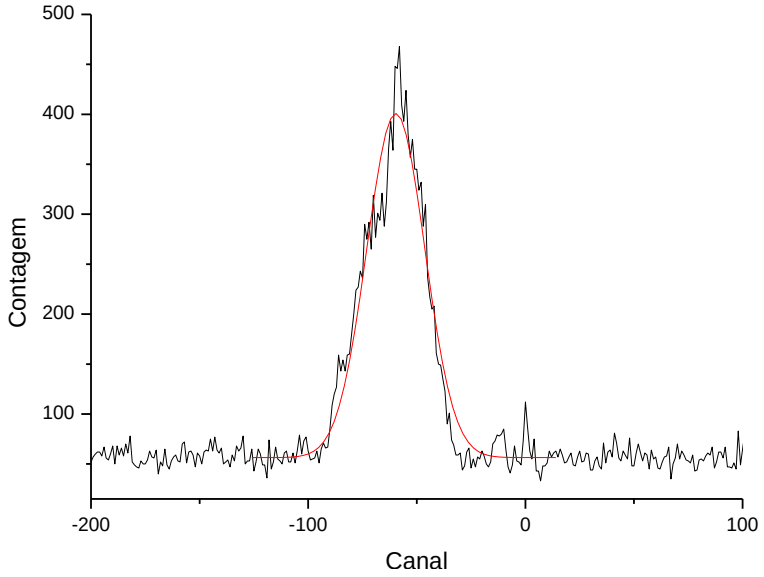

Figura 3: Espectro para Fenda de 1 mm de Abertura.

A largura a meia altura do feixe divergente (***PF***) que indica a largura do feixe que atinge a janela ativa do detector pode ser encontrada fazendo a correção por ***b*** (dividindo o valor encontrado por ***b***) obtendo ***W*** = 1,369 mm. Como a resolução intrínseca do detector é conhecida e que FWHM = 3,225 mm, então, pela equação 1 temos que ***PF*** = 3,09 mm

$$RES = \sqrt{FWHM^2 - PF^2} \quad (1)$$

Comparando com a análise teórica dos parâmetros geométricos estabelecidos no software de CAD para esta configuração do sistema, a largura do feixe foi de 3,17 mm como mostra a Figura 4.

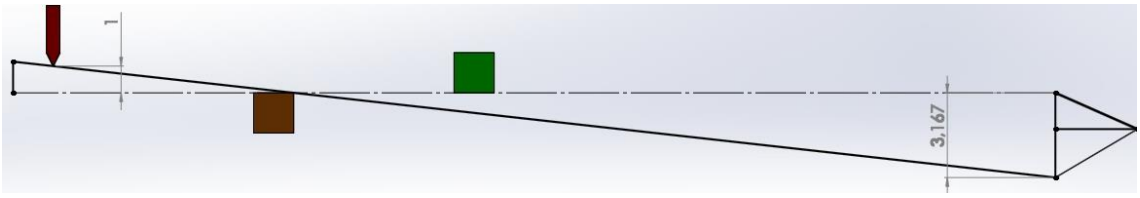

Figura 4: Análise Geométrica da Largura do Feixe na Condição de Teste Teórico para Fenda de 1 mm. Escala Vertical Ampliada em 10 Vezes.

A avaliação dos resultados do modelo teórico com o modelo experimental, observa-se que os valores encontrados são compatíveis, apresentando uma discrepância de cerca de 2,5%

que por sua vez pode estar associada a precisão da abertura da fenda e das distâncias associadas ao sistema.

Testes com fenda de 5 mm de abertura foram realizadas com tempo de 12 h. A analise do espectro gerado, realizada com a mesma metodologia para a fenda de 1 mm, apresentou uma discrepância de 8,9%. Os testes realizados no sistema de bloco de colimação com variação da fenda de 5 mm e 1 mm, apresentaram erro de 8,9% e 2,5% respectivamente, em comparação com as análises teóricas realizadas em software 3D. A diminuição do erro conforme se diminui a fenda é absolutamente favorável, visto que a resolução do equipamento é inversamente proporcional a diminuição da abertura da fenda. Em medidas de SAXS, são utilizadas fendas muito menores do que as que foram configuradas para este teste, e estes resultados apontam que nestas condições serão obtidas variações ainda menores comparado com o modelo teórico.

[1] Schnablegger H., Singh Y., *The SAXS Guide*, Getting acquainted with the principles, 3º edition (2013).

[2] Cullity, B. D., *Elements of X-Ray Diffraction*. 2ª Edição. Massachusetts: Addison-Wesley Publishing Company Inc., (1978).

[3] Alexander Bergmann, Doris Orthaber, Günther Scherf, Otto Glatter. *Improvement of SAXS measurements on Kratky slit systems by Göbel mirrors and imaging-plate detectors*, Journal of Applied Crystallography, **33**, 869-875 (2000).

[4] A. Guinier, G. Fournet, *Small-Angle Scattering of X-rays*, Wiley, New York (1955).

[5] O. Glatter, O. Kratky, *Small-Angle X-ray Scattering*, Academic, London (1982).

[6] Hendricks R.W., *Two Modifications of the Kratky Small-Angle X-ray Camera*, J. Appl. Cryst, **3**, 348 (1970).

[7] Kratky O., Stabinger H., *X-ray small angle camera with block-collimation system an instrument of colloid research*, Colloid and Polymer Science, **262**, 345-360 (1984).

[8] M. Cuendent, R. Meroz, As Estampas, *A Eletroerosão – Os Moldes*, São Paulo, Hermus (1997).

[9] Marinho, P. R. B., *Desenvolvimento de Detectores Sensíveis à Posição Multifilares e Multi-GEM para Obtenção de Imagens de Raios X*, Tese de Doutorado, CBPF, 102-140 (2006).

Acknowlegments: CAPES e FAPERJ.

Formation of $NiSi_2$ nanocrystalline platelets endotaxially grown on a Si(001) wafer

D. S. Costa[a], G. Kellermann[a], A. F. Craievic[d], L. J. Giovanetti[c], C. Huck-Iriart[c], F. G. Requejo[c], I. G. Zanella[b], R. P. Cardoso[b], C. K. B. Q. M. Oliveira[a] and I. Mazzaro[a]

[a]*Department of Physics, University Federal of Paraná, Curitiba PR, Brazil*
[b]*Department of Mechanic Engineering, University Federal of Paraná, Curitiba PR, Brazil*
[c]*Instituto de Investigaciones Fisicoquímicas Teóricas y Aplicadas (INIFTA, CONICET, Departamento de Química, Facultad de Ciencias Exactas, Universidad Nacional de La Plata), CC/16 suc. 4,1900 La Plata, Argentina*
[d]*Institute of Physics, University of São Paulo, São Paulo, Brazil*

The interest in studies of silicide nanocrystals integrated to the Si has been increased in the last decades. The reason is that $NiSi_2$ and $CoSi_2$ present high electrical conductivity, excellent thermal stability and are structurally compatible with the crystalline lattice of Si making these nanocomposites potential candidates for applications in nanoelectronic [1-2]. Therefore, new reproducible synthesis methods which require greater control of silicide nanoparticles size and shape are currently being sought for application in the processes of producing these devices in large scale. In this work an alternative method is proposed to obtain $NiSi_2$ nanoplatelets embedded in single crystalline Si wafers having the shape of nearly regular hexagons and small size dispersion. The method of preparation consists in the deposition of a Ni-doped thin film on a Si(001) wafer followed by thermal treatments to promote the diffusion on Ni atoms into Si substrate and subsequent formation of the $NiSi_2$ nanoplatelets. The sample was characterized by X-ray reflectivity and grazing-incidence small-angle X-ray scattering. The results showed the $NiSi_2$ nanoplatelets grow coherently with crystalline lattice of Si having their hexagonal surface parallel to the lattice planes of the Si{111} crystallographic form and one of their lateral sides intercepting the wafer surface. The values of the lateral size and thickness of the nanohexagons determined from X-ray scattering analysis were L = (28.0 ± 0.6) nm and t = (3.0 ± 0.5) nm, respectively.

Keywords: nanoparticles, nickel silicide, GISAXS.

Bibliography

[1] G L. P. Berning and L. L. Levenson. Diffusion of Nickel in Silicon below 475°C. Thin Solid Films, **55**, pp. 473-482 (1978).

[2] C. Y. Lee, et al. Free-Standing Single-Crystal NiSi2 Nanowires with Excellent Electrical Transport and Field Emission Properties. J. Phys. Chem. **113**, pp. 2286–2289 (2009).

Acknowlegments: CNPq; CAPES, PIPE - UFPR.

Effect of Water Content on the Porous Structure of Metakaolin-Based Geopolymers

M. D. M. Paiva[a], A. M. Percebom[b], G. Kellermann[c] , B. S. Archanjo[d], R. Verdan[d], R. Neumann[e], Romildo D. Toledo Filho[a]

[a,*] *UFRJ, ninanatal@gmail.com , toledo@coc.ufrj.br ,* [b] *PUC-Rio, apercebom@puc-rio.br,* [c] *UFPR, keller@fisica.ufpr.br ,* [d] *INMETRO, raphaelverdan@gmail.com , bsarchanjo@inmetro.gov.br ,* [e] *CETEM, rneumann@cetem.gov.br*

Cement systems should be designed to the life of the well. That implies they must work as a permanent solid barrier preventing fluid flow between different geological formations and to the surface. Therefore, a proper understanding of the mechanical properties, porosity and permeability are desirable. Geopolymers are ceramics obtained by the alkali activation of an aluminosilicate source that can replace Portland cement in oil well cementing operations. They are composed of a dense and predominantly amorphous matrix with a homogeneous footprint at macro and lower scales [1]. However, from sub-micro to nano-scales, the geopolymer morphology and nanostructure are a challenge to characterize, due to their intrinsic porosity and small agglomerated matrix particles [2].

Intrusive and small-angle scattering techniques have been used to characterize the microstructure of bulk metakaolin based geopolymers [3]. Intrusive techniques exhibit impossibility to access unconnected pores and its structure at nanoscales. Besides, adsorptions models have limitations, affecting particle and pore shape estimations [4]. Within this context, this study compares two techniques to estimate the average pore diameter and to obtain a pore size distribution for Potassium metakaolin-based geopolymers, synthetized at room temperature, with increasing water content and designed to oil well applications purposes.

BET, BJH and DFT models were applied to N_2 adsorption data to obtain the total surface area and to estimate the pore size distribution. SAXS data (Fig.1) are used to obtain the average pore sizes (using the SAS package and the Beaucage model), and the pore distributions (Fig.2 calculated with the GNOM package), adopting a spherical pores model impregnated in a homogeneous matrix. Both techniques indicate an increase in surface area, average pore diameter and coarser pore distributions, as the water content increases from the denser (Ni5) to the highest water content (Ni8) sample. Differences in the quantitative results, based on the respective model assumptions, technical limitations and uncertainties in the true pore structure are summarized on Table 1, and microstructures are illustrated in Figure 3 using SEM images.

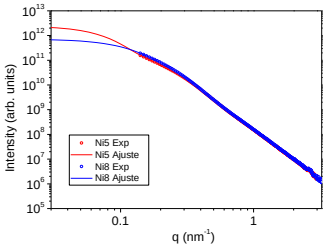

Fig.1: SAXS exp. data and fit.

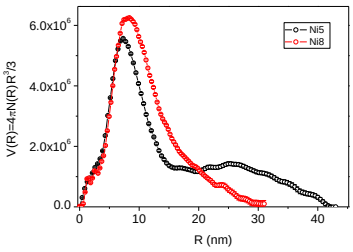

Fig.2: GNOM Vol distribution.

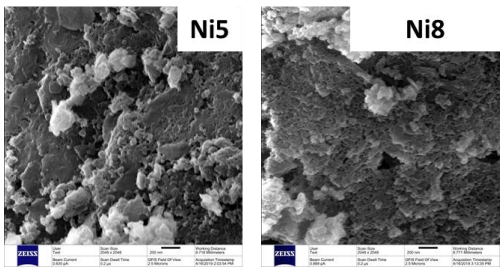

Fig.3: SEM geopolymers surfaces.

Table 1: N_2 Adsorption surface area, pore volume and SAXS average pore diameter.

System	*ρ (g/cm³)*	*BET SA (m²/g)*	*DFT SA (m²/g)*	*Davg SAXS (nm)*	*Vol BJH (cm³/g)*	*Water (%wt)*	*UCS 7days (MPa)*
Ni5	1,9	42	38	15	0,20	25,7	63
Ni8	1,7	69	36	16	0,39	34,5	15

[1] Paiva, M.D.M. et al. Journal of Petroleum Science and Engineering. 169:748-759 (2018).
[2] Kriven, W.M. Geopolymer-based composites. In Comprehensive Composite Materials II; Oxford Academic Press: Oxford, UK; Vol 5, pp. 269–280 (2018).
[3] Benavent, V., et al. Effect of composition and aging on the porous structure of metakaolin-based geopolymers. Journal of Applied Crystallography, 49(6), 2116–2128 (2016).
[4] Zhang, Z., et. al. Effect of drying procedures on pore structure and phase evolution of alkali-activated cements. Cement and Concrete Composites, 96, 194–203 (2019).

Acknowledgments: UFRJ; CETEM; LNLS; Inmetro.

Outros temas

Response of Hirshfeld Surfaces to temperature or pressure gradients in the coordination polymer emim[Mn(btc)]

C. B. Pinto[a], L. H. R. Dos Santos[a], B. L. Rodrigues[a].

[a]*Departamento de Química, Universidade Federal de Minas Gerais, Belo Horizonte, Brasil.*

Structural variations occurring under non-ambient conditions are of interest to crystal engineering[1], as they might provide insight regarding materials behavior and thermodynamics. The coordination polymer emim[Mn(btc)] (emim=1-ethyl,3-methyl imidazolium; btc=1,3,5-benzenetricarboxylate) has been studied under temperature[2] (T) and pressure[3] (P) gradients, resulting not only on anisotropic responses of the unit cell, but also on variations in bond distance and Mn^{II} coordination. In order to analyze variations on the metal-center environment, this study presents the Hirshfeld surface (HS) and fingerprint plots (FP)[4] generated for the Mn^{II} center on each previously determined structure in the multi-pressure and temperature studies[2,3].

The structural variations upon increasing P are more drastic, due to the formation of a new Mn-O bond. The HS's (Figure 1a) present several variations concerning surface volume (V), area (A), globularity (G), asphericity (Ω), shape index (S) and d_i *vs.* d_e (FP). G for example increases with P, indicating that the surfaces are closer to a spherical shape. Mn-O bond distances decrease and can be correlated to S values. The variations of the HS with T are less pronounced (Figure 1b), but inspection of quantitative parameters highlights the changes. Both A and V increase with T, while G decreases. Overall, the values of Ω are much closer to zero when varying T than they are when varying P, indicating higher similarity of the surfaces to an isotropic object. Mn-O bond distances increase with T, but S does not respond very accurately.

Even though the changes in HS's are very subtle, quantitative information regarding the surface shape can be taken as indicators of changes in metal center environment, allowing a better comprehension of structure behavior in non-ambient conditions. These correlations could eventually be used to predict the behavior of other materials, thus providing an accurate tool for the establishment of structure-property relationships useful for crystal engineering.

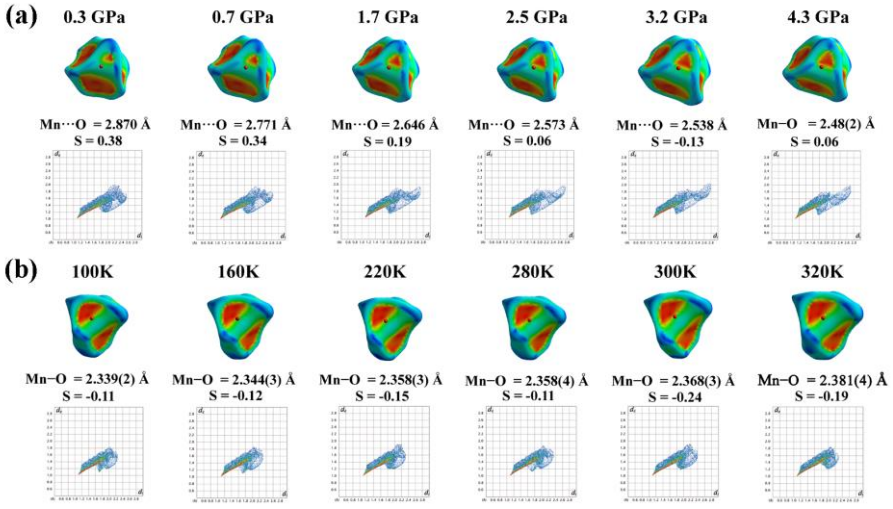

Figure 1: HS and FP for the Mn^{II} metal center with (a) increasing P and (b) increasing T.

[1] Desiraju, G.R., *IUCrJ*, **1**, 380-381 (2014).

[2] Madsen, S.R., Lock, N., Overgaard, J., Iversen, B.B., *Acta Cryst.*, B**70**, 595-601 (2014).

[3] Madsen, S.R., Moggach, S.A., Overgaard, J., Iversen, B.B., *Acta Cryst.*, B**72**, 389-394 (2016).

[4] Turner, M.J., McKinnon, J.J., Wolff, S.K., Grimwood, D.J., Spackman, P.R., Jayatilaka, D., Spackman, M.A., CrystalExplorer17 (2017). University of Western Australia.

Acknowledgments: CAPES; PPGQ-UFMG.

Crystal and electronic structures of $YbFe_2Zn_{20-x}Cd_x$ (x = 0.0, 1.0, 1.3 and 1.4) heavy fermions compounds

A. Fahl[a], R. Grossi[a], D. Rigitano[a], M. Cabrera-Baez[b], M. A. Avila[b], C. Adriano[a], E. Granado[a].

[a] *"Gleb Wataghin" Institute of Physics, University of Campinas - UNICAMP,Campinas, São Paulo, CEP 13083-859, Brazil.*

[b] *CCNH, Universidade Federal do ABC - UFABC, Santo André, São Paulo, CEP 09210-58, Brazil.*

The partial (up to 7%) substitution of Zn by Cd in the Yb-based intermetallic cage heavy fermion series $YbFe_2Zn_{20-x}Cd_x$ (x = 0.0, 1.0, 1.3 and 1.4) is known to induce a slight (~20%) reduction of the Sommerfeld specific heat coefficient γ and a huge (two orders of magnitude) reduction of the T^2 resistivity coefficient *A* [1][2]. This surprisingly distinct behavior of *A* and γ with Cd amount x calls our attention for more detailed studies. In this work, Single-Crystal X-Ray diffraction and Yb L_3-edge X-Ray absorption spectroscopy experiments are performed. The Cd ions are shown by single-crystal X-Ray diffraction to occupy a specific crystallographic site (16*c*) of the cubic structure (space group $Fd\bar{3}m$) (see *Fig.1.1)*, implying a practical limit of 10% for the Cd substitution of Zn atoms in the chemical formula [3]. The local atomic structure determined by Extended X-Ray Absorption Fine Structure (EXAFS) is consistent with the mean structure found by the single-crystal x-ray diffraction. The Yb valence determined by X-Ray Near Edge Structure (XANES) is shown to remain close to +2.85 for all series, with no variation with the Cd amount x or temperature beyond the experimental error (±0.04). These results lead us to continue the studies by incorporating news experimental techniques as Raman spectroscopy, X-Ray Emission Spectroscopy (XES) and Angle-resolved Photoemission Spectroscopy, and also numerical calculations of band structure by first principles calculation using the Density Functional Theory (DFT) with the objectives of investigate the vibrational and electronic properties of the systems $YbT_2Zn_{20-x}Cd_x$ (T = Fe, Co).

a) 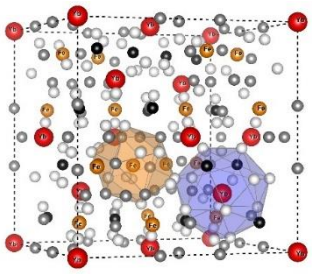 *b)* 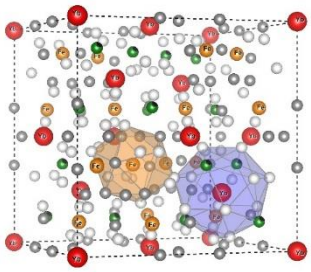

Figure 1: a) Unit cell of the $YbFe_2Zn_{20}$ compound (space group $Fd\bar{3}m$) with lattice parameter a=14.005(2)Å, the black, grey and white spheres represent the Zn atoms at the 16c, 48f, and 96g crystallographic site respectively. b) Unit cell of the $YbFe_2Zn_{18.6}Cd_{1.4}$ compound (space group $Fd\bar{3}m$) with lattice parameter a=14.109(2) Å the black/green, grey and white spheres represent the Zn atoms at the 16c, 48f, and 96g crystallographic site respectively [3].

[1] Cabrera-Baez. M., Ribeiro, R. A. and Avila, M. A., *Journal of physics: Condensed Matter*, **28**, 375601 (2016).

[2] Torikachivili, M. S. *et al*. *PNAS*, **104**, 24, 9960-9963 (2007).

[3] Fahl, A., *Estrutura cristalina e valência do Yb no composto de Férmions Pesados $YbFe_2Zn_{20}$ com substituição de Zn por Cd.* Dissertação de mestrado (Instituto de Física "*Gleb Wataghin*" – Universidade Estadual de Campinas, 2019).

Acknowledgments: We like to thank CNPq, CAPES and FAPESP for the financial support and the LNLS staff for technical support.

Magnetic Structure of RNiSi$_3$ (R = Gd and Tb)

Rodolfo Tartaglia[a], Fabiana R. Arantes[b], Carlos W. Galdino[a], D. Rigitano[a], U. F. Kaneko[c], M. A. Avila[b], and E. Granado[a]

[a] *"Gleb Wataghin" Institute of Physics, University of Campinas, Campinas, Brazil.*
[b] *CCNH, Universidade Federal do ABC, Santo André, Brazil.*
[c] *Brazilian Synchrotron Light Laboratory, Brazilian Center for Research in Energy and Materials, Campinas, Brazil.*

The intermetallic family RNiSi$_3$ (R = rare earth) presents interesting antiferromagnetic ground states evolving with R and under applied magnetic field for some of the compounds.[1] In spite of this, the magnetic structures need to be determined for a better understanding of the physics of this system. In this work, resonant X-ray magnetic diffraction experiments were performed on single crystals of GdNiSi$_3$ and TbNiSi$_3$ at zero field. It is known that photons are also sensitive to the electronic magnetic moments, leading to the appearance of magnetic Bragg peaks in the magnetically ordered phase of the material. Also, when the X-ray energy is close to an absorption edge related to the magnetism of the magnetic element, an enhancement of the signal is observed, causing a resonant scattering condition.[2] The diffraction experiments on GdNiSi$_3$ and TbNiSi$_3$ were done at the XDS (X-ray Diffraction and Spectroscopy) beamline of LNLS. The primitive magnetic unit cell matches the chemical cell below the Néel temperatures T_N = 22.2 and 33.2 K, respectively. The magnetic structure is the same for both compounds, with ferromagnetic *ac* planes stacked in an antiferromagnetic + - + - pattern, with the rare-earth magnetic moments pointing along the **a** direction (magnetic space group *Cmmm'*).[3] This structure contrasts with the + - - + stacking and magnetic moment along **b** axis previously reported for YbNiSi$_3$,[4] indicating a sign reversal of the coupling constant between second-neighbor R planes as R is varied form Gd and Tb to Yb.

[1] F. R. Arantes, D. Aristzabal-Giraldo, S. H. Masunaga, F. N. Costa, F. F. Ferreira, T. Takabatake, L. Mendonça-Ferreira, R. A. Ribeiro, and M. A. Avila, *Phys. Rev. Materials*, **2**, 044402 (2018).

[2] J. P. Hill and D. F. McMorrow, *Acta Cryst.*, **52**, 236 (1996).

[3] R. Tartaglia, F. R. Arantes, C. W. Galdino, D. Rigitano, U. F. Kaneko, M. A. Avila, and E. Granado, *Phys. Rev. B*, **99**, 094428 (2019).

[4] Y. Kobayashi, T. Onimaru, M. A. Avila, K. Sasai, M. Soda, K. Hirota, and T. Takabatake, *J. Phys. Soc. Jpn.*, **77**, 124701 (2008).

Acknowlegments: This work was supported by CAPES and FAPESP (Grant 2017/04913-1).

SAGUI beamline of Sirius: current development

Guilherme A. Calligaris, Luciano B. Candido, Antonio M. Gasperini,
José C. Corsaletti, Humberto R. Junior, Bernd C. Meyer, Márcio M. Soares

Brazilian Synchrotron Light Laboratory (LNLS), Brazilian Center for Research in Energy and Materials (CNPEM), Campinas, SP, 13083-970, Brazil

The SAGUI – Scattering Analysis Beamline – is an undulator source beamline currently under design for the Sirius second phase. It is core proposal aims SAXS experiments as well as general scattering/diffraction measurements, from liquids and solids samples. Because of such multi-purpose feature, it intends to encompass the broad user community from both SAXS1 and XRD2 UVX beamlines, but also with new approaches in mind. Therefore, SAGUI is organized in three main experimental stations divided into two experimental hutches. The first of them has an experimental station (42 m from source) dedicated to Small and Wide Angle X-ray Scattering (SAXS/WAXS) in several sample environments (likewise the SAXS1 – UVX), with the requirement to include high throughput capabilities both for liquids and solids, and so increasing the beamtime efficiency. The second hutch contains the other two experimental stations. The farthest of them, at 58 m and based on the current XRD2 diffractometer, will be dedicated for scattering and diffraction techniques which relies on bulky/weighty sample environments, such as the Langmuir Trough or the spin-coating setups that are currently available at XRD2. Lastly, the central experimental station is made of a new 6+2 circles diffractometer that will take advantage of the sweet spot in terms of energy range (5 – 24 keV) at 53 m, with a beam size of 34(H) X 8(V) microns (FWHM) provided by the beamline achromatic optics. Furthermore, this setup aims new possibilities of sample environment (cryostats, magnetic fields) and techniques due to the improved payload, flux and beam size, such as Magnetic Diffraction, X-Ray Standing Waves, surface diffraction, and microdiffraction, and at the same time addressing the current XRD2 techniques (GISAXS, GID, XRR, RSM, XRMD, etc). Because of such versatility, the optical focalization intends to preserve the undulator source characteristics but also deliver the necessary flexibility and stability to move the focal position between the experimental stations.

Here, the SAGUI beamline concept will be presented and features from all three experimental stations will be discussed, together with its radiation source and optics aspects. Regarding single crystal experiments, current progress on advanced techniques such as X-ray Standing Wave (XSW) [1, 2] and three-dimensional Reciprocal Space Maps (3D-RSM) [3, 4] will also be shown.

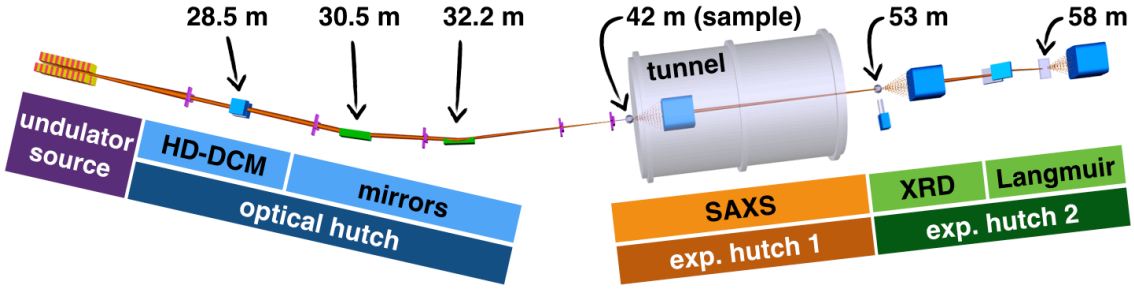

Figure 1: Schematic view of SAGUI beamline. Nominal distances from source of optical components (HD-DCM – High Dynamics Double Crystal Monochromator and x-ray mirrors) and sample enviroments (experimental hutches 1 and 2) are shown.

[1] Pietsch, U., Holy, V., and Baumbach, T. *High-Resolution X-Ray Scattering: From Thin Films to Lateral Nanostructures*. 2nd ed., Springer, 2004.
[2] Batterman, B. W., *Physical Review*, (1964), **133**, A759-A764.
[3] Zegenhagen, J. and Kazimirov, A. *The X-Ray Standing Wave Technique: Principles and Applications*. World Scientific, 2013.
[4] Xu, H., et al., *Appl Phys Lett*, (2019), **114**, 242901.

EXAFS analysis of structural disorder in the $Co_3O_2BO_3$ ludwigite

C. W. Galdino[ab], D. Freitas[c], G. M. Azevedo[b], M. A. Continentino[d], E. Granado[a].

[a]*Instituto de Física "Gleb Wataghin", UNICAMP, Campinas, Brazil.*
[b]*Laboratório Nacional de Luz Síncrotron (LNLS), Campinas, Brazil.*
[c]*Instituto de Física, UFF, Niterói, Brazil.*
[d]*Centro Brasileiro de Pesquisas Físicas (CBPF), Rio de Janeiro, Brazil.*

Homometallic ludwigites with chemical formula $(M^{2+})(M^{3+})O_2BO_3$ are mixed-valent complex oxides with potentially interesting physical phenomena. It was recently shown that a hybrid of reduced-multiwalled carbon nanotubes and $Co_3O_2BO_3$ have outstanding performance as an oxygen evolution reaction (OER) electrocatalyst, where the slow OER kinetics presents the main bottleneck regarding the storage of renewable energy and clean energy generation [1]. The novel catalyst containing $Co_3O_2BO_3$ have an overpontential lower than that for the state of the art RuO_2 catalyst [2]. The remarkable OER electrocatalyst performance of the ludwigite was mainly attributed to its local distorted octahedral environment, which increases the unit cell volume and enhance its catalytic active surface area. In addition to that, atomic positional disorder may play a significant role in the Co ludwigite unit cells volume size. However, the possibility of structural disorder in $Co_3O_2BO_3$ lacks a dedicated study in contrast to other heterometallic ludwigites, which are known to present disordered structures [3]. Finally, understanding the role of structural disorder in these materials may help the synthesis of robuster and more efficient OER electrocatalyst for green energy production.

This work investigates structural disorder in $Co_3O_2BO_3$ as a function of temperature by applying reverse Monte Carlo (RMC) methods in EXAFS data analysis. The EXAFS spectra were extracted using traditional methods [4] from Co K edge X-ray absorption spectroscopy experiments performed at the XAFS2 beamline of LNLS. Then, RMC methods were applied to refine the Co ludwigite atomic position by introducing random small amounts of disorder in the system until the refined crystal structure EXAFS spectrum reproduces experimental data. In addition to that, the convergence in reasonable time of simulated results depends upon the use of an evolutionary algorithm (EA), which allows us to cover a much bigger area of the configurational space much faster than regular methods. The EXAFS-RMC/EA analysis was performed using EvAX (Evolutionary Algorithms for XAS analysis) [5].

In this work we will show experimental and simulated EXAFS for $Co_3O_2BO_3$ for various temperatures from 6 to 900 K. Simulated spectra resemble remarkably well experimental data and we discuss the influence of structural disorder on physical phenomena. We conclude that local disorder regarding Co octahedral environment is very rigid and does not change significantly up to 400 K. Above this temperature, changes in the local octahedral environment are possibly connected to two charge ordering transitions at 480 K and 500 K. The possibility of a spin-state crossover in $Co_3O_2BO_3$ will also be discussed.

[1] Fabbri, et al. Catal. Sci. Technol. **4**, 3800 (2014)
[2] Kundu, et al. ChemElectroChem **5**, 1670 (2018)
[3] S. Sofronova, and I. Nazarenko. Cryst Res Tech **52**, 1600338 (2017)
[4] M. Newville, J. of Phys.: Conf. Series, **430**, 012007 (2013)
[5] J. Timoshenko, A. Kuzmin, J. Purans, J. Phys.: Condens. Matter **26**, 055401 (2014)

Acknowledgments: This work was supported by CNPq Grants 134752/2016-3 and 308607/2018-0, FAPESP Grant 2018/20142-8, and CAPES, Brazil.

A study on the limit of application of the kinematical theory of X-ray diffraction

D.F. Dias[a,b], A.N. C. Lima[a], M. A. R. Miranda[a], J. M. Sasaki[a].

[a]*Physics department, Federal University of Ceará, Fortaleza Brazil.*
[b]*Brazilian Synchrotron Light Laboratory (LNLS), Brazilian Center for Research in Energy and Materials (CNPEM), Campinas, Brazil.*

The key to practically all the properties of matter is in the crystal structure, to know how the atoms are distributed in space is a fundamental information for modern science. X-ray diffraction is among the most suited techniques to obtain this atomic structure from measured angular position and intensities of the diffraction peaks. In order to describe the process of X-ray diffraction, it was initially used the kinematical theory, also known as geometric theory, because basically uses geometric factors, such as Bragg's law, for the description of the phenomenon. Over time, some experiments showed a disagreement with the geometric theory[1], for example the experiment realized by G. Borrmann, that observed an anomalous transmission effect on the X-ray beam when passing through a crystal of great thickness [2]. Another theory was developed, the so-called dynamical theory of X-ray diffraction, which takes into account several physical principles, such as the multiple scattering and index of refraction inside the crystal, and dynamical theory has been able to explain the Borrmann effect. With the advancement of science, new applications using dynamical theory began to be developed, such as X-ray diffraction imaging, where the observed contrast in the images originated from the difference between kinematical and dynamical intensities, x-ray standing wave (XSW), where the multiple reflections inside the crystal, give rise to a standing wave, which together with a fluorescence detector, provide a tool capable of elementary mapping the unit cell. Moreover, in X-ray optics where single crystals with a high degree of perfection are used as monochromators, dynamical theory is used to explain exactly the properties of the beam, such as energy. For this study we simulate measurements of X-ray diffraction using both the diffraction theories and we observe in what size of crystallite, the diffraction theories begin to diverge. The result shows that if the crystal has a thickness of 13.7% of extinction length, the intensities calculated by the kinematical and dynamical theories have a difference of 5%. The extinction length is linked with beam attenuation due to scattering within the sample. Taking into account the absorption of the crystal, this size is still smaller. We also developed an expression to calculate the critical thickness for any percentage difference. Finally, we also showed that the linear absorption decreases this critical thickness.

[1] BATTERMAN, B. W. & COLE, H., Rev. Mod. Phys., **36**, 681–717 (1964).

[2] Borrmann, G., Physik. Z., **43**, 157 (1941).

Acknowlegments: CNPq.

Python – Arduino Based Scientific Instrumentation for Single Crystal Experiments

D. F. C. Ferrando[a], J. W. B. de Araújo[b] , E. M. Kakuno[a].

[a]*Universidade Federal do Pampa, Bagé, Brasil.*

[b]*Universidade Federal do Rio Grande, Rio Grande, Brasil.*

To aid the assembly of crystallographic experiments that do not follow the standard setup, especially those done with single crystals, which often demand hardware to control motors, read temperature, linear and angular position and so on, mainly controlled by a computer. This work presents simple and flexible instrumentation, which is controlled globally by Python software and locally by Arduino software, as we can see in figure 1.

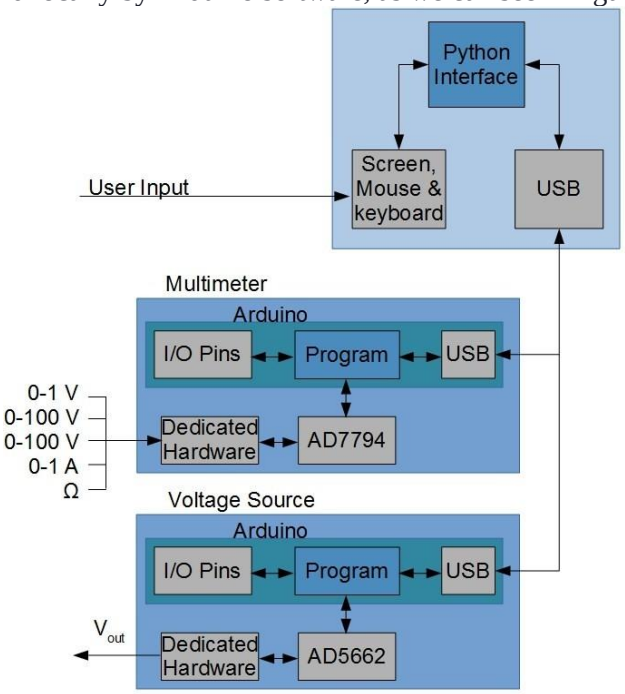

Figure 1: General view of the general instrumentation based on Python-Arduino.

For users to easily reconfigure the instrumentation hardware, it uses the Arduino platform as a base. The equipment has two modules: the first one is called a Multimeter, consisting of an Arduino-controlled ADC (digital-analog converter), the AD7794 [1] with 0.01% accuracy of internal voltage reference. This module measures DC voltage (a) 0 to 100V , (b) 0 to 1.0V, (c) 0 to 1.0 A, (d) resistance and (e) general digital I / O ports. The second module is a voltage source controlled by an Arduino with two configurations. The first configuration is a very accurate voltage source with 0.01% voltage accuracy based on the AD588 voltage reference and an 18-bit high precision AD5781 digital-analog converter (DAC). The second configuration uses a DAC with internal reference voltage with a voltage accuracy of 0.1% to 0.25% and 14 to 16 bits (AD5682, DAC714, among others), with the feed back to the Multimeter module to improve precision. The Multimeter and voltage source modules are designed to work alone.

References

[1] Analog Devices, Inc. AD779x Instrumentation Converters Frequently Asked Questions, 2010. (https://www.analog.com/media/en/technical-documentation/frequently-asked-questions/AD779x_FAQ_Instru_Conv.pdf).

Acknowlegments: CAPES / PIBID / Residência Pedagógica